MICROSCALE CROSSFLOW HEAT EXCHANGER

FABRICATED BY LASER-BASED XUROGRAPHY

by

Faisal Abdulazeez Fathiel

A thesis submitted to the faculty of
The University of Utah
in partial fulfillment of the requirements for the degree of

Master of Science

Department of Mechanical Engineering

The University of Utah

December 2012

The University of Utah Graduate School

STATEMENT OF THESIS APPROVAL

The following faculty members served as the supervisory committee chair and

members for the thesis of _____ Faisal Abdulazeez Fathiel _____

.

Dates at right indicate the members' approval of the thesis.

_____ Timothy Ameel _____	, Chair	10-25-2012	Date Approved
_____ Kuan Chen _____	, Member	10-25-2012	Date Approved
_____ Meredith Metzger _____	, Member	10-25-2012	Date Approved

The thesis has also been approved by _____ Timothy Ameel _____

Chair of the Department/School/College of _____ Mechanical Engineering _____

and by Charles A. Wight, Dean of The Graduate School

ABSTRACT

Commercial applications of microfluidic systems have been expanding exponentially over the last decade. Most commercial systems are fabricated using silicon processing; however, development costs remain high. For fundamental process development, a less expensive alternative is desirable. Xurography is an inexpensive rapid prototyping technology for microfluidic systems that is becoming more prevalent in research labs. In this technology, patterns are cut in double-sided adhesive polyimide tape, which is then sandwiched between two substrates. Traditionally, a cutting tool forms the patterns, which are relatively imprecise and subject to defects. To improve the cutting process, a laser has been implemented in this work. Due to the laser energy input, features are found to be more precise, but subject to soot production and melting. Laser-based xurography has been used to create five multilayer heat exchangers to explore the feasibility of thermal processing in devices sealed with the polyimide tape. The crossflow and counterflow heat exchangers were tested under a wide range of conditions; however, turbulent flow was not achieved due to pressure drop limitations. The devices performed leak free at temperatures up to 75 $°C$ and pressures as high as 2520 kPa. Heat exchanger effectiveness matched theoretical predictions within experimental uncertainties. Using an exergy analysis, it was determined that the heat exchangers performed most efficiently at low Reynolds number. This work represents the first time laser-based xurography has been used to develop multilayer microfluidic devices.

To

My mother

My father

My brothers and sisters

TABLE OF CONTENTS

LIST OF FIGURES

LIST OF TABLES

NOMENCLATURE

C	Capacity rate [$kJ/kg/K$]
D_h	Channel hydraulic diameter [m]
h	Enthalpy [kJ/kg]
h	Convective heat transfer coefficient [$W/m^2/K$]
L	Channel length [m]
m	Mass [kg]
$\dot{m}$	Mass flow rate [kg/s]
NTU	Number of transfer units
Nu	Nusselt number
P	Pressure [MPa]
q	Heat rate [W]
Re	Reynolds number
s	Entropy [$kJ/kg/K$]
T	Temperature [K]
t	Time [sec]
U	Overall heat transfer coefficient [$W/m^2/K$]
V	Flow velocity [m/s]
W	Channel width [m]
$\dot{X}$	Exergy rate [W]
Z	Channel height [m]

Greek Symbols

α Channel aspect ratio

δ Density [kg/m^3]

ΔP Pressure drop [kPa]

$\mathcal{E}$ Heat exchanger effectiveness

k Thermal conductivity [$W/m/K$]

$\eta_{II,ch}$ Exergy efficiency, ratio of cold to hot

$\eta_{II,oi}$ Exergy efficiency, ratio of output to input

μ Dynamic viscosity [$Pa.s$]

Subscripts

1   First measurement

2   Second measurement

avg   Average

c   Cold

ch   Ratio of cold to hot

h   Hot

i   Inlet

o   Outlet

oi   Ratio of output to input

w   Water

ACKNOWLEDGEMENTS

CHAPTER 1

INTRODUCTION

1.1 Motivation

As a result of recent advances in microfabrication, the number of microfluidic applications is growing rapidly. Microfluidic devices have dimensions on the order of micrometers and include micro-reactors, micro-heat sinks, micro-biochips and many other applications [1]. These devices are found in many fields including the entirely new fields of lab-on-a-chip, which have been enabled by the increased understanding of fluid behavior at the microscale [1]. Microfluidics has significantly impacted medicine, bioengineering and many other industries [2]. Some microfluidic devices require heating and/or cooling of fluids to perform their deigned function. Fortunately, convective heat transfer at the microscale is relatively enhanced, primarily due to the increase in surface-area-to-volume ratio. Given that heat transfer is an important phenomenon at the microscale, a significant amount of research has been conducted over the last two decades to further understand this fundamental transport phenomenon.

Heat exchangers are widely used in many engineering applications. The importance of heat exchangers has increased during the past quarter century, due tosociety's ever growing interest in energy sustainability, energy recovery, conservation, and the efficient implementation of new energy sources. Environmental concerns are also part of this increased awareness of energy usage and heat exchangers are finding new

uses in the areas of waste disposal, water pollution, air pollution, and thermal pollution [1].

Understanding the heat transfer phenomena associated with convection and conduction is essential in the design and analysis of a heat exchanger. Additionally, heat loss is a variable that may have a significant impact on the overall heat exchanger effectiveness. Heat loss may occur in many different ways, such as radiation to the surrounding environment and conduction and/or convection to the ambient fluid. Convection may be either free or forced depending on the surrounding air flow. Moreover, heat may be lost by conduction to any parts attached to the heat exchanger. At the microscale, external insulation is typically relatively thin, yet the heat transfer driving potential to/from the environment may be equivalent to that in macroscale devices. Thus, heat losses to the surroundings, typically not included in macroscale heat exchanger thermal analysis, must be included for accurate modeling of microscale heat exchangers.

The successful design of a microscale heat exchanger requires knowledge of the heat transfer characteristics of microchannels. Unfortunately, only limited experimental data for the heat transfer in microscale heat exchangers are available. On the other hand, a plethora of data is available in the literature for internal convection, including flows that are single phase, two phase, and undergoing phase change. Early on, some researchers found significant departure at the microscale from the accepted conventional-sized tube correlations for internal convection [3, 4]. More recently, researchers have found that the conventional correlations and models applied at the macroscale are actually in agreement with the available microscale heat transfer experiments [5]. Currently, members of the

thermal science community are in general agreement that the conventional-sized tube correlations are in accord with the available microscale experiments.

With this background, the overriding objective of this work to investigate the heat transfer phenomena in a microscale crossflow heat exchanger manufactured by a rapid prototyping technology called xurography. This fabrication technology enables the creation of microfluidic devices with lower cost and turn-around time than traditional microfabrication technologies. Additionally, a laser cutting methodology is developed to enable curved surfaces to be employed in xurography applications.

1.2 Introduction to Xurographic

The development of microfluidic systems based on microfabrication technologies has attracted tremendous scientific and industrial attention. Researchers started the development using conventional semiconductor materials [6]. Silicon was a common material used for these microfluidic systems, because of its ability to create high precision geometries. Glass, polydimethylsiloxane (PDMS), and acrylic are other materials used for substrates in the development of microfluidic systems [7]. These materials, however, result in some important drawbacks, including limitations on fabrication methods, testing, and packaging, in addition to relatively high costs. However, the high precision of these technologies is sometimes required for microfluidic systems.

Given the ever-increasing demand for new microfluidic applications, research activities have grown over the last decade in this field. As a result, rapid prototyping technologies have become an important foundational step in further developing the field. The advantage of rapid prototyping over traditional micro-machining techniques is that the device can be fabricated quickly and at lower cost. A recent novel manufacturing

technique termed "xurography" has been developed as an effective method for manufacturing microfluidic channels [8]. Xurography is defined as the process of cutting the designed microchannel out of a double-sided adhesive tape (typically Kapton®) using a cutting tool, such as a razor edge. Kolekar [9] reported on xurography that employs a cutting plotter to manufacture the microchannel. In the present study, a new methodology that employs a laser was used to cut the Kapton® tape. The advantages of xurography include: fast fabrication, no clean room dependence, and low-cost equipment and materials in comparison to other microfabrication technologies. The new laser-cutting methodology will be discussed further in Chapter 3.

1.3 Summary

This study was undertaken to answer several fundamental questions:

1. Can a two layer crossflow heat exchanger be manufactured using xurography? No multilayer microfluidic device has yet to be reported in the literature.

2. Can a laser be employed to cut the double–sided adhesive tape, enabling the possibility of curved cuts, without significant damage to the tape? If successful, the more complex patterns than can be generated using a laser cutting process will significantly improve the xurography technology.

3. What are the temperature limits for a xurographic heat exchanger? No xurographic manufactured thermal devices have been reported in the literature, so it is unclear what the upper temperature limits are for device of this type.

4. Does the microscale cross flow heat exchanger performance, in terms of the relationship between effectiveness, capacity ratio, and the number of transfer units (NTU), agree with theoretical correlations?

A literature review discussing past research on microscale heat exchangers, will be presented in Chapter 2. Several cross flow heat exchangers were fabricated by xurography, using a laser cutting process to create the microchannel geometries. Details of the heat exchanger design and fabrication are provided in Chapter 3, along with the development of the laser cutting process. These heat exchangers were tested in a controlled laboratory environment. The test section, experimental flow loop, data acquisition and data reduction processes are presented in Chapter 4. The thermal performance of the heat exchangers is presented in Chapter 5 along with the test results and discussion. Finally, Chapter 6 presents a summary of the project along with conclusions and recommendations.

CHAPTER 2

LITERATURE REVIEW

2.1 Introduction

The literature for microscale crossflow heat exchangers is somewhat sparse. Most of the published articles present results for the hydraulic effects in the microchannels, while very few articles report on the heat transfer phenomena. The main references used for this study are the general fundamentals of heat exchangers typically found in heat transfer textbooks, and some published articles. This review presents previously reported studies on pressure drop, heat exchanger effectiveness, heat exchanger exergy analysis, and crossflow heat exchanger correction factor. These same issues are also reported for similar heat exchangers.

2.2 Literature Review

2.2.1 Pressure Drop

One of the most important performance characteristics of a heat exchanger is pressure drop. Technical reports or property manuals for any heat exchanger would be of limited value if they did not include the pressure drop characteristics for that particular heat exchanger. Pressure drop is an important input to determine the total pressure drop in the network. Pressure drop is also necessary to select the pump that will produce the

flow for the system. Pressure drop in heat exchangers is primarily dependent on the skin friction losses in the fluid conduits. These losses depend on the friction factor, whichis inversely proportional to mass flow rate and Reynolds number *Re*. The friction factor is an indication of the pressure drop per unit of length. In the first decade of research on friction factor in microchannels, most reported data were found to be inconsistent with theory and accepted correlations. Later, it was determined that many of these early works had inherent errors that produced the erroneous conclusion. Obot [10] reported that there were two major reasons for the reported friction factor inconsistencies. First, the mass flow rate, which is understandably low, is subject to high uncertainty. Second, the locations of the pressure transducers, from which pressure drop is determined, were often improperly placed. Often pressure was measured upstream and downstream of the microchannel system and minor losses due to fittings, contractions, expansions, and channel direction changes were only approximated. Obot [10] estimated mass flow rate uncertainties were typically on the order of (2-5%), where the friction factor uncertainty was reported as (10-15%) by various researchers. Peng and Wang [11] and Wang and Peng [12] found that the measured pressure drop deviated considerably from the classical value and that it was more strongly dependent on the Reynolds number *Re*. In their investigation, the pressure drop and heat transfer for water flow through rectangular microchannels with different aspect ratios and hydraulic diameters in the range 0.15 to 0.34 *mm* were evaluated.

In addition to friction factor, other fluid flow characteristics have been investigated to assess their agreement (or disagreement) with accepted theory and correlations. Wu and Little [13] obtained eight datasets for eight channels: seven of the

channels had variable roughness and the other had a smooth surface. In the development of a miniature Joule-Thomson device, they created rectangular microchannels with hydraulic diameters in the range from 50 to 80 μm. The roughened channels were found to have an improved heat transfer coefficient, but also an increased friction factor. The analysis also showed that the Reynolds analogy was invalid. Acosta et al. [14] reported a study based on three flat rectangular microchannels with high aspect ratio (20, 30 and 40). Friction factor data and the critical Reynolds number Re_{cr} were found to be in agreement with existing correlations for smooth channels. Pfahler et al. [15] reported a study for microchannel friction factor for N-propanol flows with Re ranging between 50 and 300 in microchannels with cross-sectional area ranging from 80 to 7000 μm^2. The primary objective of the study was to determine the length scale at which the continuum assumption and the applicability of Navier-Stokes equations to predict the fluid behavior begin to break down. They found that most flow characteristics were in rough agreement with those predicted from the Navier-Stokes equations. They also found that the Poiseuille number (f x $Re = C$ for laminar flow) agreed with theory for most of their channels. However, for the channel of depth 0.8 μm, C was found to be dependent on Re and was also a factor of three greater than theoretical predictions. Peng et al. [14, 15] carried out studies in rectangular microchannels with different aspect ratios and 0.133 < d_h < 0, where the range of Re was between 50 and 3,000. It was found that Re_{cr} was significantly lower than the accepted value for smooth channels of large hydraulic diameter d_h. Choi et al. [3] and Yu et al. [17] reported the frictional factor for microtubes with inner diameters ranging from 6.9 to 102 μm for 20 < Re < 20,000 and 200 < Re < 20,000, respectively. They found that in both cases the microtube laminar flow friction

factor was below the theoretical prediction for a circular tube and that the turbulent friction factors were slightly below the accepted correlations. The early studies of Choi et al. [3] and Yu et al. [17], like many others from that era, were most likely flawed for a number of reasons. Papautsky et al. [18] indicated that microchannel flow study errors can be categorized into three distinct areas: measurements of channel dimensions, measurements of pressure and flow rate, and surface effects.

Pfahler et al. [19] conducted another experimental investigation on both gases (nitrogen and helium) and liquids (isopropyl alcohol and silicon oil) in microchannels etched in silicon with depths of 0.5 - 50 *μm*. Friction factor values were found to be less than those predicted from the conventional incompressible fluid theory. In their experimental investigation, Makihara et al. [20] found that the measured values for friction factor for micro-capillary tubes agreed with the predicted values determined from the Navier-Stokes equations. Gui and Scaring [21] reported an investigation based upon data from Rahman and Gui [22]. In their experiment with water and a refrigerant, Re_{cr} was found to be 1400 instead of the generally accepted value of 2300. Their studies were conducted in three microchannels of 1.0 *mm* width and depths of 221, 254, and 278 *μm*.

2.2.2 Heat Exchanger Effectiveness

Heat exchanger effectiveness, defined as the ratio of the actual heat transfer between the hot and cold fluids to the maximum possible interfluid heat transfer, is an important parameter for any heat exchanger. However, after reviewing all the available literature, it appears that no researcher has reported effectiveness data for microscale heat exchangers. Thus, heat exchanger effectiveness is one of the primary parameters to be reported in this study.

2.2.3 Heat Transfer Studies

A number of studies have been reported in the literature for heat transfer in microchannels and microscale heat exchangers; several of the more important studies are presented here. Peng et al. [16] reported an experimental investigation of convection in rectangular microchannels with d_h ranging from 0.133 to 0.367 *mm* and aspect ratios in the range 0.333 to 1.0. They indicated that the upper bound on the laminar flow regime was in the range of Re = 200 - 700 and that turbulent convective heat transfer was achieved at Re = 400 – 1500. Re_{cr} was found to decrease with decreasing channel size. The aspect ratio and d_h were found to have a significant effect on the heat transfer and flow characteristics. Laminar heat transfer was greatest for an aspect ratio of 0.75 while turbulent heat transfer peaked in the aspect ratio range of 0.5 - 0.75. Wang and Peng et al. [24] investigated water and methanol flow in rectangular microchannels. They found that fully developed turbulent flow was initiated in the range Re = 1,000 - 1,500 and that Re_{cr} was in the range 300 - 800. Fully developed turbulent heat transfer was predicted by the well-known Dittus-Boelter correlation [23] with a different empirical multiplicative coefficient.

Yu et al. [17] reported in an experimental investigation of a dry nitrogen and water in microtubes with diameter of 19, 25 and 102 *μm, Re* ranging from 250 to 20,000, and the Prandtl number *Pr* in the range 0.7 - 5.0. They found that the heat transfer coefficient *h* was enhanced in comparison to laminar theory and turbulent correlations while the friction factor was less than accepted values. Note that these results are inconsistent with the Reynolds analogy, which predicts that heat transfer and frictional losses should change concurrently in the same direction.

Morini [24] presents an excellent review of the experimental heat transfer literature for microchannels. He indicates that Nusselt number data are frequently in disagreement with conventional theory but that they also appear to be inconsistent with one another. Various explanations for these discrepancies have been proposed, including rarefaction and compressibility effects, property variation effects, viscous dissipation effects, surface roughness, and experimental uncertainties. Morini [24] concluded that many more systematic studies are required to generate sufficient data to fully understand the transport mechanisms that may be underlying the apparent variation in heat transfer and flow characteristics in microchannels. Kandlikar and Steinke [25] also conducted an in-depth comparison of the experimental data available for microscale convection heat transfer. Their objective was to identify discrepancies in the reported literature. They found that the available data were generally in good agreement with macroscale theories and correlations.

2.2.4 Exergy (Availability)

Exergy, also known as availability, is a measure of energy usefulness. In a steady state exergy analysis of a heat exchanger, the total exergy flux to and from the device (due to mass transfer and heat exchange with the surroundings) less the exergy destruction within the device must sum to zero. A heat exchanger exergy analysis is one means to combine the desired interfluid heat transfer with the energy loss due to frictional effects in a cost-benefit analysis. The microscale heat exchanger in this work will be analyzed from the point of view of the second law of thermodynamics using exergy efficiency (defined in Chapter 3). A perusal of the available literature on microscale heat exchanger experiments did not uncover any work that reported an exergy analysis for the

tested heat exchangers.

2.2.5 Heat Exchanger Correction Factor

Since the flow of the two fluids in a crossflow heat exchanger is not in a parallel configuration, a correction factor must be applied when analyzing the heat exchanger using the log mean temperature difference method. None of the available articles that report on experiments for microscale crossflow heat exchangers present data for the correction factor. Most heat transfer textbooks include data and a theoretical expression for the correction factor that is dependent on the inlet and outlet temperatures of the two fluids. This theoretical expression will be used to determine the theoretical correction factor in this study. A correction factor will also be determined from the experimental data using the original methodology proposed by Bowman et al. [26] facilitated by a code developed in the Engineering Equation Solver (*EES*) software.

2.2.6 Similar Heat Exchangers

A xurographic microscale crossflow heat exchanger is manufactured and tested for the first time in this research. Many researchers have investigated the fluid flow and heat transfer characteristics in other types, or in some cases similar, microscale heat exchangers. Bier et al. [27] used precision cutting of foils to manufacture a crossflow microscale heat exchanger in which water was the working fluid. They were able to generate volumetric heat transfer coefficients of more than 300 $MW/m^3/K$ for a log mean temperature difference of approximately 60 K. Friedrich and Kang [28] used diamond machining to manufacture a microscale crossflow heat exchanger with water as a working fluid. Individual copper plates were stacked and diffusion bonded to form the

heat exchanger. With conservative operating conditions, they were able to generate a volumetric heat transfer coefficient of nearly 45 $MW/m^3/K$, which is nearly 20 times that of more conventional compact heat exchangers. Ravigururajan et al. [29] conducted a single-phase fluid investigation on a parallel-flow microscale heat exchanger using R-124 as the working fluid. They reported heat transfer coefficients that were 200% greater than accepted correlations. Jiang et al. [30] investigated the fluid flow and heat transfer performance in both a microchannel and a micro-porous media heat exchanger. The thermal performance of the porous media heat exchanger was better than that with microchannels; however, the pressure drop of the former was larger. The maximum volumetric heat transfer coefficient for porous media and deep microchannel heat exchangers was 86 $MW/m^3/K$ and 38 $MW/m^3/K$, respectively. Harris et al. [31] investigated both polymer and nickel microscale heat exchangers that were fabricate using embossing techniques and LIGA fabricated mold inserts. The heat exchangers were operated with two fluids, air and water. The devices achieved heat transfer/volume rates that were five times that for conventional-scale counterparts. Alm et al. [32] manufactured microscale counterflow and crossflow heat exchangers from ceramic using stereolithography and low-pressure injection molding. Heat transfer coefficients up to 22 $kW/m^2/K$ were achieved with water in the crossflow heat exchanger. The authors reported that the joining process for the ceramic components caused blockages, which subsequently increased the pressure drop. Garcia-Hernando et al. [33] tested two counterflow microscale heat exchangers characterized by microchannels of 100 x 100 and 200 x 200 μm square cross sections, using deionized water. They found that the heat transfer data agreed with the predictions from theory. Brandner and Schubert [34]

manufactured a microscale heat exchanger using single metal foils that were diffusion bonded to form the monolithic body. Up to several thousand integrated microchannels were used. The channel cross-section ranged from semi-elliptic, to full-elliptic and rectangular. Channel dimensions were 160 x 50, 160 x 100 and 200 x 100, respectively. Hydraulic diameters were 68, 120, and 133 μm, respectively. The number of channels per passage was 2279, 1118, and 650, respectively. Extremely high heat transfer-to-volume ratios, up to 30 kW/m^3, were achieved. Kelly et al. [35] reported a study of a microscale crossflow heat exchanger fabricated using derivatives of the LIGA process. The bonding for the two polymer sections was accomplished using urethane adhesive, strong spray adhesive, mist spray adhesive, ultraviolet glue, heat sensitive glue, and methyl-methacrylate bonding solutions. The working fluids were air and water. Kelly et al. found that devices constructed using this process can handle both industrial and commercial level thermal loads, typically much larger than $10kW$. When considering all of these microscale heat exchangers, it is clear that high heat transfer rates per unit volume are achievable but that fabrication time and costs are high. In contrast, xurography presents a fabrication process that can realize a working heat exchanger in as little as one day for very low cost.

2.3 Summary

Many researchers have reported on the development of microscale heat exchangers, which have encompassed a wide variety of flow configurations. Extremely high volumetric heat transfer coefficients have been reported suggesting these devices will continue to have application where relatively small flow rates and deployment space are desirable. Many different technologies have been applied to fabricate these devices;

however, for the most part the fabrication processes have been expensive and time consuming. Thus, alternative approaches, which enable fast turnaround and are inexpensive, are desirable for the fabrication of microfluidic devices in general, and for micro heat exchangers specifically. To date, no work has been reported in the literature on microscale devices fabricated by xurography that incorporate heat transfer. Additionally, no multilayer xurographic devices have ever been reported. Thus, this work was undertaken to answer the previously reported questions, to develop data sets that illuminate the performance of this classification of heat exchangers, and to determine the feasibility of a xurographic heat exchanger. In the next chapter, a detailed manufacturing process is discussed for the microscale xurographic heat exchanger. The discussion will include the new application of laser to cut the Kapton® tape for use as a construction substrate for the microchannel system.

CHAPTER 3

DESIGN, FABRICATION AND CHARACTERIZATION

3.1 Introduction and Motivation

Manufacturing micro-electro-mechanical systems (MEMS) and microfluidic devices has never been an easy undertaking. Gad-el-Hak [36] suggested in his book, *The MEMS Handbook*, the idea of hiring an ant to do the work, which is not a bad idea, although highly impractical. Fortunately, the available technology today enables researchers to produce a micro-structure device from a variety of technologies.

In this chapter, several of the tasks undertaken early in the project are reported. These tasks include: 1) modeling efforts to determine expected performance of the microscale heat exchanger, 2) a Pretest uncertainty analysis to determine the feasibility of the experiments, to select data acquisition instrumentation based on minimal uncertainty, and to create the data reduction methodology to produce minimum uncertainty in the reported parameters, 3) the implementation of the xurographic methodology, and 4) the development of a laser cutting methodology for use in xurography.

3.2 Modeling

3.2.1 Preliminary System Modeling from Theory

Engineering Equation Solver (*EES*) is software used to obtain numerical solutions

to sets of algebraic or nonlinear equations. The code can be used to solve integral and differential equations, for optimization, to provide uncertainty analyses, for linear andnonlinear regression, and to generate publication-quality plots. The first step of this design process is to predict howthe device will behave in terms of measureable properties of pressure, temperature and mass flow rate. From these, it is also of interest how other performance metrics, such as viscosity, density, specific heat, heat rate, heat flux, etc., will change. All the aforementioned thermodynamic and transport properties are functions of temperature. Thus, the value of each property will change with the change of the temperature. As a first step in the design process, a constant value for these properties is used and the properties are corrected in a subsequent step. The Reynolds number, Prandtl number, Nusselt number, pressure drop, friction factor and the expected outlet temperature are predicted for each fluid. The results are then compared with data, which have been reported by many researchers and referenced in several textbooks [37, 38, and 39].

The inlet temperatures for the hot and cold fluids are assumed to be $70°C$ and $20°C$, respectively. The first physical model for the microscale crossflow heat exchanger has three microchannels, each with a width of 600 $μm$. The height of the channel is set to 100 $μm$, which is the approximate thickness of the Kapton® polyimide tape. The Kapton® polyimide tape consists of three layers: a 35 $μm$ adhesive, the 30 $μm$ polyimide tape and then another adhesive layer of 35 $μm$ (thicknesses are approximate). The total thickness is 100 $μm$ for the Kapton® polyimide tape, which defines the microchannel height.

Several *EES* models have been created. The number of microchannels was varied to include 3, 6, 9 and 12 microchannels for each side. The number of microchannels was initially three because of concerns related to the capability to manufacture a higher number of microchannels using the laser cutting technology. On the other hand, the first device tested had 15 microchannels on each side.

Results from the *EES* models were found to be in agreement with the available reported data [37, 38, and 39]. All equations and correlations for the *EES* model are presented in section 4.4. Example results from the modeling are presented and discussed in the Appendix.

To improve the initial *EES* models, the working fluid properties, such as viscosity, density, thermal conductivity and specific heat, were modified to be functions of temperature. Property correlations for water density, viscosity, thermal conductivity, and specific heat at constant pressure were obtained from University of Applied Science, Faculty of Mechanical Engineering, Department of Technical Thermodynamics, Germany [51]. Through a connection at the National Institute of Standards and Technology (*NIST*).

Several different channel patterns were designed and fabricated before the final designs were selected. The first fabricated pattern, created with traditional xurography, as shown in Fig. 3.1, was a single-layer device consisting of three microchannels with widths of 600 *μm*. It was found that this design was undesirable for the study, as discussed in section 3.5.1.

The second pattern, designed for the laser-cutting technology, consisted of six microchannels with sharp corners, designated as Pattern #1 in Fig. 3.2. Each

microchannel was 900 *μm* wide. The next design (Pattern # 2, figure 3.2) consisted of nine microchannels each 450 *μm* in width. Different manifold headers were used for that design. These patterns indicated that the laser-cutting technology is capable of producing small microchannels (widths on the order of 500 – 600 *μm*) with curved features. Pattern #3 in Fig. 3.2 shows a nine-channel system where each channel was 50 *mm* and 27.333 *mm* in length and width, respectively. This design also implemented smooth curved channel inlet sections for the first time.

The final design pattern is shown in Fig. 3.3. The naming convection for each design is based on the microchannel width and the number of microchannels (e.g., 15 X 0.6 *mm*). Some of the design criteria have been applied to guide the final design process.

- The minimum separation distance between the outermost channels or other cut features and the tape edge was selected to be 8 *mm*. This minimum wall thickness was designed to provide adequate adhesion surface area so as to minimize the possibility of leaks to the exterior of the device. Alshareef [40] tested the integrity (lack of water leakage) of microchannels, produced using a blade cutter, when subjected to a range of pressure differences across the separation wall. Leakage was visually observed using colored distilled water. Several wall thicknesses were tested for a range of pressure differences. The 1 *mm* wall thickness was found to be leak free for pressures less than 1.7 *MPa*. These tests were performed without the clamping system.

- Based on Alshareef's [40] data, the separation walls for the microchannel were 1.1 *mm* or more.

- To create a crossflow heat exchanger with the maximum surface area participating in the heat transfer between the two fluids, the patterned surface areas of

both the hot and cold sides were designed to be square-shaped. The same *AutoCAD* pattern was used to cut both faces using the laser technology. Using these design guidelines, the tape sections were laser cut. The final device microchannel patterns are shown in Figs. 3.3 to 3.5.

- The first device manufactured and tested consisted of 15 microchannels of 600 *μm* length. This design was considered the base device. The other two designs are modifications of the base design using the same overall surface area for the microchannel pattern and maintaining the same manifold headers.

3.2.2 Higher Level Modeling Based on Theory

A second, more accurate, model was developed to serve as the basis for the data reduction and uncertainty analyses. The code was verified by comparing results with those generated from the *EES* model. Details of the model are provided in section 4.4. *Matlab* was used as the tool to facilitate the model development. As in the latter stages of the previously described *EES* model, temperature dependent property correlations were also applied in the second model. The *Matlab* model was used to generate approximate data for use in the Pretest uncertainty analysis, presented in section 3.4.

3.3 Heat Transfer Surface Area

The thermal conductivity of the 3-layer Kapton® tape is relatively low; the accepted value provided by the manufacturer is $k = 0.12$ *W/m/K* for the direction perpendicular to the layers. Likewise, the thermal conductivity of the glass slide is also relatively low at $k = 0.96$ *W/m/K*. Thus, it was initially assumed that the heat transfer through the Kapton® tape and glass side would be low compared to the heat transferred

through the metal partition. If true, the heat transfer surface area used in the heat exchanger performance analysis should be modified. To assess this possibility, both two-dimensional (2-D) and three-dimensional (3-D) models of the heat exchanger were created in *Comsol*. Symmetry was liberally applied to reduce the area or volume that had to be modeled. Fig. 3.6 is a typical isothermal plot for the 2-D heat exchanger model. Important features indicated in Fig. 3.6 are the glass slide, microchannel, Kapton® tape, and the metallic partition. The top of the glass slide was assumed to be perfectly insulated (adiabatic) and adiabatic boundary conditions were assumed on the left and right surfaces due to symmetry. Isothermal boundary conditions, consistent with the fluid temperature, were assumed for the three surfaces of the microchannel. The lower surface of the partition, which also represents the top surface of the orthogonal hot microchannel, was assumed to be isothermal, at a temperature consistent with the hot fluid. Nominal temperatures were assumed for the system. For the results presented in Fig. 3.6, the microchannel walls were assumed to be at $20°C$ and the partition bottom surface was assumed to have a temperature of $85°C$. In Fig. 3.6, it is clear that the majority of heat is transferred into the microchannel through its bottom (metal partition) surface. An assessment of the heat rate through the three surfaces of the microchannels indicates only 4% is transferred through the combined glass and Kapton® tape surfaces, which is essentially negligible. Thus, the heat transfer surface area for the heat exchanger analysis is approximated by only the surface in contact with the metal partition, rather than the entire wetted surface. Fig. 3.6 2-D isothermal plot for a section of the microchannel heat exchanger. The isothermal microchannel surfaces assumed for the 2-D model were a reasonable approximation of actual conditions; however, a better approximation could be

achieved by including the fluid flow in the channels. A 3-D model that allowed fluid flow to be incorporated accomplished this upgrade. Fig. 3.7 presents an example of the 3-D simulation results. The 3-D model has the same basic geometry as the 2-D model with two major differences: 1) the complete bottom microchannel is included (only the microchannel surface was included in the 2-D model), and 2) a 0.1 *mm* extrusion is utilized to create the third dimension. All exterior boundaries are assumed to be perfectly insulated. In Fig. 3.7, the hot fluid microchannel is near the middle of the model and the cold-water microchannel is at the bottom of the model.

As with the 2-D model, the 3-D model indicated that the heat transferred through the Kapton® tape is negligible when compared to the total amount of heat transferred through the metal partition. In general, good agreement was found between the results for the two numerical models.

3.4 Pretest Uncertainty Analysis

According to Kline [41], there are six primary uses of an uncertainty analysis during the design and planning phases of an experiment, including:

1. To enforce a complete examination of the experimental procedure, including the potential sources of error.

2. To advise when improved instruments and/or procedures are necessary to achieve desired output accuracy.

3. To minimize instrument cost for a given output accuracy.

4. To identify instruments and/or procedures those have the greatest impact in the accuracy of the output parameters.

5. To determine if the experiment can meet the desired level of accuracy. If not, the experiment may be abandoned or redesigned.

For this experiment, the Pretest uncertainty analysis was performed to provide details to assess all of the above uses, except number 3.

The Pretest uncertainty analysis was conducted computationally following the procedure outlined by Moffat [42,43,44], which results in reported uncertainties containing only precision error. Uncertainty in an output parameter, or result, δR is found by taking the square root of the sum of the products of the sensitivity coefficients θ_i, equivalent to the partial derivatives in equation 3.1, and the measurement uncertainties δx_i.

$$\delta R = \left[\sum_{i=1}^{n} \left[\frac{\partial R}{\partial x_i} \delta x_i \right] \right]^{1/2} \qquad (3.1)$$

The sensitivity coefficients were computed using the data reduction program introduced in the previous section using the method proposed by Moffat [42, 43, and 44]. In this procedure, estimates for the δx_i are first provided as input to the code. Sensitivity coefficients can then be determined using a central difference approximation for the partial derivative using a suitable perturbation.

A sample of the input data used for a typical Pretest uncertainty analysis, based on the data acquisition system and data reduction procedure outlined in Chapter 4, is provided in the Appendix. Variable values were estimated based on expected performance predicted by the theoretical system model presented in Section 3.2.2. Estimates for measurement uncertainties were based on manufacturer's data and expected instrument uncertainty following calibration.

The Pretest uncertainty results indicate that the cold-side pressure drop has the greatest uncertainty of 11.7%. This most significant contribution to this uncertainty is the pressure measurement at the cold inlet. The uncertainty data also indicate that the most critical measurement in the experiment is the mass flow rate, which can adversely affect the uncertainty in Re and other parameters.

The Pretest uncertainty analysis results in the Appendix indicate that the expected uncertainties for the results are acceptable. After careful consideration of these data, it was concluded that 1) data of acceptable uncertainty can be generated so there is no need to abandon the experiment, 2) the data acquisition equipment can provide the desired accuracy in the results, 3) the initial procedure for data acquisition and data reduction is acceptable in terms of providing results with acceptable uncertainty, and 4) the determination of mass flow rate from the mass measured by the scales in a selected time interval is the most critical measurement in the experiment and should be taken with the most care.

3.5 Xurography

Many microchannel manufacturing processes have been reported by researchers; Ashman and Kandlikar et al. [45] reported the microchannel fabrication processes as the following:

1. Micro-machining, a diverse category that includes diffusion bonding and diamond tool milling/grinding as common micro-machining methodologies

2. Stereolithography

3. Chemical Etching

4. LIGA

Note that xurography is not mentioned as a microchannel fabrication methodology. While not a traditional microfabrication technology, xurography is finding more application in numerous research labs around the world due to its inherent advantages of low cost, ease of manufacturing, and fast fabrication. These qualities make xurography a technology that is suitable for rapid prototyping. Xurography has been proven to be an effective method for microfluidic channel manufacturing. The manufacturing of a microchannel using xurography has traditionally been achieved using a knife plotter to cut the double-sided adhesive tape. To enhance the technology, laser cutting of the double-sided adhesive tape was explored as a means of creating curved microchannel features. A thorough explanation of the traditional xurographic process has been provided by Nguyen [46].

A review of the two cutting techniques, including the design and cutting process, is discussed in the following section. Both technologies have several common features, including the graphic design that is delivered to the cutting tool. The two tools use different software to drive the cutting process, namely *Adobe Illustrator* for the cutting-plotter (blade cutting) and *AutoCAD* for the laser cutting process.

3.5.1 Blade Cutting

Manufacturing a microchannel using xurography has been typically achieved by using a cutting plotter, as first suggested by Bartholomeusz et al. [47]. In this technique, the double-sided adhesive tape is fixed on a piece of wider tape, which has first been placed on a piece of paper. Since the cutting process is contact based, the double-sided adhesive tape must be prevented from moving during the cutting process. The

numerically controlled cutting plotter is essentially a printer with the cutting knife in place of the printing jets or printing head. This cutting process has several advantages and disadvantages listed below.

3.5.1.1 Advantages

- Inexpensive rapid prototyping technique.

- The basic equipment (cutting plotter) is inexpensive.

- The consumable materials (double-sided adhesive tape, substrate material) are inexpensive.

- Feature resolution on the order of 10 μm is possible.

- A clean room facility is unnecessary.

- The cut microchannel has good edge acuity with minimal undesired burrs.

3.5.1.2 Disadvantages

- The width of the cut microchannel is limited to a minimum of 300 μm.

- Consistent precise production is challenging.

- Perfectly straight channel sections are difficult to produce.

- An overlap of the cutting path is required at both the beginning and end points in order to achieve a smooth and complete cut that facilitates the tape removal process (peeling process).

- The cutting plotter cannot produce circular or curved geometries with high resolution (only straight cuts are typically possible).

- The production of multiple separate cuts of high accuracy on the same piece of tape is problematic due to tape movement during cutting.

A significant disadvantage of the cutting technique for the manufacture of microchannels is the inconsistency of channel width. Data from Torgerson et al. [48] indicate that difference between the cut channel width and the cutting plotter setting may be as high as 27%. The laser cutting technique was explored as a method to increase precision and to enable curved cuts.

3.5.2 Laser Cutting

A VersaLaser VLS3.60 laser system was used to cut the double-sided Kapton® tape. The VLS3.60 laser system is widely used in educational institutions for graphic and product design, materials research and in architecture programs. The laser system is a single laser platform with six laser cartridges with power ranging from 10 to 60 *W*. In practice, the laser beam is applied vertically to cut the Kapton® tape. Thus, a plan view of the design pattern is required.

The cutting procedure with the VLS3.60 can be summarized as the following: 1) Create a plan view pattern design using *AutoCAD*. 2) Import the design into the laser machine environment using *AutoCAD*. 3) Bond the Kapton® tape to both surfaces of the metal material, which serves as the major heat transfer media between the hot and cold microchannels. 4) Focus the laser beam using the manufacturer's recommended procedure. 5) Set the laser beam power, density and speed. 6) Activate the machine to laser cut the tape.

In practice, it was determined that step 5 is the most critical to achieving the desired cut. Desired traits are a precise complete cut with minimal burning of the material, minimal soot production, and no scoring of the substrate. To achieve this result, many trials were conducted to determine the optimal combination of laser power,

intensity and speed for a fixed *z*-axis elevation (distance between the laser lens and object being cut). Initial trials indicated that the required settings to produce acceptable cuts were dependent on substrate thickness, *z*-axis elevation, and the presence or absence of the plastic cover sheet on the Kapton® tape. Table 3.1 includes the laser settings for a selection of trials conducted to select the optimum laser properties for cutting the Kapton® tape. The laser settings and results presented in Table 3.1 are based on a single laser pass. Power, set as a percentage of full power, impacts the cutting depth. Higher power settings result in deeper cuts. Processing speed is set as a percentage of the maximum rate of travel of the motion system. This setting also affects the cutting depth. Color refers to settings that are automatically applied to different elements of the graphic being printed (cut) and allows interpretation of raster and vector elements in the graphic. The laser pulsing frequency is set in pulses per linear inch (PPI). Table 3.2 provides similar data for trials conducted using multiple cutting passes.

The trials reported in Tables 3.1 and 3.2 are samples of the many iterations applied to determine the optimum laser settings for effective cutting of the Kapton® tape without etching the substrate. The color setting was found to be useful in controlling settings when cutting the same geometry with different substrate materials or to produce different cutting depths on the same substrate.

The best two sets of laser control settings used to laser cut the Kapton® tape are listed in Table 3.3. The first set was used to cut the tape only (without the plastic coating) while the second set was used to cut the tape including the plastic coating.

The laser cutting technique has several advantages and disadvantages, which are listed below.

3.5.2.1 Advantages

- The material to be cut can be rigidly placed in the system.

- With no physical contact associated with the cutting process, the test article experiences no movement.

- High precision curved geometries may be produced.

- Since the cutting mechanism is produced with a laser beam, there is no tool wear.

- A wide variety of materials can be cut or etched.

- The cutting process is relatively fast.

- The microchannel walls have reduced relative roughness compared to surfaces created by a physical cutting process.

3.5.2.2 Disadvantages

- The laser cutting process can produce burned and/or melted edges.

- Soot and ash, in the form of a black powder, can migrate into the microchannels.

- The edges of the microchannels may be black as a result of the burning process.

The manufactured microchannels were symmetrical and had precise dimensions, unlike the microchannels produced with the cutting plotter. Ash created from the burned tape left an undesirable appearance and required removal before the microchannels were capped. The cleaning process was accomplished by simple rinsing with water. Unfortunately, the rinsing process was unable to completely remove all the burned and melted material from the tape. Loose ash was removed but the edges remained blackened. A physical cleaning process was not attempted since this may have resulted in undesired modification of the microchannel dimensions. Chemical treatments to remove the burned material were not considered. In the future, chemical treatment should be studied to

improve the overall quality of the cut geometries. The blackened cuts that defined the microchannel edges resulted in high uncertainty for the measured microchannel width. When using an optical microscope, it was difficult to achieve an accurate measurement for the microchannel width without first cleaning the blackened edges.

3.6 Fabrication, Manufacturing and Assembly of the Heat Exchanger

As previously mentioned, many different technologies have been used to fabricate a system of microchannels that are the primary component in microscale heat exchangers. In the previous section, xurography was introduced as a means to create microchannel systems; laser cutting of double-sided adhesive Kapton® tape is used in this study to generate the microchannel patterns. In this section, additional details are provided on the assembly process that takes the patterned Kapton® tape to a complete heat exchanger.

The heat exchanger consists of five separate layers. Stacked from bottom to top, these layers are:

1) A 5.08 *cm* x 5.08 *cm* (2" x 2") glass slide of 3.2 *mm* (1/8") thickness.

2) A 5.08 *cm* x 5.08 *cm* (2" x 2") layer of double-sided adhesive Kapton® polyimide tape. Each adhesive layer is approximately 35 *μm* thick. The tape is approximately 30 *μm* thick; thus, the total thickness of the adhesive and tape is approximately 100 *μm*. The microchannels have been defined through the laser cutting and tape peeling process. The microchannels (3 to 15 channels) run N to S in this layer.

3) A 5.08 *cm* x 5.08 *cm* (2" x 2") partition of high thermal conductivity metal.

4) A 5.08 *cm* x 5.08 *cm* (2" x 2") layer of double-sided adhesive Kapton® polyimide tape. The microchannels (3 to 15 channels) run E to W in this layer to create the cross flow arrangement.

5) A 5.08 *cm* x 5.08 *cm* (2" x 2") glass slide of 3.2 *mm* (1/8") thickness.

Two vias are created in each glass slide by mechanical drilling with a Dremel rotary tool. The vias are aligned with the manifold sections in each microchannel system and provide fluid inlet and outlet for each microchannel system. Nanoports are bonded over each via on the exterior of the glass slide. The nanoports serve as fittings for the plastic tubing that delivers fluid to/from the heat exchanger. Details on the drilling process and nanoport bonding are provided by Nguyen [46]. Nanoport curing is conducted in an oven at 175°C for 45-60 *min*.

Brass and copper were chosen for the partition material due to their high thermal conductivity, availability, and ease of polishing such that good adhesion with the Kapton® tape occurs. The thermal conductivity *k* for brass is 109 *W/m/K*. For copper *k* = 401 *W/m/K*. Thin partitions were selected to facilitate thermal transport through the partition; however, it was determined that thin metallic foils would not provide the necessary rigidity for assembly. As a compromise, the thickness of the brass piece is 1.35 *mm,* and the copper piece is 0.85 *mm* thick.

The metallic partitions are cut from stock sheets into 5.08 *cm* x 5.08 *cm* (2" x 2") pieces using a bench shear cutter. To insure flatness, a 30-ton hydraulic mechanical press then compresses the partition material, which has been sandwiched between two heavy steel pieces. Burrs, created by the cutting process, are then removed from the edges of the partitions using sand paper in a dry sanding process. The sanded surfaces and edges

are evaluated using a right-angle tool to ensure each corner of the partition is right angled. The partition is then cleaned using liquid isopropyl. This process removes the oil collected on the surface during the pressing process and the metallic particles generated by the sanding process. If the partition is cut from pristine stock material, the finishing process is a light polishing. For material in rougher condition, several polishing step are undertaken. Polishing is conducted with a rotating disc polisher using successively finer grit paper (50 μm, 15 μm, 0.5 μm particle size). Polisher speeds range from 50 to 500 *rpm*, where the slower speed is used with the largest grit paper. Water is used as the lubricant. The last mechanical machining step is buffing. In this process, a piece of cloth is used with a liquid chemical buffing agent. Fig. 3.8 shows a sample of the polished brass compared to unpolished brass piece (used as a metallic partition).

After the mechanical polishing of the metallic partition The Kapton® tape pieces are bonded to each face of the partition. The partition is held from the side to insure no fingerprints are left on the surface. The metallic partition is slowly transferred to the exposed adhesive on the tape to minimize the inclusion of air at the bonding interface. After sticking the first side of the partition to one of the tapes, the second side is bonded to the second tape similarly. Unwanted Kapton® tape is removed using a blade and a roller is used to evacuate any trapped air bubbles. The next step is to cut the Kapton® tape sections using the laser cutter. Following the cutting process, the surfaces are cleaned using water and a dry cloth. The surface cleaning process is done gently and slowly so as not to damage the cuts. Before removing the coating, the glass top piece is laid on the Kapton® tape (before removing the plastic coating) and the vias are marked. Using a high-speed Dremel drill with a diamond-coated bit, the marked vias are drilled in

the glass cover slides. Each piece of glass is marked to insure the best alignment between the vias and manifolds. Finally, the cut Kapton® tape sections are removed to create the microchannel sections

Several steps are taken to insure that the microchannels on the two sections are at right angles to each other. The first step insures that each corner of the metallic partition forms a right angle, as described above. In the second step, the metallic partition is placed in the corner of the machining area in the laser machine. The laser machine has 90° corners, which allows any right-angled piece to precisely fit into the corner. In the third step, a 5.08 *cm* x 5.08 *cm* (2" x 2") square is drawn, where the microchannels are centered in this square. This square allows the laser beam to focus on each corner, insuring the center position of the microchannels.

Kapton® tape curing is conducted in an oven at 120°*C* for 45-60 *min*. A clamping system was initially applied to the five-layer heat exchanger test section to provide additional mechanical force to minimize the potential for leakage. It was later determined that the clamp was unnecessary. The test sections were operated at gauge pressures up to 2.5 *MPa* (365 *psig*) at the inlet, which correlates to *Re* ~ 1600 in the channels, without signs of leakage. Thus, the clamping system was abandoned. Fig. 3.9 shows a 3-D SolidWorks model of the final device parts before assembly. A 3-D SolidWorks model of the assemble device is shown in Fig. 3.10. In Fig. 3.11, images of devices at various stages of fabrication are shown. The images include a slide with one of the first fabricated patterns, two slides showing samples of the patterns created by laser cutting with different iterations of the control settings, metallic partitions after laser cutting (both before and after peeling the tape) and two assembled devices (one with a

brass partition and the second with a copper partition).

3.7 Summary

Three different types of models have been introduced in this chapter. The first-level analytical model, which is a system of coupled nonlinear equations, was applied to design the heat exchanger and to assess operational limits. The higher-level analytical model was developed for two purposes: data reduction and the uncertainty analysis. The uncertainty analysis indicated that the proposed experiment could be conducted with acceptable uncertainty and with the proposed data acquisition system. The finite-element model of the heat exchanger indicated that the heat transfer surface area for the heat exchanger performance analysis should be represented by only the microchannel surface in contact with the metal partition. A novel laser cutting process for the xurographic microchannel fabrication technology was also introduced. Laser cutting was found to mitigate problems with the traditional cutting plotter. Channel geometries are more accurate and precise. Cut surfaces are smoother, but have an undesirable coating of burned and/or melted Kapton® material and adhesive. The laser cutting method also enables curved cuts. The heat exchanger microchannel systems have been designed and the complete assembly processed has been outlined. The following chapter will present the experimental apparatus, procedure, data acquisition and data reduction.

Table 3.1 Effect of laser control settings on finished product for a single cycle.

#	Power	Speed	PPI	Color	Results
1	2.0%	10%	990	(B)	Tape not removable
2	2.0%	5%	990	(B)	Tape not removable
3	3.0%	5%	990	(B)	Peeling is difficult, results in channel destruction
4	3.0%	5%	990	(R)	Peeling is difficult, results in channel destruction
5	3.0%	5%	990	(Y)	Peeling is difficult, results in channel destruction
6	1.0%	2%	1000	(B)	Tape is not removable
7	2.0%	2%	1000	(B)	Tape is removable without substrate etching
8	2.0%	2.5%	1000	(B)	Peeling is difficult, results in channel destruction
9	2.0%	2.2%	1000	(B)	Tape is removable without substrate etching
10	2.0%	2.1%	1000	(B)	Tape is removable without substrate etching
11	1.0%	3.5%	1000	(B)	Tape is totally burned, significant substrate etching
12	2.0%	2.5%	1000	(B)	Tape is removable, minimal substrate etching
13	3.0%	4.0%	1000	(B)	Tape is burned, substrate has some etching
14	5.0%	4.0%	1000	(B)	Tape is removable, slight substrate etching

Table 3.2 Effect of laser control settings on finished product for multiple passes.

#	Power	Speed	PPI	Color	Results
1	1.0%	5%	1000	(B)	first iteration, only cover etched; second iteration, tape burned but not removable
2	2.0%	10%	1000	(B)	first iteration, only cover etched; second iteration, tape burned without peeling
3	1.0%	10%	1000	(B)	@ 5 iterations, only cover etched @10 iterations, only cover etched @20 iterations, only cover etched
4	3.0%	5%	1000	(Y)	Tape is etched on second iteration
5	3.0%	2%	1000	(Y)	Tape is etched on second iteration

Table 3.3 Optimum laser control settings.

| #	Power	Speed	PPI	Color	Results
1	2.0%	2.2%	1000	(B)	Fine cut results, easy to peel
2	5.0%	4.0%	1000	(B)	Fine cut results, easy to peel
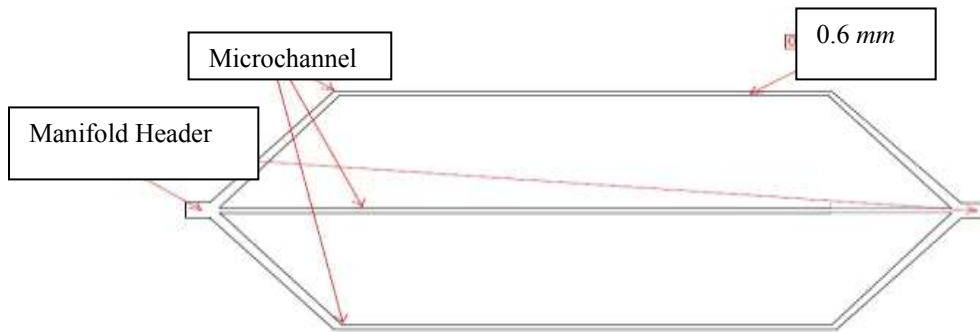
Fig. 3.1 Initial design. The middle microchannel was 59 *mm* long while the parallel sections of the outer microchannels are 39 *mm* in length.
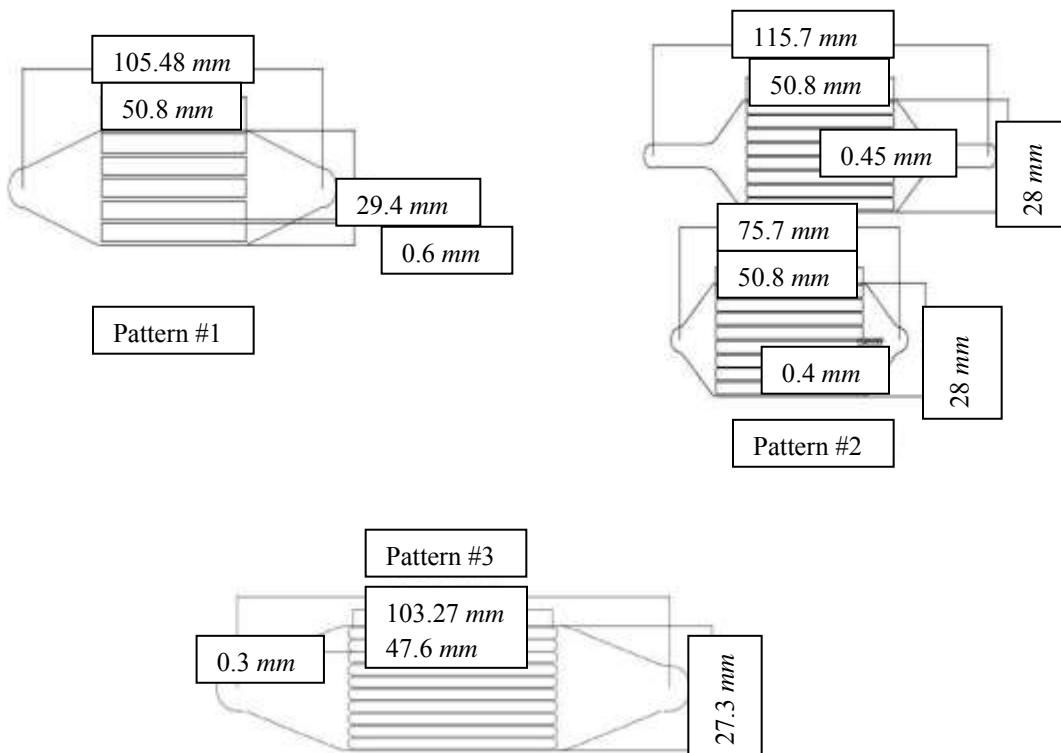

Fig. 3.2 First generation microchannel systems designed for laser cutting.
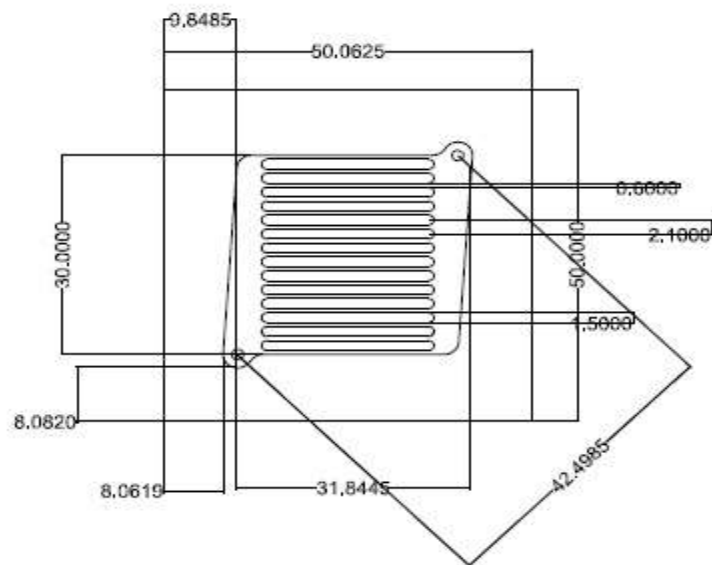
Fig. 3.3 Microchannel 15X0.6 *mm*. All dimensions in *mm*.
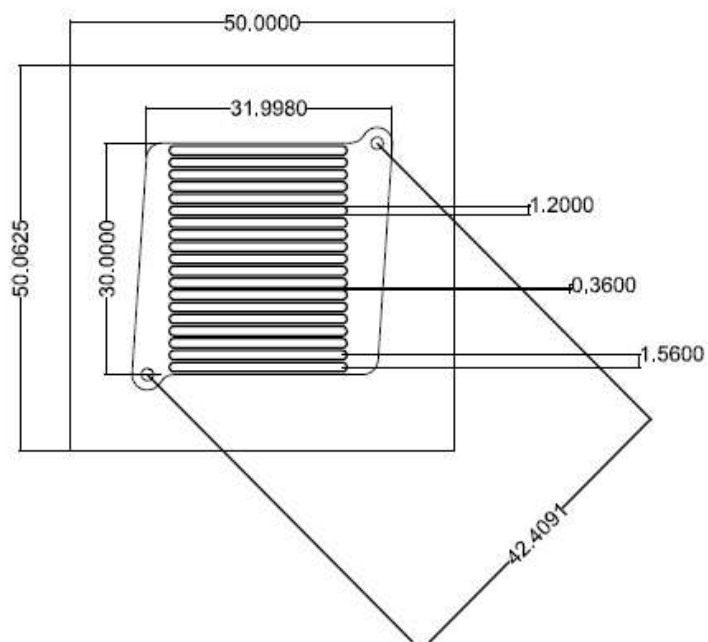
Fig. 3.4 Microchannel 20 X 0.36 *mm* . All dimensions in *mm*.
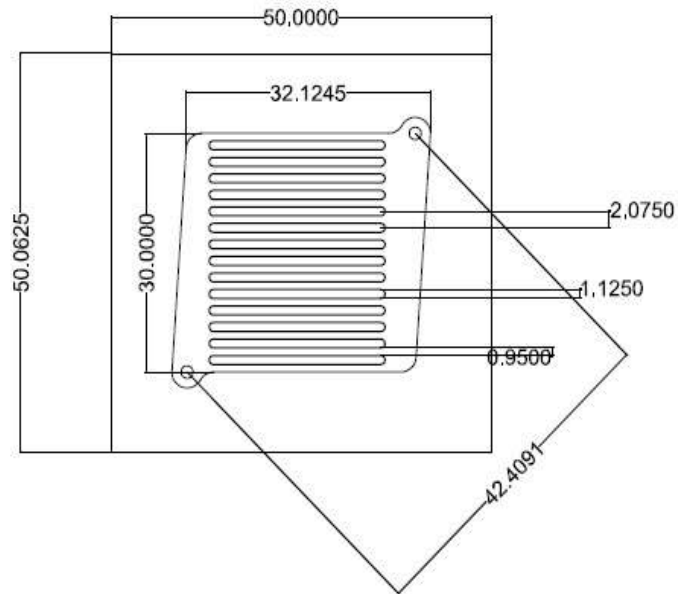
Fig. 3.5 Microchannel 15X0.9 *mm*. All dimensions in *mm*.
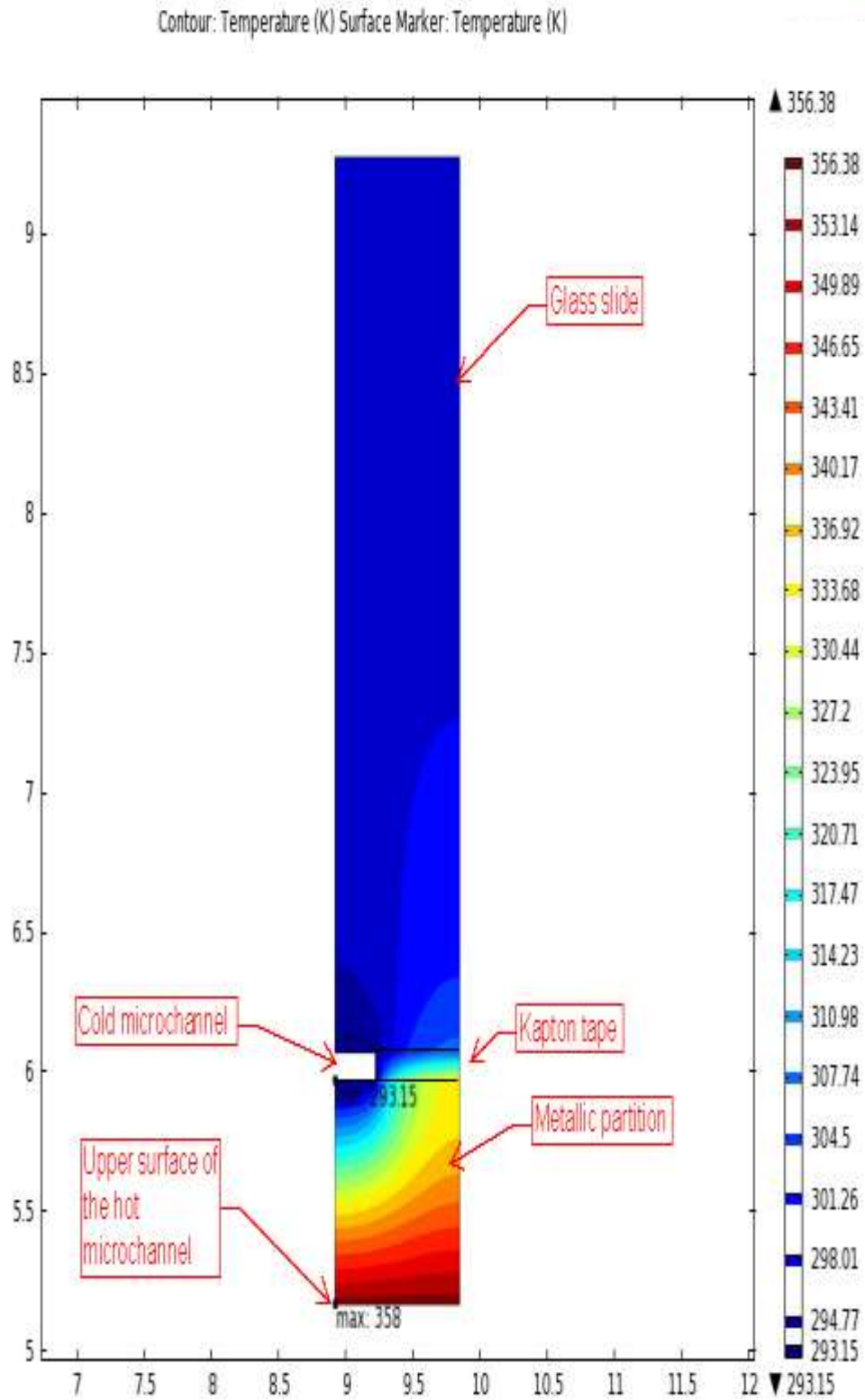
Fig. 3.6 2-D isothermal plot for a section of the microchannel heat exchanger
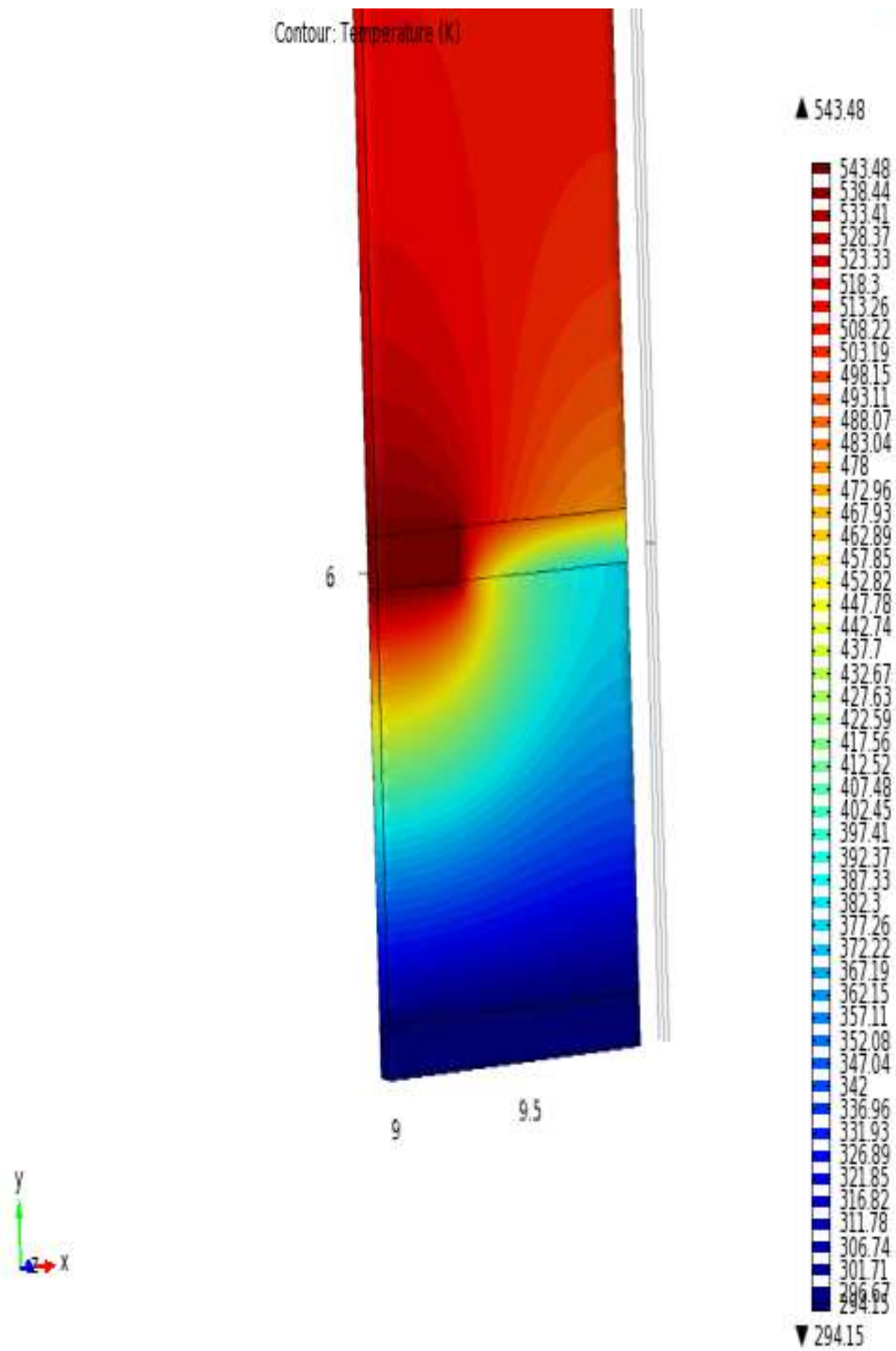
Fig. 3.7 Isothermal contours from the 3-D simulation of a microchannel heat exchanger

Fig. 3.8 Comparison of unpolished and polished brass partition pieces.

Nano-port

Glass slide

Kapton® tape

Metallic Partition

Kapton® tape

Glass slide
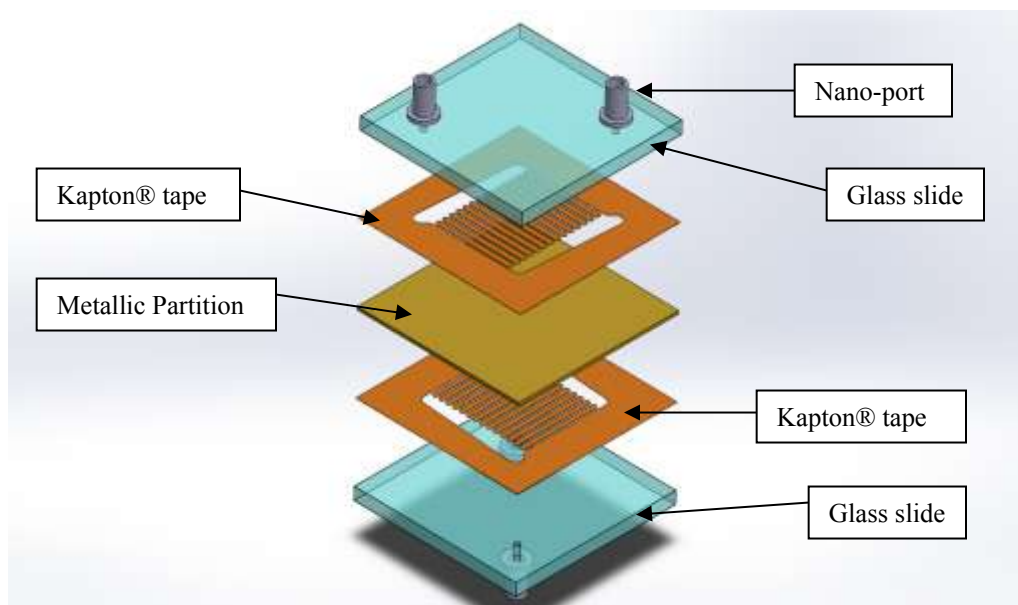
Fig 3.9 SolidWorks model of the crossflow heat exchanger fabricated by xurography before assembly
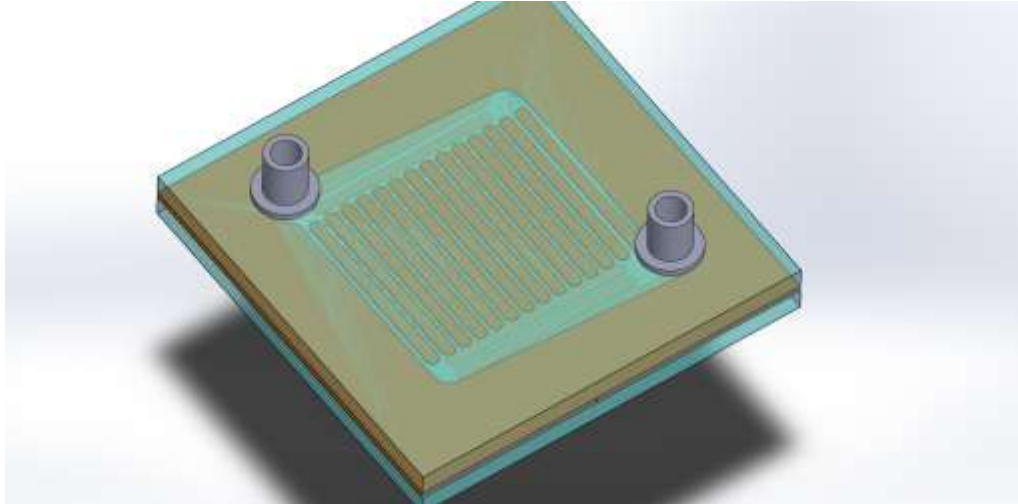
Fig. 3.10 SolidWorks model of assembled crossflow heat exchanger fabricated by xurography.
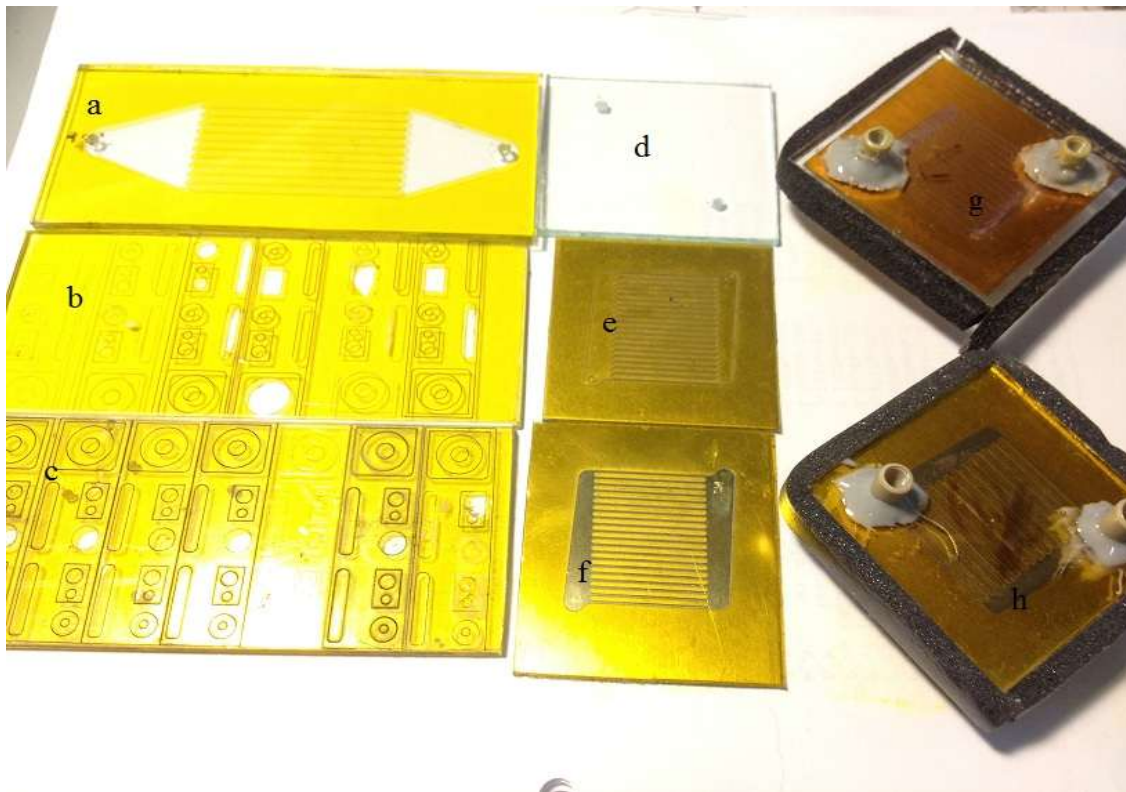

Fig. 3.11 Images of the crossflow heat exchangers at various stages of production. a) One of the first patterns created by laser cutting. b) Glass slides with cut patterns for different iterations of the cutting control settings. c) Glass slide with drilled vias. d) Metal partition with cut tape before peeling. e) Metal partition after peeling and removal of coating. f) Assembled device with copper partition. g) Assembled device with brass partition.

CHAPTER 4

EXPERIMENTAL APPARATUS, DATA ACQUISITION

AND DATA REDUCTION

4.1 Introduction

Experimental details are provided in this chapter. An existing flow loop was modified to accommodate an additional fluid so the crossflow heat exchanger could be tested. All experimental equipment and instrumentation are described. The test procedure is outlined and the data reduction process, including all correlations, is introduced.

4.2 Apparatus, Instrumentation, and Data Acquisition

The working fluid for the both the hot and cold sides of the heat exchanger is water. An open flow loop flow was used for both fluids. The flow loop schematic is shown in Fig. 4.1. A Parker piston-type accumulator (3.785 L, 101.6 mm bore) is used to drive the flow by charging the gas-side of the accumulator piston with a type K nitrogen tank. The nitrogen is supplied to the accumulator by a Tescom pressure regulator. The Tescom pressure regulator allows control of the nitrogen pressure supplied to the accumulator. A 6BHT series Teflon lined hose with a 9.5 mm (⅜ in) outer diameter connects the nitrogen tank to the accumulator. Two Swagelok T-valves are used on the accumulator, one on the inlet side (the gas side) to control the nitrogen inflow and to

switch to the vacuum pump, and another on the outlet side (the fluid side) to control the outflow of water. The valve on the gas side controls two processes: First, the accumulatorcan be charged with nitrogen to drive the water from the accumulator to the tested device; second, the gas side of the accumulator can be evacuated by a Gast vacuum pump to draw water into the accumulator. When the liquid side T-valve is opened to the water column and the gas side is evacuated, water flows into the accumulator. When the accumulator is charged with nitrogen and water, the gas pressure drives water out of the accumulator into the pipe network.

A Swagelok filter of 7 μm porosity serves to remove solid impurities from the water. A water heater, manufactured by PolyScience, is used as a heat source for the hot fluid. The heat supplied by the water heater to the system's distilled water is transferred to the working fluid via the water heater tube-in-tube heat exchanger.

Omega T-type shielded thermocouples measure the fluid temperature at the heat exchanger inlet and outlet. The thermocouple measurement uncertainty is $\pm 0.1°C$ following calibration. Setra 522 series pressure sensors, with an uncertainty of $\pm 0.15\%$ of full scale, measure pressure at the heat exchanger inlet and outlet for both fluids. The fluids are collected in separate containers at the end of each open flow loop. The accumulated fluid mass is measured in real time by Scientific SL600 mass balances. The data acquisition system internal clock records the time interval associated with the accumulated mass. The uncertainty of the mass balances is ± 0.01 g. The computer internal clock imposes a ± 0.01 s of uncertainty. The mass containers are plastic beakers (600 g maximum capacity) with plastic covers and TF-200 PTFE membrane filters to

minimize mass loss due to evaporation. A high level of evaporation is possible since the outlet temperature for both fluids exceeds $35°C$.

The time interval for the mass flow rate measurement was set to automatically change dependent on the response of the experiment equipment. Each instrument has a different response time. It was observed that the slowest response is for the mass balances, and this response differs depending on the flow rate. For low flow rates, the uncertainty is high. Thus, the time intervals recorded for low flow rates are higher than that for high flow rates. Additionally, the recorded data are refined further by the mass flow rate uncertainty in the data reduction code.

A National Instruments PX-1010 controlled the data acquisition process. The data acquisition system acquires, records, and displays data in real time for the time interval, pressure measurements, temperature measurements, and mass flow rates. A LabVIEW program is designed to calculate and display other derived parameters, such as the amount of heat transferred to/from each fluid, C_r, and Re.   The flow loop, including all major components, is shown in Fig. 4.2.

4.3 Experimental Procedure

As the maximum load capacity for the mass balance is 600 g, the experiment is not allowed to approach the maximum load. When the load of one of the plastic beakers approaches 550 g the experiment is stopped to empty the beakers. The experiment is controlled to run until steady state is reached. The indication for reaching steady state is when the displayed temperature of all thermocouples is constant and within the uncertainty value of the thermocouples. After reaching steady state, the data set is saved

so it may be analyzed in a later step using *Matlab*. If the accumulator is empty, the pressure is released and the vacuum pump is operated to refill the accumulator.

The experiment is started at the lowest possible pressure. The lowest recorded pressure is 48 *kPa* (7 *psig*). The maximum is 2.51 *MPa* (365 *psig*) for one device and approximately 1.38 *MPa* (200 *psig*) for the rest of the devices. The reason for not exceeding 1.38 *MPa* (200 *psig*) as the maximum applied pressure at the inlet is the inability of achieving turbulent flow. The maximum *Re* was approximately 1900 with a 2.51 *MPa* (365 *psig*) of inlet pressure. Pressure intervals are set at 34.5 *kPa* (5 *psig*) when the applied pressure is below 689 *kPa* (100 *psig*) and 103 *kPa* (15 *psig*) at higher inlet pressure. The collected data are in **.txt* format.

4.4 Data Reduction

The working fluid properties are calculated using thermodynamic and transport property functions developed for *MatLab* use by the University of Applied Science, Faculty of Mechanical Engineering, Department of Technical Thermodynamics, Germany [51]. The water property functions require temperature and pressure as inputs. These functions are used to calculate dynamic viscosity, density, heat capacity, entropy, enthalpy, and thermal conductivity for water. An average temperature, calculated from the inlet and outlet temperatures, is used to calculate dynamic viscosity, heat capacity, thermal conductivity, and density for both the cold and hot fluids. The individual temperatures for each inlet and outlet are used to calculate entropy and enthalpy for each fluid at those specific points.

The saved data sets are analyzed and converted to the desired output parameters using a *Matlab* code. The code is designed to calculate Reynolds number for both the hot

and cold sides (Re_h and Re_c), the average Reynolds number (Re_{avg}), and the mass flow rate for each fluid ($\dot{m}_h, \dot{m}_c$). The cold fluid heat capacity rate C_c, the hot fluid heat capacity rate C_h, and the capacity rate ratio C_r are obtained from other quantities using their definitions. The minimum and maximum heat capacity rates, C_{min} and C_{max}, respectively, are assigned according to the maximum and the minimum capacities for the cold and hot fluids. The heat rate from the hot fluid q_h, the heat rate to the cold fluid q_c, and the average heat rate q_{avg} are also calculated. The theoretical friction factor f and the theoretical Nusselt number Nu_{th} are determined along with the theoretical convective heat transfer coefficient h and the theoretical overall heat transfer coefficient U_{th}. For comparison purposes, the experimental overall heat transfer coefficient U_{exp}, the experimental and theoretical effectiveness (ε_{exp} and ε_{th}), and the experimental and theoretical number of transferred units (NTU_{exp} and NTU_{th}) are calculated. Additionally, the exergy efficiency based on two different expressions is calculated. Definitions and equations that describe all of the variables introduced in this paragraph are provided in the next section.

4.4.1 Correlations

Reynolds number is defined as the ratio of inertial and viscous forces,

$$Re = \frac{\rho V D_h}{\mu} \tag{4.1}$$

As noted, the dynamic viscosity, μ, and the density, ρ, of water are calculated using the thermodynamic and transport property functions referenced in the previous section. D_h is the microchannel hydraulic diameter for each individual channel and V is the mean velocity for a channel obtained from the mass flow rate, which is defined as

$$\dot{m} = \rho V A_c. \tag{4.2}$$

where A_c is the tube cross-sectional area. The hydraulic diameter for the rectangular microchannels is defined as

$$D_h = \frac{2ZW}{Z+W} \tag{4.3}$$

where Z is the channel depth and W is the channel width.

Re_{avg} is computed from the hot and cold fluid Reynolds numbers based on the flow in a single microchannel

$$Re_{avg} = \frac{Re_c + Re_h}{2} \tag{4.4}$$

The mass flow rate is calculated from the experimental data as follows:

$$\dot{m} = \frac{m_2 - m_1}{t_2 - t_1} \tag{4.5}$$

where m is the mass, t is time, and subscripts 1 and 2 refer to the start and end times for the mass measurement. The heat capacity rate is defined as

$$C = \dot{m} c_p \tag{4.6}$$

where c_p is the fluid specific heat at constant pressure. When the heat capacity rates are computed for both fluids, C_{min} and C_{max} are found using *Matlab* functions for the maximum and minimum values,

$$C_{min} = \min(C_c, C_h) \tag{4.7}$$

$$C_{max} = \max(C_c, C_h) \tag{4.8}$$

The heat capacity rate ratio C_r is defined as

$$C_r = \frac{C_{min}}{C_{max}} \tag{4.9}$$

The heat rate transferred to/from each fluid is determined from an application of the first law of thermodynamics,

$$q = \dot{m}c_p(T_{in} - T_{out})$$ (4.10)

where T_{in} and T_{out} are the inlet and outlet fluid temperatures. Assuming the heat exchanger is adiabatic, the heat rate to the cold fluid q_c should equal the heat rate from the hot fluid q_h. Unfortunately, perfect insulation is difficult to achieve. Thus, $q_c \neq q_h$ and an average heat rate q_{avg} for the heat transfer between the fluids is of interest.

$$q_{avg} = \frac{q_c + q_h}{2}$$ (4.11)

Nusselt number is defined as the ratio of convective to conductive heat transfer at a boundary (surface).

$$Nu = \frac{hD_h}{k}$$ (4.12)

where h is the heat transfer coefficient and k is the fluid thermal conductivity. For this work, both theoretical and experimental Nusselt numbers and overall heat transfer coefficients are calculated and compared. The theoretical Nusselt number Nu_{th} for flow that is fully developed both thermally and hydrodynamically is dependent only on the microchannel aspect ratio α. A correlation for Nu_{th} has been developed using published data [23].

$$Nu_{th} = 7.496 - 10.06\alpha^3 + 22.726\alpha^2 - 17.195\alpha$$ (4.13)

For fully developed laminar flow in rectangular ducts the friction factor f is dependent on Re and α. A correlation for rectangular channels has been developed for this relationship using published data [50].

$$fRe = -50.416\alpha^3 + 132.75\alpha^2 - 121.217\alpha + 95.705$$ (4.14)

The friction factor is not a primary focus in this study; it has been calculated for theoretical purposes only in the early design steps. After determining the theoretical Nusselt number, the theoretical value of h is calculated from Eq. (4.12) for both fluids.

These values are then be used to determine the theoretical overall heat transfer coefficient U_{th}.

$$U_{th} = \left[\frac{A_{sc}}{A_{sh}h_h} + \frac{1}{h_c}\right]^{-1} \tag{4.15}$$

where A_{sh} and A_{sc} are the heat transfer surface areas of the hot and cold channels, respectively, and h_h and h_c are the convective heat transfer coefficients for the hot and cold fluids, respectively. The heat transfer area is calculated as

$$A_s = 2(L + W) \tag{4.16}$$

where L is the channel length and W is the channel width.

The theoretical number of transferred units NTU_{th} is calculated based on its definition,

$$NTU_{th} = \frac{U_{th}A_{sc}}{C_{min}} \tag{4.17}$$

Using the definition of NTU, the experimental number of transferred units NTU_{exp} is calculated as follows

$$NTU_{exp} = \frac{U_{exp}A_{sc}}{C_{min}} \tag{4.18}$$

The Logarithmic Mean Temperature Difference (*LMTD*) is calculated from its definition and is used in an expression for heat rate between the two fluids to determine the experimental overall heat transfer coefficient U_{exp}.

$$LMTD = \frac{\Delta T_2 - \Delta T_1}{ln(\Delta T_2 / T_1)} \tag{4.19}$$

where ΔT_1 and ΔT_2 refer to the differences in hot and cold fluid temperatures at the two ends of the heat exchanger. The experimental overall heat transfer U_{exp} is calculated as follows after calculating the correction factor (*f*) using *EES*,

$$U_{exp} = \frac{q_{avg}}{LMTDA_{sc}F} \tag{4.20}$$

Here F is the correction factor that accounts for the differences between the crossflow heat exchanger and a concentric tube heat exchanger in counterflow operation (assumed in Eq. 4.19). The correction factor is calculated from a built-in function in *EES* [26].

The theoretical effectiveness ε_{th} is calculated from the analytical relationships developed for crossflow and counterflow heat exchangers [23]. The exact expression applied is dependent on the specific heat exchanger design (crossflow or counterflow) being analyzed.

Crossflow (single pass, both fluids unmixed):

$$\varepsilon_{th} = 1 - exp\left[\left(\frac{1}{C_r}\right) NTU^{0.22}\{exp[-C_r NTU^{0.78}] - 1\}\right] \tag{4.21}$$

Counterflow:

$$\varepsilon_{th} = \frac{1 - exp[-NTU(1 - C_r)]}{1 - C_r exp[-NTU(1 - C_r)]} \tag{4.22}$$

The definition of heat exchanger effectiveness is used to determine the experimental effectiveness.

$$\varepsilon_{exp} = \frac{q_{avg}}{q_{max}} \tag{4.23}$$

where q_{max} is defined as

$$q_{max} = C_{min}(T_{h,i} - T_{c,i}) \tag{4.24}$$

and $T_{h,i}$ and $T_{c,i}$ are the hot and cold fluid inlet temperatures, respectively.

Exergy efficiency $\eta_{II,oi}$, or second-law efficiency, provides a means to assess heat exchanger performance that includes exergy destruction due to frictional effects and exergy transfer between the hot and cold fluids. Exergy efficiency for a heat exchanger is typically defined in one of two ways, both of which find use in the general literature.

One form ($\eta_{II,ch}$) is the ratio of exergy recovered (increase of cold fluid exergy) to the exergy expended (decrease in hot fluid exergy) [52],

$$\eta_{II,ch} = \frac{\dot{X}_{c,o} - \dot{X}_{c,i}}{\dot{X}_{h,i} - \dot{X}_{h,o}} \tag{4.25}$$

where $\dot{X}$ is the rate of exergy transfer associated with the mass flow entering (i) or leaving (o) the heat exchanger, defined as

$$\dot{X} = \dot{m}[(h - h_0) - T_0(s - s_0)] \tag{4.26}$$

In this context, h is enthalpy and s is entropy for the state of interest, T_0 is the reference temperature, h_0 and s_0 are the enthalpy and entropy at the reference state, and changes in the kinetic and potential energy forms of exergy are assumed to be negligible. Enthalpy and entropy values are calculated using the previously described water property functions. The second form of exergy efficiency ($\eta_{II,oi}$) is the ratio of exergy leaving the heat exchanger to the exergy entering the heat exchanger [52],

$$\eta_{II,oi} = \frac{\dot{X}_{c,o} + \dot{X}_{h,o}}{\dot{X}_{c,i} + \dot{X}_{h,i}} \tag{4.27}$$

Both forms of exergy efficiency are presented in Chapter 5. Chapter 5 also presents the Posttest uncertainty analysis, experimental observations, experimental data, discussion of the results, and a summary of the experimental work.
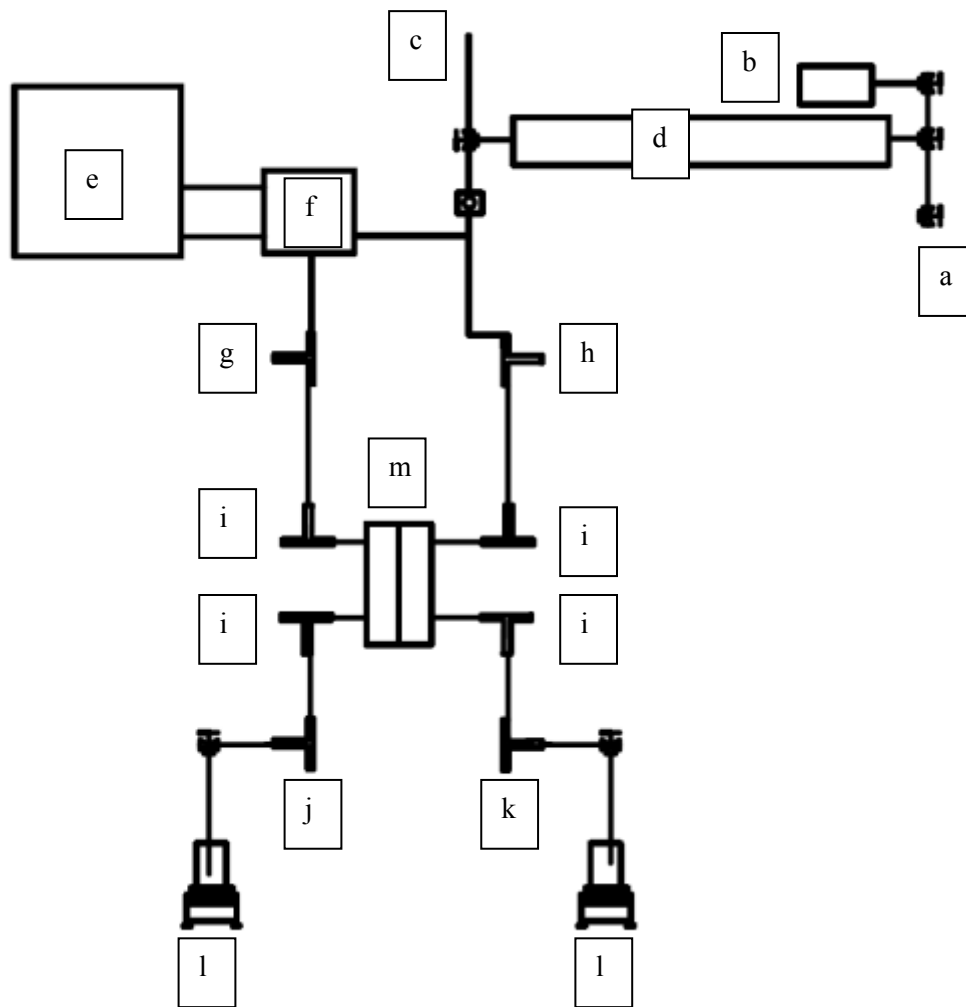
Fig. 4.1 Schematic of the experimental flow loop. a) Driving pressure inlet. b) Vaccum pump. c) Refil water tank. d) Accumulator. e) Water heating unit. f) Tube-in-tube heat exchanger. g) Hotside inlet water pressure sensor. h) Coldside inlet water pressure sensor. i) T-type thermocouples. j) Hotside outlet pressure sensor. k) Codleside outlet pressure sensor. l) Mass balance. m) Undertest device.
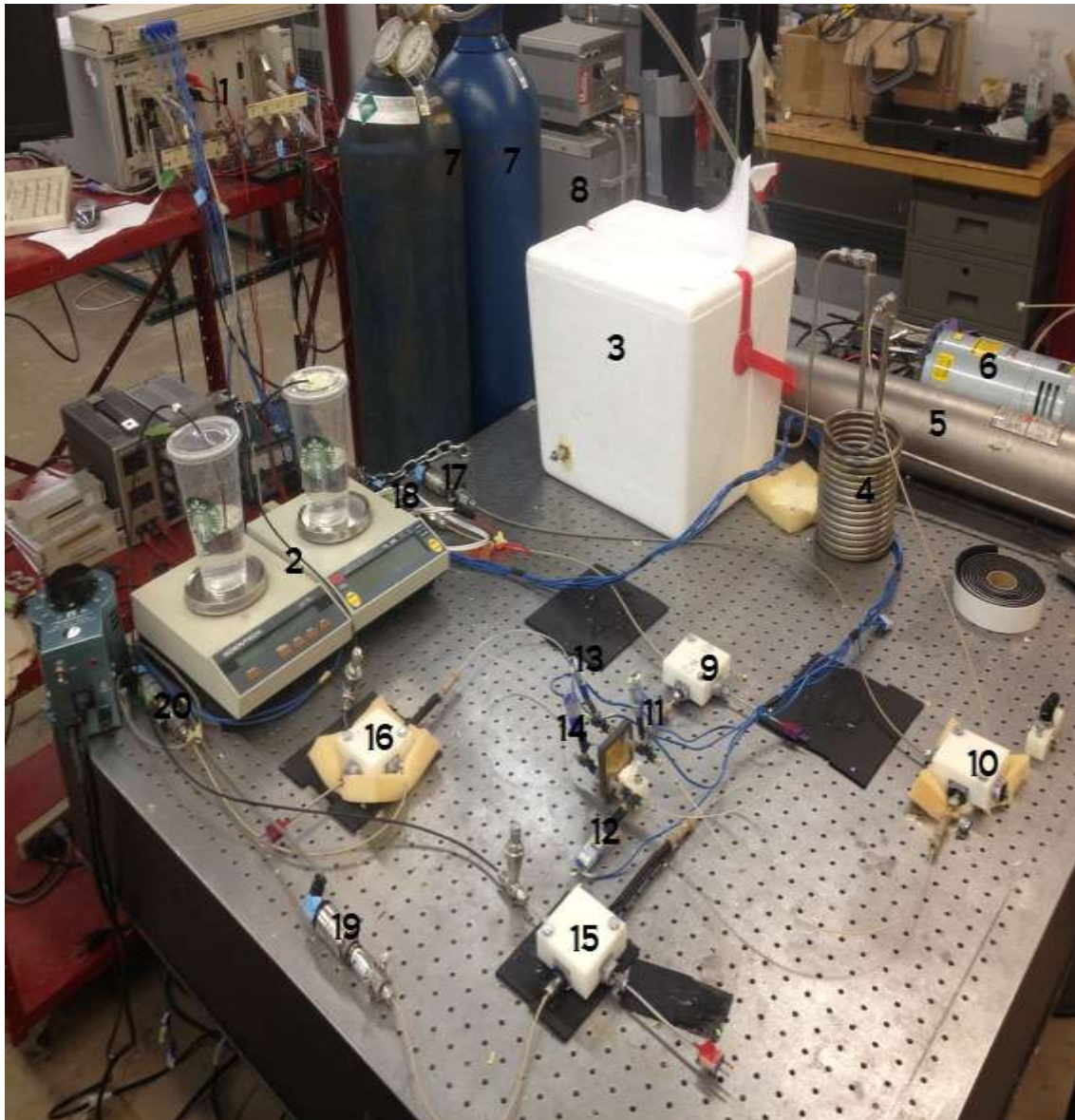
Fig. 4.2 The experimental flow loop with all major components identified. 1) Data acquisition system. 2) Mass balances. 3) Heat exchanger to heat the hot fluid. 4) Cold side working fluid coil. 5) Accumulator. 6) Vacuum pump. 7) Nitrogen tank. 8) Water heater. 9) Hot fluid inlet union. 10) Cold fluid inlet union. 11) Cold fluid inlet thermocouple. 12) Cold fluid outlet thermocouple. 13) Hot fluid inlet thermocouple. 14) Hot fluid outlet thermocouple. 15) Cold fluid outlet union. 16) Hot fluid outlet union. 17) Cold fluid inlet pressure sensor. 18) Hot fluid inlet pressure sensor. 19) Cold fluid outlet pressure sensor. 20) Hot fluid outlet pressure sensor.

CHAPTER 5

RESULTS AND DISCUSSION

Five separate microchannel heat exchangers were fabricated and tested. Four of the devices were constructed and operated in a crossflow configuration and the other device was constructed for counterflow operation. The number of channels was the same in both layers of a single device, but the number of channels varied between devices. The overall platform for each layer was the same for all devices, namely 5.08 mm X 5.08 mm (2 in X 2 in). Given the fixed overall platform, but with variation in channel width and wall thickness, the number of channels was different for each device.

The microchannel heat exchangers were tested for a variety of conditions with the objective of obtaining the widest operating range in terms of *NTU*, C_r, and ε. Comparisons were made between the experimental and theoretical forms of these three key performance parameters. The working fluid in all cases was de-ionized water.

5.1 Characterization

As mentioned above, five devices were constructed and tested. Four have a crossflow configuration, consistent with the type of heat exchanger emphasized in thiswork. The fifth device was constructed for counterflow operation. The nominal device in this study is the crossflow heat exchanger with 600 *μm* channel width with a brass partition. Three of the crossflow devices are manufactured with a brass partition,

but with different channel widths. The fourth device has the same channel dimension as the nominal device (600 *μm*) but is assembled using a copper partition. The fifth devicealso has channels of 600 *μm* width, but with a counterflow channel configuration and brass partition. All devices have an identical manifold design and total surface area (device platform). Because of the identical total surface area shared by all the devices, the difference between the nominal device and the 950 *μm* channel width device is the microchannel separation wall thickness. In the 950 *μm* device, the channel walls are narrower than those of the nominal device, while the number of channels is the same. For the 360 *μm* and 600 *μm* devices the number of channels is 20 and 15, respectively, while the separation wall thickness is 1.125 *mm* and 1.2 *mm*, respectively. Channel height is determined by the Kapton® tape thickness, which in nominally 100 *μm*. Kolekar [9] measured the Kapton® tape thickness with and without a clamping system and found that it ranges between 92 and 106 *μm*. A nominal tape thickness of 100 *μm* was assumed for the microchannel height in this study. This study emphasizes a proof of concept for xurographic heat exchangers rather than an experiment designed to extract experimental data such as friction factor and heat transfer coefficient. Thus, precise measurements of channel dimensions are not required. Tables 5.1 and 5.2 provide dimensions and other physical characteristics for the fabricated heat exchangers.

5.2 Observations

In the course of running the experiments, several observations related to system performance were made. For instance, it was observed that the hot fluid inlet temperature is proportional to the total mass flow rate (i.e., the mass flow rate leaving the accumulator). The total mass flow rate increases by increasing the pressure applied to the

gas side of the accumulator. The single flow stream leaving the accumulator is split into two streams, one that is heated and delivered to the hot side of the heat exchanger and the other that is cooled and delivered to the cold side. Thus, the two flow rates are coupled. This flow loop design feature makes it difficult to maintain a constant hot fluid inlet temperature as the overall mass flow rate changes. The water heater and tube-in-tube heat exchanger system used to heat the hot fluid has limited control. Therefore, the fine adjustments to the hot water heater that are necessary to maintain a constant hot water supply temperature to the heat exchanger as mass flow rate is adjusted is not possible. This lack of temperature control impacts both the hot and cold fluid outlet temperatures as well.

It was also discovered that temperature measurements of the fluid inlet and outlet temperatures are adversely affected as the distance between the heat exchanger fluid ports and the thermocouple locations increases. This inaccuracy, first observed when a first law of thermodynamics analysis was conducted on the heat exchanger, results from the axial conduction in the tube fittings at the heat exchanger ports and heat loss from the connecting tubes to the surroundings. The large surface-to-volume ratio of the tubing used to deliver the working fluid from the union to the Nano-port increases the effect of heat loss from the tubing. To mitigate this effect, the thermocouples were moved to locations as close to the heat exchanger ports as was physically possible. The maximum operating pressure and temperature were 2,516.6 *kPa* (365 *psig*) and 75 *°C*, respectively. The devices operated well under high pressure, although some leakage occurred, but not directly as a result of the high pressure. Leakage was typically a result of incomplete bonding between the Nano-ports and the glass substrates. The poor adhesion was likely

due to chemical changes to the adhesive caused by exposure to above room temperatures during shipping. Device fabrication was found to be straightforward after the proper fabrication procedure was determined (through some trial-and-error). Fabrication of stacked (multi-layer) microscale heat exchangers by xurography was found to be possible. The metallic partition material did not affect the bonding process; however, smooth surfaces were found to produce better adhesion. The laser cutting process produced burned or melted edges regardless of the laser setting combination. This unfortunate outcome made channel width measurement problematic and left residual material in the channels in some cases.

5.3 Posttest Uncertainty

The Posttest uncertainty analysis follows the same procedure as the Pretest uncertainty analysis. The only difference is that the measurement uncertainties include repeatability errors in addition to precision errors. The results of the uncertainty analysis in the form of relative experimental uncertainties (percentage) for typical values of the most significant parameters are presented in table 5.3. most significant parameters are presented in Table 5.3.

5.4 Heat Exchanger Performance

The crossflow and counterflow heat exchangers were tested and the raw data were converted to performance parameters. Heat exchangers are often evaluated by their effectiveness, which is a function of *NTU* and the capacity rate ratio. Depending on the heat exchanger objective, inter-fluid heat transfer rate or the outlet fluid temperatures may be of interest to a designer. All of these performance parameters are presented in the

next sections, typically as functions of fluid mass flow rate or Reynolds number. Other parameters that further elucidate heat exchanger function are overall heat transfer coefficient and exergy efficiency.

5.4.1 Typical Performance Parameters

A traditional $\varepsilon(NTU, C_r)$ plot is presented in fig. 5.1 for the nominal device (15 X 600 μm channels, crossflow operation). Solid lines represent the theoretical effectiveness calculated from eq. 4.21 for different values of C_r. Symbols present the experimental data. Note that what appears to be a single symbol (for instance at $NTU \sim 0.56$) is actually a set of data that have nearly the same values. While it is difficult to ascertain from this data set, the experimental data agree well with theory (fig. 5.2 clarifies the agreement). Similarly, data trends agree within experimental uncertainty with theory. The average variance in ε_{exp}, with respect to theoretical values at the same C_r and NTU, is 7.28%. Even with the coupled cold and hot fluid flows, which prevents control of individual flow streams, a wide range of C_r was obtained (0.2 – 0.9). Similarly, a reasonable range was achieved for NTU (0.5 – 3.7) and ε_{exp} (0.37 – 0.93). Note that the maximum effectiveness correlates with the minimum capacity rate ratio, which was obtained with the lowest total mass flow rate. For this flow loop, increasing the mass flow rate decreases C_r, while ε_{exp} and NTU increase.

An expanded view of the data in fig. 5.1 is shown in fig. 5.2 for $C_r = 0.92$. These data more clearly demonstrate that the experimental data agree with the theoretical expression (eq. 4.21) within the experimental uncertainty. Of the 21 data at $C_r \cong 0.92$, nearly 80% agree with theory. Note that the $\varepsilon_{exp}(NTU)$ curve appears nearly linear over

this small *NTU* range. This data set also demonstrates that multiple data are actually represented by an apparent single symbol in fig. 5.1, as noted above. The narrow range of *NTU* for this value of C_r stems from the limited mass flow rate control in the flow loop. While it is desirable to have mass flow rate control over both fluids over a wide range, the single accumulator that supplies the batch flow prevents that type of operation. Similar data are presented in fig. 5.3 for the counterflow heat exchanger that incorporates 15 X 600 *μm* channels on both layers. A portion of this data set is presented in fig. 5.3 for $C_r \cong 0.85$. For fig. 5.3, the solid lines calculated from eq. 4.22 represent the theoretical relationship. Note that the parameter range is much smaller for this heat exchanger than for the nominal device operating in crossflow, even though both devices have the same number and size of channels.

These differences are likely due to minor disparities in the two heat exchangers and in the flow loop connections to the devices. In addition, the system lacked individual flow control for the two fluids, since a single pressure source and flow control valve was used. When coupled, these differences prevented equivalent parameter space to be explored for the two heat exchangers. Even though the parameter space is limited, experimental data agree reasonably well with theory. As shown in fig. 5.3, the majority of the data at $C_r = 0.85$ agree with theory within the ε_{exp} uncertainty. Note that uncertainty appears to be much better for this data set than in fig. 5.2; however, it should be noted that the ε_{exp} range is much larger in fig. 5.3 than in fig. 5.2.

All of the crossflow heat exchangers show the same trends for $\varepsilon_{exp}(NTU, C_r)$ as the nominal device, as shown in fig. 5.4. Agreement with theory is again good for all crossflow heat exchangers. The range of data, however, is not the same for all devices.

The nominal heat exchanger has the largest range on all three performance parameters. The heat exchanger with the smallest channels has the smallest range for the parameters of interest. Since pressure drop increases significantly with a reduction in channel size for an equivalent flow rate, the total mass flow rate was limited in the device with the smallest channels. This resulted in the limited range of effectiveness and *NTU* for that device.

Fig. 5.5 presents comparisons of $\varepsilon(C_r, NTU)$ experimental data with theory for all four cross flow heat exchangers. Experimental data are color coordinated with the solid lines, which represent theoretical predictions at C_r values selected based on mean values for appropriate groups of experimental data. Symbol size for the experimental data is based on effectiveness uncertainty. Thus, symbols that overlap theoretical lines of the same color indicate experimental data that agree with theory. All four crossflow heat exchangers exhibit performance in which $\varepsilon(C_r, NTU)$ agrees in most cases with the theoretical predictions. The most significant deviation from theory occurs for NTU > 2.5. It may be concluded from these data, that performance predictions for multilayer cross flow heat exchangers made by xurography may be made using the theoretical relationships for the general class of crossflow heat exchangers.

5.4.2 Other Parameters of Interest

The following figures show that there was not much difference between the minimum and maximum heat capacities and between the hot and cold mass flow rates, owing to the limited flow control discussed earlier. Fig. 5.6 presents C_{max} and C_{min} data for all heat exchangers. A reasonable range was obtained for each heat capacity. However, for most of the heat exchangers, these data produce a capacity rate ratio that is

in the range of 0.85 to 1.0. The smallest C_r is obtained for the 15 X 0.60 μm crossflow heat exchanger at the lowest flow rates. Even though it appears C_{min} and C_{max} are nearly equivalent at the lowest flow rates, C_r achieves its smallest value of 0.2 in this range.

Similar trends are observed when comparing the mass flow rates for the cold and hot fluids for all heat exchangers (fig. 5.7). These data highlight the way in which the flow splits into the two flow streams upon exiting the single accumulator. Given the flow loop design and valves, individual control of the two fluids was limited. As a result, the mass flow rates were close in value for almost all experiments. As noted above for the comparison of the minimum and maximum heat capacities, the greatest deviation from the equal mass flow rate scenario occurred at the lowest total mass flow rate.

Figs. 5.8 to 5.11 present the hot fluid mass flow rate, the minimum and the maximum heat capacities, and the average inter-fluid heat rate with respect to the hot fluid Reynolds number Re_h, respectively. The trends for the hot fluid mass flow rate (fig. 5.8) are as expected for the crossflow heat exchangers. The linear increase of $\dot{m}_h$ with Re_h is due to the fact that Re_h is proportional to $\dot{m}_h$. Similarly, Re_h is inversely proportional to D_h, so the increase in $\dot{m}_h$ with the decrease in D_h at fixed Re_h is expected. $\dot{m}_h$ data for both 600 μm channel crossflow heat exchangers are nearly equivalent, with the exception of the high Re_h data for the copper partition device. The differences between the $\dot{m}_h$ data for the crossflow and counterflow devices with equivalent channel sizes has been discussed previously.

Figs. 5.9 and 5.10 present data for the minimum and maximum heat capacities, respectively, as functions of the hot fluid Reynolds number. These trends follow that for $\dot{m}_h(Re_h)$, which is expected since C is proportional to $\dot{m}_h$.

The average heat transfer rate between the two fluids is presented in fig. 5.11 as a function of the hot fluid Reynolds number. Recall that the two mass flow rates are coupled, due to the flow loop design, which controls the mass flow rates with a single valve. Thus, changes in $\dot{m}_h$ are tracked by similar changes in $\dot{m}_c$. For both fluids, an increase in mass flow rate (which accompanies an increase in Re_h) results in an expected nearly linear increase in q, since q is directly proportional to mass flow rate (see eq. 4.10). The trend of $q(Re_h)$ for the copper partition crossflow heat exchanger appears to be closer to $Re_h^{1/2}$ rather than the linear response. While the $Re_h^{1/2}$ trend is expected for laminar external flow, there is no rationale for the trend observed for this internal flow case. Most likely, the lack of flow control that results in low C_r at low flow rates caused the nonlinear behavior for this heat exchanger at low Re_h. The effect of channel size at fixed Re_h is not as clear as in figs. 5.8 – 5.10. For laminar fully developed flow in a channel, Nu is constant. Thus, as D_h decreases, h is expected to increase. These effects in both channels should reduce the thermal resistance between the two fluids and q should increase. This effect appears to occur for the smaller two channel sizes when $Re_h > 1000$. However, with the exception of the 950 μm channel crossflow heat exchanger, there is little difference between the q_{avg} data for different channel widths for $Re_h < 1000$.

The hot fluid Reynolds number effects on fluid temperatures are displayed in figs. 5.12 – 5.14. The hot fluid inlet temperature (fig. 5.12) initially increases rapidly with Re_h. However, for $Re_h > 600$, $T_{h,i}$ reaches a nearly constant value. This effect has been discussed previously and is in part due to the insufficient temperature control of the hot water heater that was used to control the hot water inlet temperature. The $T_{h,o}$ response (fig. 5.13) follows that of $T_{h,i}$ as expected, except $T_{h,o}$ continues to increase for $Re_h > 600$,

although the increase slows for $Re_h > 1200$. This trend with Re_h is due to the nearly linear increase of q_{avg} with Re_h (fig. 5.11), which leads directly to an increase in $T_{h,o}$ with Re_h. If hot fluid temperature change is the desired objective, the best performer was the 600 μm counterflow heat exchanger and the worst (lowest ΔT) was the 600 μm crossflow heat exchanger with copper partition.

The cold fluid was not heated or cooled before introducing it to the heat exchanger. Thus, the cold fluid inlet temperature was nearly the same for each trial and is not presented here. The effect of Re_h, which follows that of Re_c, on $T_{c,o}$ is shown in Fig. 5.14. $T_{c,o}$ increases nearly linearly up to Re_h of approximately 1000 – 1200. For larger values of Re_h, $T_{c,o}$ is nearly constant, similar to the $T_{h,o}$ trend. If the heat exchanger objective is to heat the cold fluid, the best performers are the two 600 μm crossflow devices while the counterflow device achieves the lowest temperature rise.

The effect of Re_h on the experimental NTU is shown in Fig. 5.15. Using the definition of NTU (eq. 4.17), it is clear from the $NTU_{exp}(Re_h)$ trend in Fig. 5.15 that C_{min} is the dominant term. As Re_h increases, the two mass flow rates increase (see fig. 5.8), which leads to an increase in C_{min} (see fig. 5.8). Concurrently, U_{exp} is expected to be nearly constant for laminar fully developed flow; thus NTU_{exp} decreases with Re_h.

Experimental effectiveness also decreases with an increase in Re_h, as shown in fig. 5.16. Given the coupling between NTU_{exp} and ε_{exp}, as demonstrated in figs. 5.1 – 5.4, the response of ε_{exp} with Re_h is expected, as it follows that shown in Fig. 5.15 for NTU_{exp}.

The effect of Re_h on U_{exp}, calculated from eq. 4.20, for the five heat exchangers, is shown in Fig. 5.17. The q_{avg} response to Re_h is also exhibited here. The greater slope of the $q_{avg}(Re_h)$ curves at low Re_h are also observed in fig. 5.17 for U_{exp}. For $Re_h > 300$, the

trend for U_{exp} is nearly linear for all heat exchangers, as it is for q_{avg}. Thus, it could be concluded that the U_{exp} response is directly correlated with that for q_{avg}. The effect of channel size, and thus heat transfer surface area, is more difficult to explain. The largest values of U_{exp} are for the smallest channels, which, given the manner in which U_{exp} was calculated (eq. 4.20), is understandable given that q_{avg} for the 360 μm channel heat exchanger is nearly the same as that for the other devices. Also note that q_{avg} is greatest for the 950 μm channel device; however, U_{exp} for that device is about the same as the other devices owing to the effect of the heat transfer surface area.

5.4.3 Exergy Efficiency

The exergy efficiency for all five heat exchangers is presented using two expressions. Equation 4.25 gives the expression for $\eta_{II,ch}$, which is the ratio of the exergy recovered (cold fluid exergy increase) to the exergy expended (hot fluid exergy decrease). Equation 4.27 gives the second definition for exergy efficiency $\eta_{II,oi}$, which is the ratio of exergy leaving the heat exchanger to the exergy entering the heat exchanger. The effect of Re_h on $\eta_{II,ch}$ is shown in fig. 5.18. Similarly, the effect of Re_h on $\eta_{II,oi}$ is shown in fig. 5.19. Note that the trends for both forms of exergy efficiency with Re_h are approximately the same. At very low Re_h, the exergy transfer that accompanies the heat transfer overcomes the exergy destruction associated with frictional losses. However, at approximately $Re_h = 150$, the frictional effects begin to dominate causing an increase in exergy destruction with Re_h that exceeds the increase in exergy transfer associated with the increase in q_{avg} between the fluids. Thus, the exergy efficiency continually decreases with Re_h. This trend suggests that these heat exchangers should be operated at low flow rates and Reynolds numbers if one is interested in the maximum second law efficiency.

Of note is that the counterflow heat exchanger outperforms all the crossflow heat exchangers in terms of exergy efficiency. Also note that the effects of the different heat exchanger designs on exergy efficiency is the same for both definitions.

5.3 Summary

Five microchannel heat exchangers have been fabricated using the xurographic technology that utilizes a laser cutting process. The microchannels were characterized and the devices were tested to ascertain their thermal performance. It was determined that better performance was delivered by the crossflow configuration, which was the primary type of device studied. For comparison purposes, a counterflow heat exchanger was also tested. Experimental data in the form of ε, NTU, and C_r were generated; however, the range of these parameters was severely limited when compared to typical theoretical performance presentations. These restrictions were a result of the flow loop design, which coupled the mass flow rates of the two flow streams. Good agreement was found with theory for the xurographic heat exchangers. The data indicate that the two mass flow rates and heat capacities were nearly equivalent for all conditions, due to the flow control issue. As expected, the mass flow rates, and minimum and maximum capacities were found to vary linearly with the hot fluid Reynolds number. While the average inter-fluid heat transfer rate increases with Re_h, the effect of channel size was not clearly defined. Outlet fluid temperatures were found to increase with Re_h following the trend of q_{avg}. NTU was found to decrease nearly exponentially with Re_h due to the influence of C_{min}. The trend with Re_h for effectiveness is similar to that for NTU. As a result, the best performance in terms of effectiveness is found to occur at low Re_h. It was also found that devices with a copper partition performed better than the device built with

a brass partition for the same flow configuration. This performance difference is due to the disparity in thermal conductivity for the two materials (k for copper is about 2.5 times that for brass).

Considering exergy efficiency, the counterflow heat exchanger outperformed all the crossflow heat exchangers. It was determined that all the heat exchangers performed best in the range $50 < Re_h < 150$. At higher Re_h, frictional losses increase the exergy destruction, which overwhelms the increase in exergy transfer with the heat transfer. Thus exergy efficiency decreases with Re_h for Re_h greater than approximately 150.

Table 5.1 Heat exchanger dimensions. Channel height is 100 μm for each device. Other devices with equivalent channel widths have the same dimensions as those presented here.

Device Designation	Number of channels	Separation wall thickness (*mm*)	Channel width (*μm*)	Total wet area (*mm*)	Channel length (*mm*)
15 X 600	15	1.5	600	211.5	23.5
15 X 950	15	1.125	950	334.875	23.5
20 X 360	20	1.2	360	169.2	23.5

Table 5.2 Device dimensions, materials, and configuration.

#	Channel width (*μm*)	Metallic partition	Number of channels	Configuration	Correction factor F	D_h (*mm*)
1	600	Brass	15	Crossflow	0.9201	0.171
2	360	Brass	20	Crossflow	0.9022	0.157
3	950	Brass	15	Crossflow	0.9044	0.181
4	600	Copper	15	Crossflow	0.9406	0.171
5	600	Brass	15	Counterflow	1.0000	0.171

Table 5.3 Typical values of Posttest relative uncertainties (%) for the most significant parameters. B refers to brass partition, C refers to copper partition.

Variable [units]	15 X 600 μm, B-Cross	15 X 950 μm, B-Cross	20 X 360 μm, B-Cross	15 X 600 μm, C-Cross	15 X 600 μm, B-Counter
$\dot{m}_h$ [kg/s]	1.758	0.806	0.675	1.955	0.709
$\dot{m}_c$ [kg/s]	2.119	0.880	0.828	2.296	0.847
Re_h	4.244	3.256	6.198	4.687	3.840
Re_c	4.619	3.470	5.856	4.884	4.093
q_h [kW]	12.376	8.759	11.570	12.211	11.300
q_c [kW]	9.517	9.270	10.831	11.519	12.369
q_{avg} [kW]	7.943	6.356	7.961	8.561	8.314
C_{max} [kW/K]	1.379	0.788	0.714	2.154	0.713
C_{min} [kW/K]	2.010	0.848	0.847	2.521	0.847
U_{exp} [kW/m^{2}K]	19.558	12.253	13.126	18.761	10.938
NTU_{exp}	1.758	0.806	0.675	1.955	0.709
ε_{exp}	2.119	0.880	0.828	2.296	0.847
$\eta_{II,oi}$	4.244	3.256	6.198	4.687	3.840
$\eta_{II,ch}$	4.619	3.470	5.856	4.884	4.093
C_r	12.376	8.759	11.570	12.211	11.300
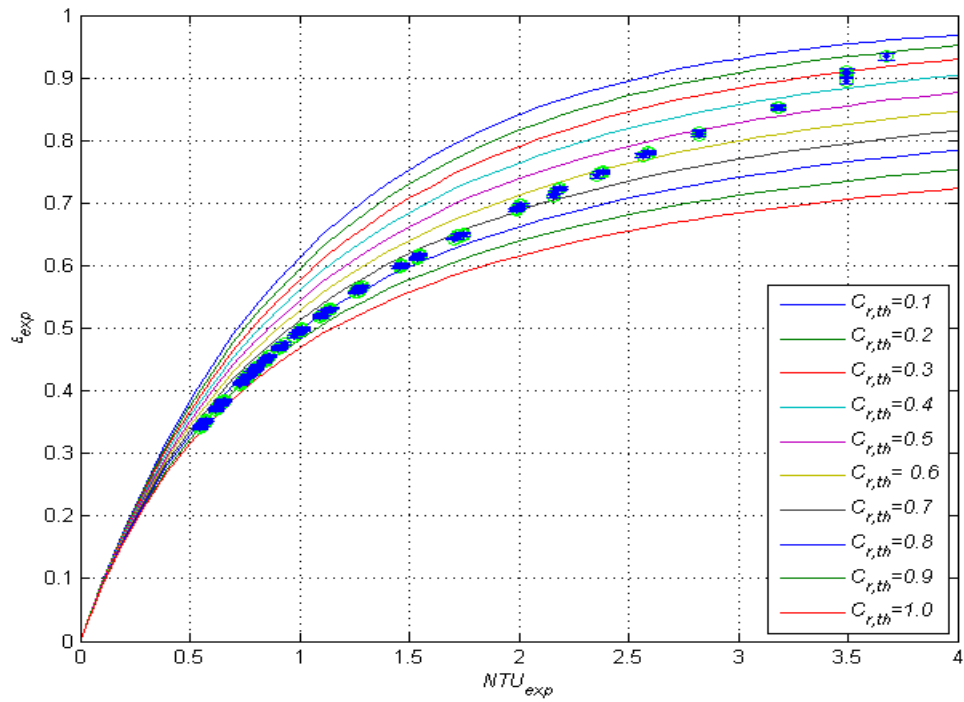
Fig. 5.1 Effectiveness as a function of *NTU* and C_r for the nominal device, which contains 15 X 600 *μm* channels in each layer, with crossflow operation.
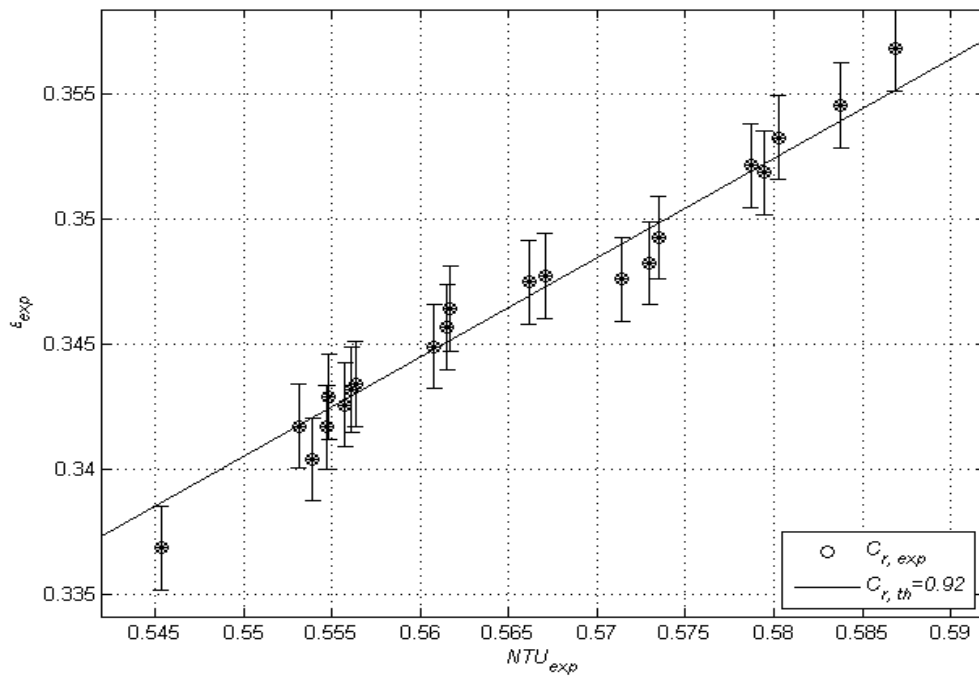
Fig. 5.2 Effectiveness validation for the nominal device (15 X 600 *μm* channels, crossflow operation)
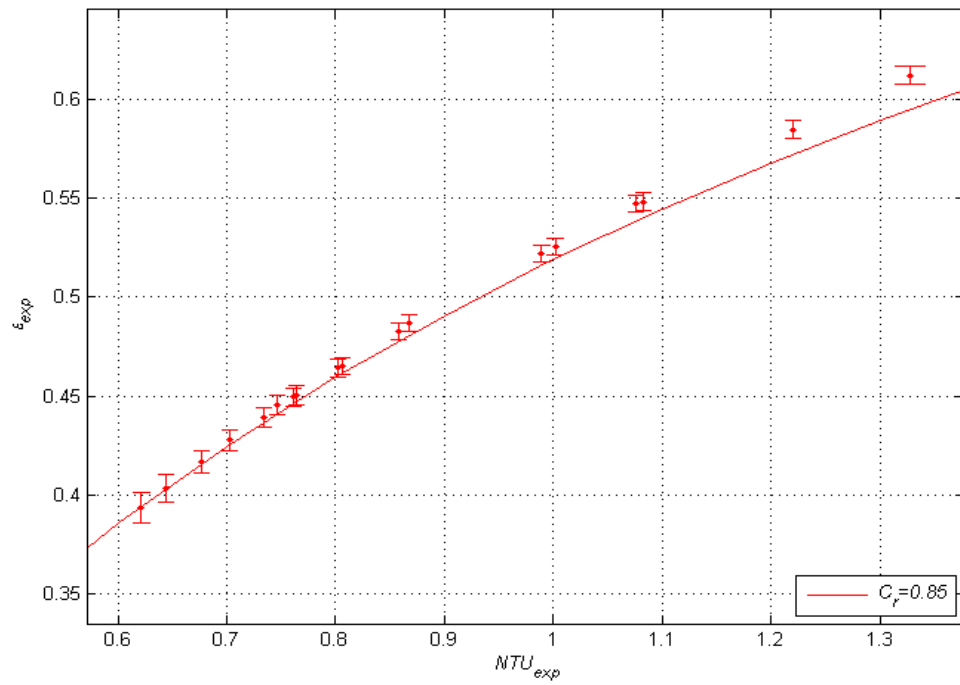
Fig. 5.3 Expanded view of the data at $C_r \cong 0.85$ for the counterflow heat exchanger.
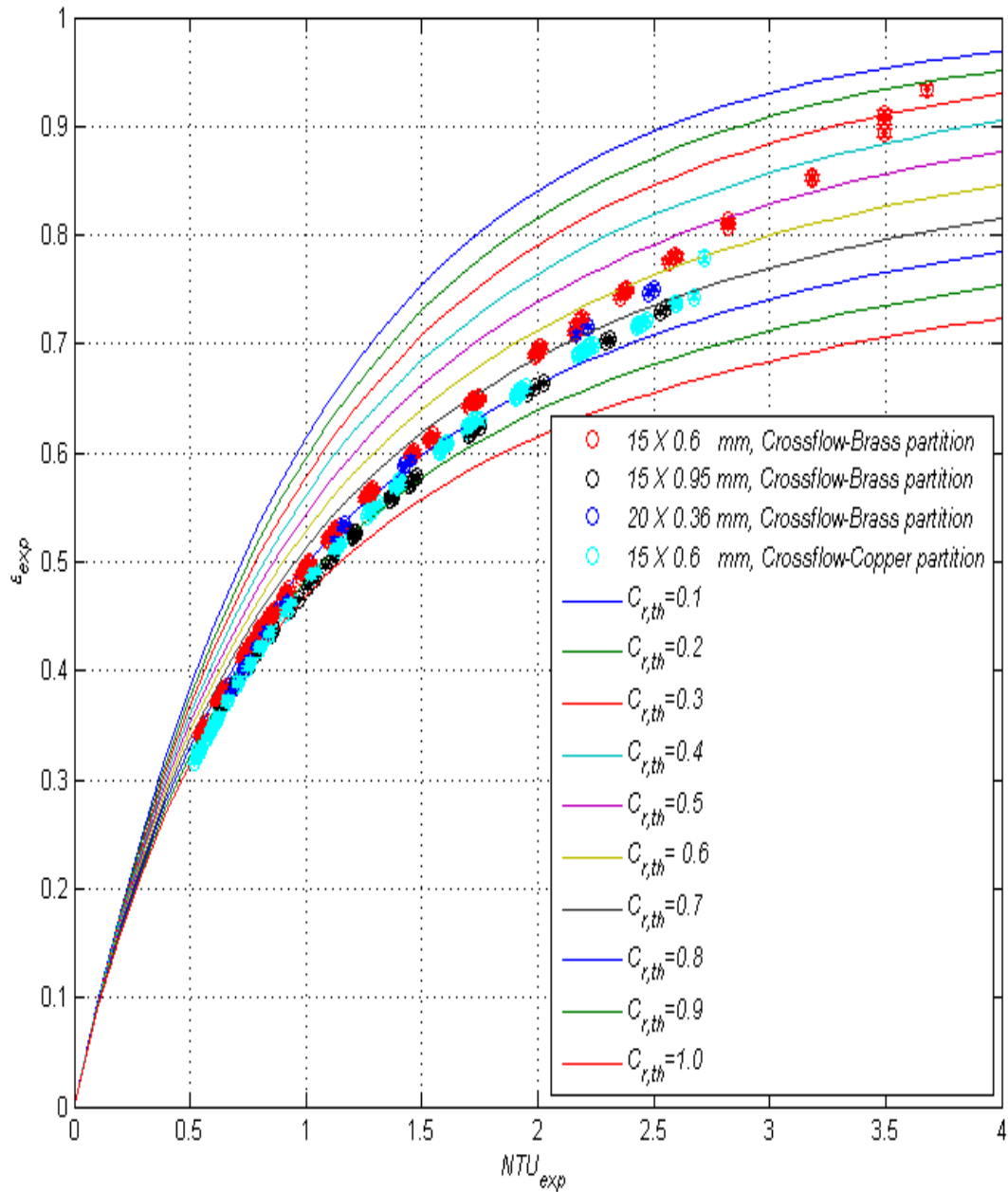
Fig. 5.4 Effectiveness as a function of *NTU* for different capacity rate ratios for the four crossflow heat exchangers.
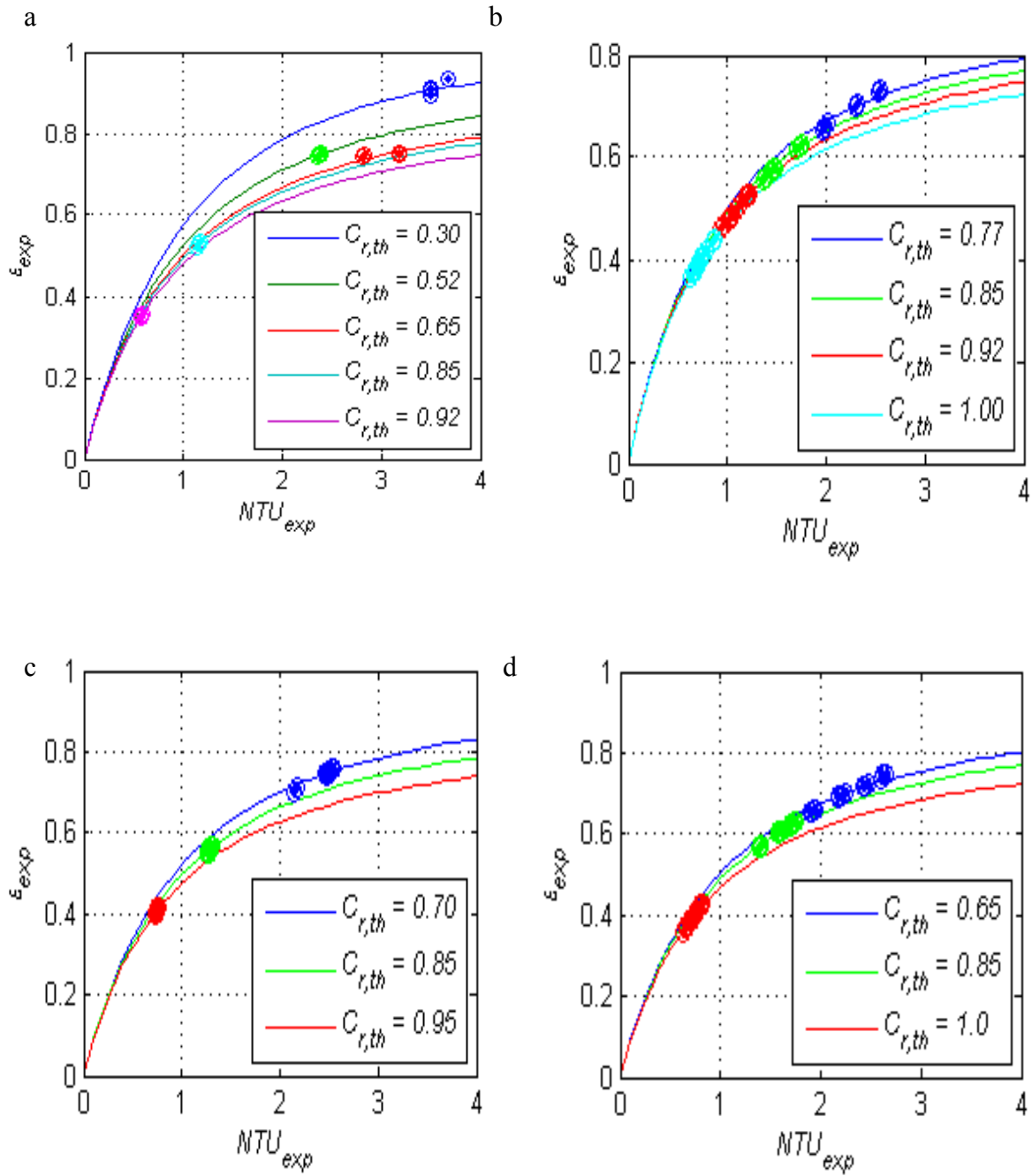
Fig. 5.5 Comparison of experimental and theoretical effectiveness for all four crossflow heat exchangers. a) 15 X 0.6 *mm*, crossflow, brass HEX, b) 15 X 0.95 *mm*, crossflow, brass HEX, c) 20 X 0.36 *mm*, crossflow, brass HEX, d) 20 X 0.36 *mm*, crossflow, copper HEX.
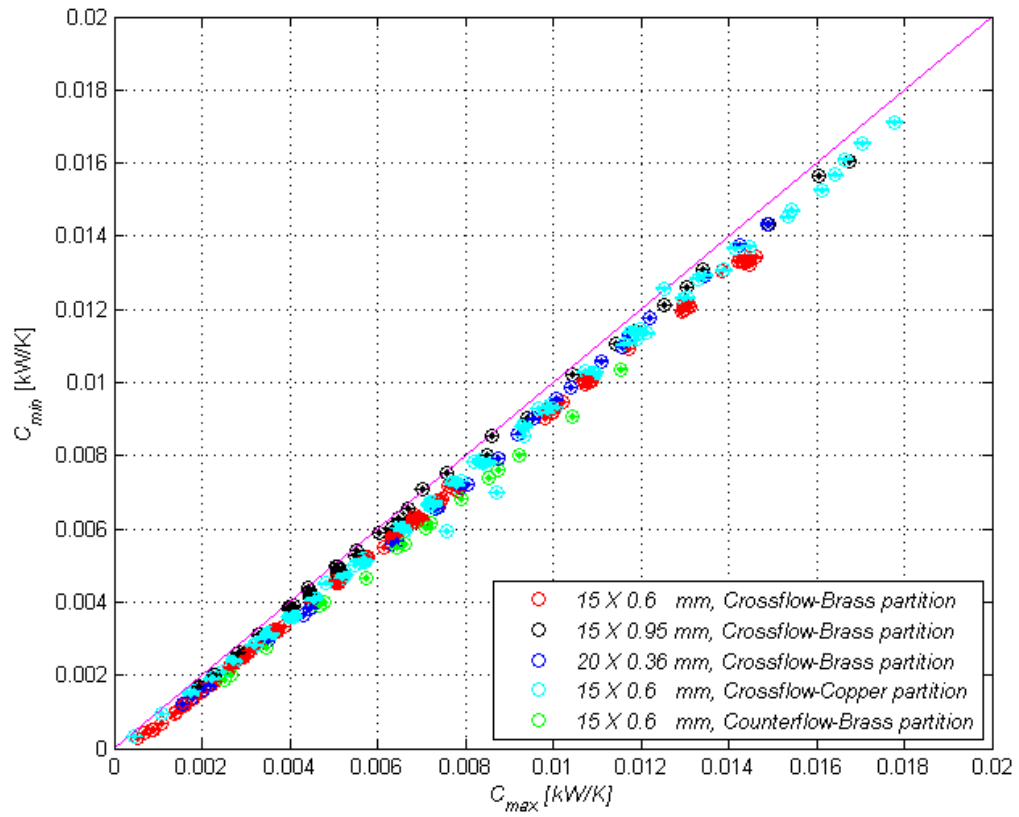
Fig. 5.6 Comparison of minimum and maximum heat capacities for all heat exchangers.
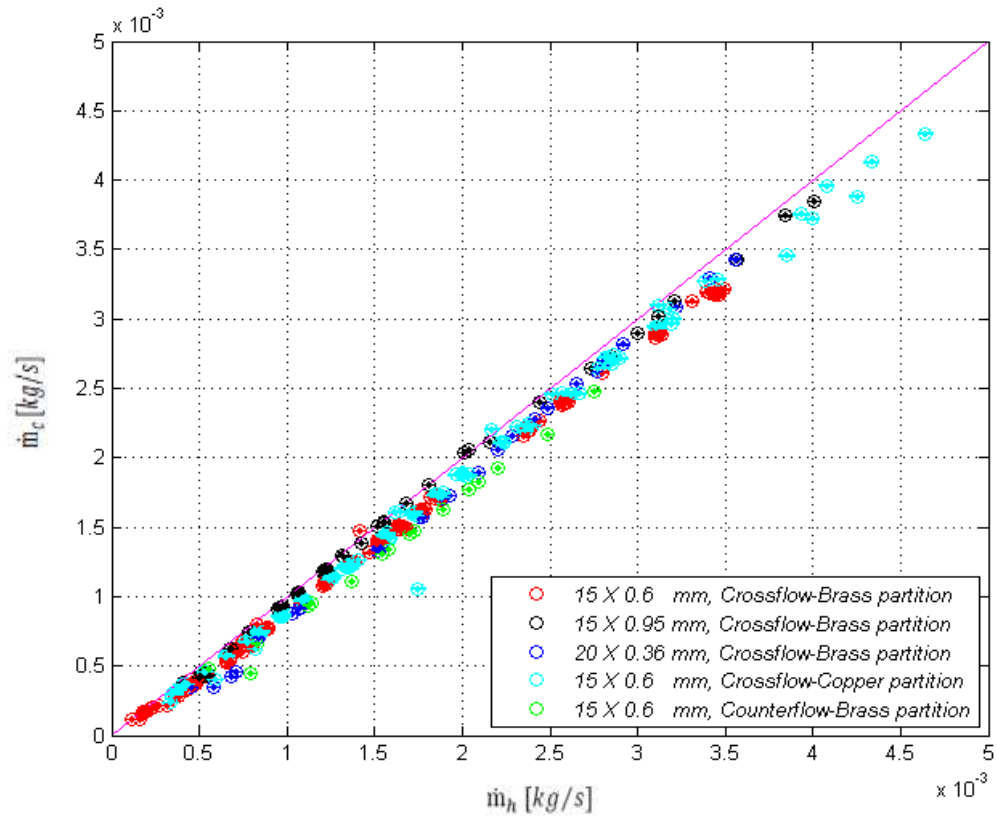
Fig. 5.7 Comparison of hot and cold fluid mass flow rates for all heat exchangers.
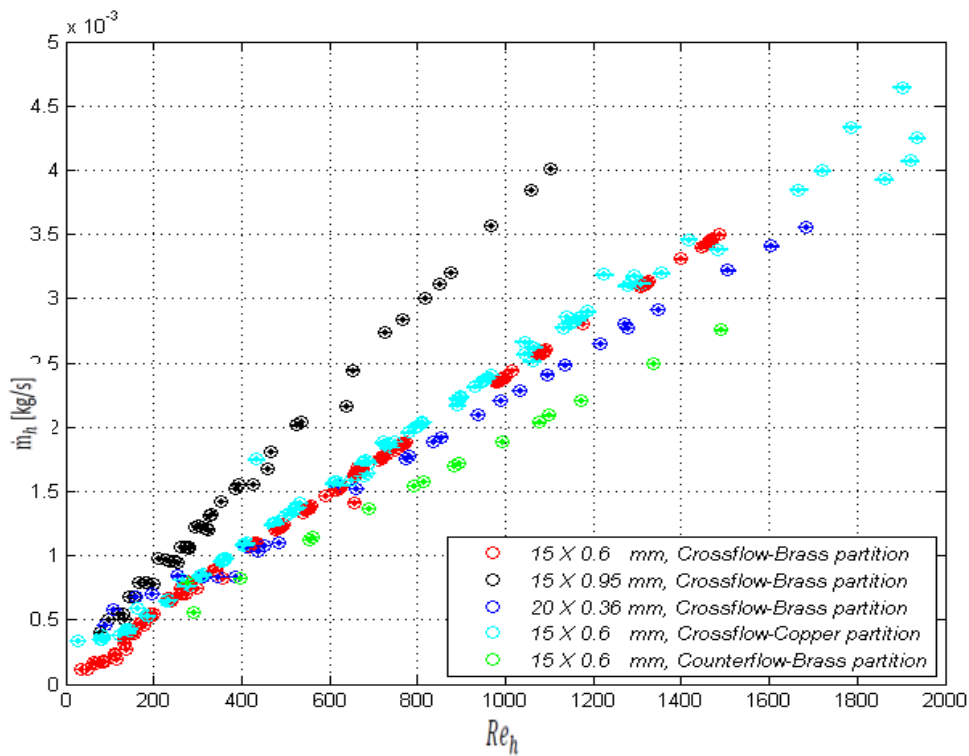
Fig. 5.8 Hot fluid mass flow rate and Reynolds number for all heat exchangers
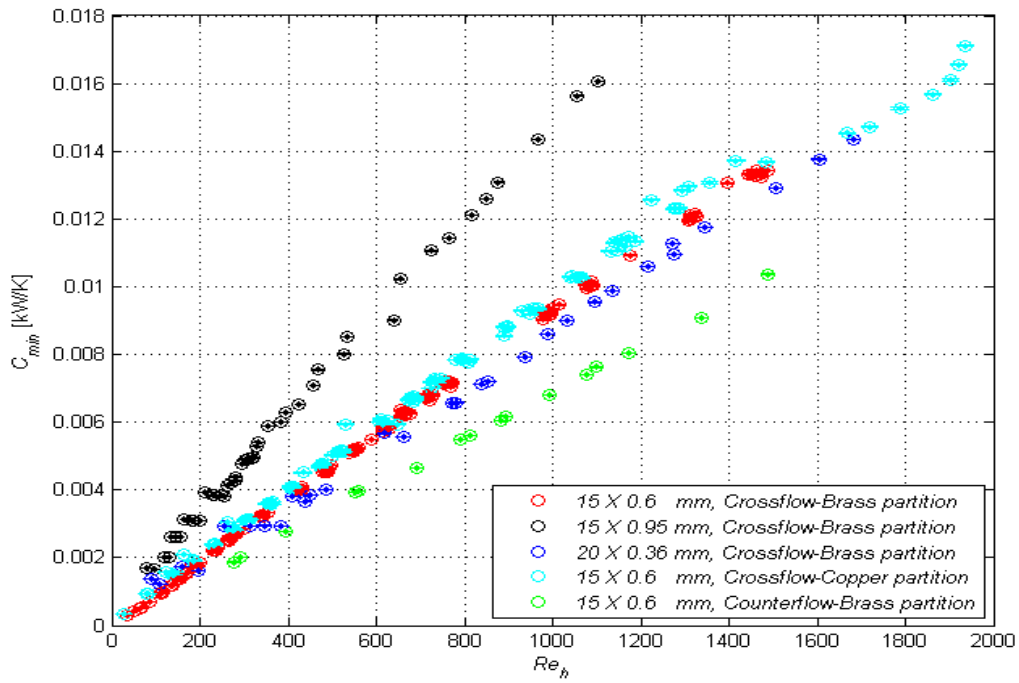
Fig. 5.9 Minimum heat capacity as a function of hot fluid Reynolds number for all heat exchangers
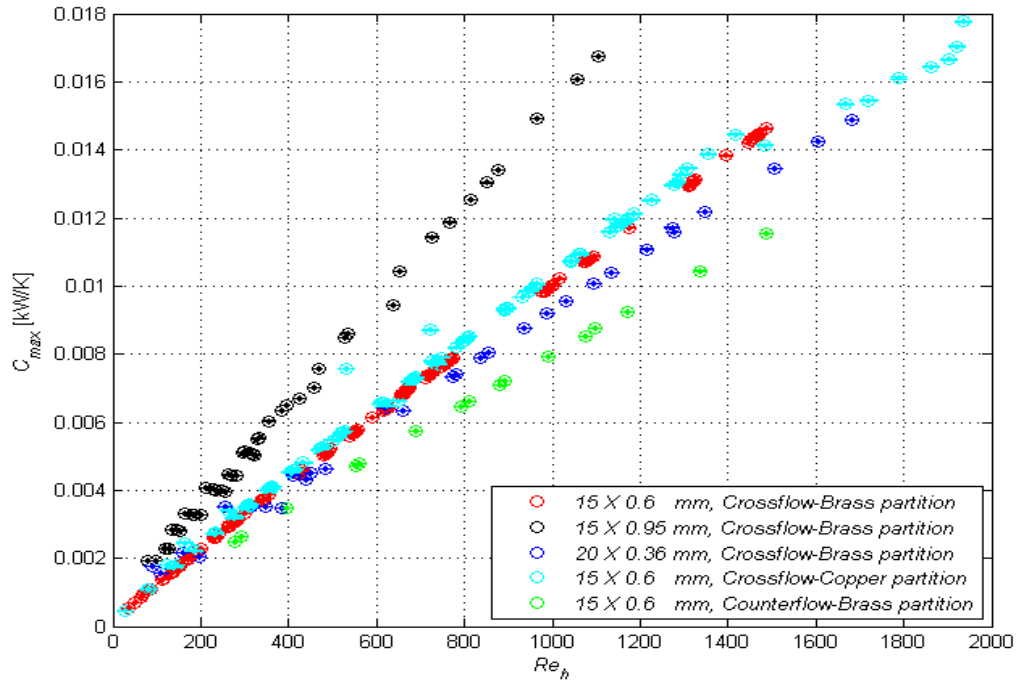
Fig. 5.10 Maximum heat capacity as a function of hot fluid Reynolds number for all heat exchangers
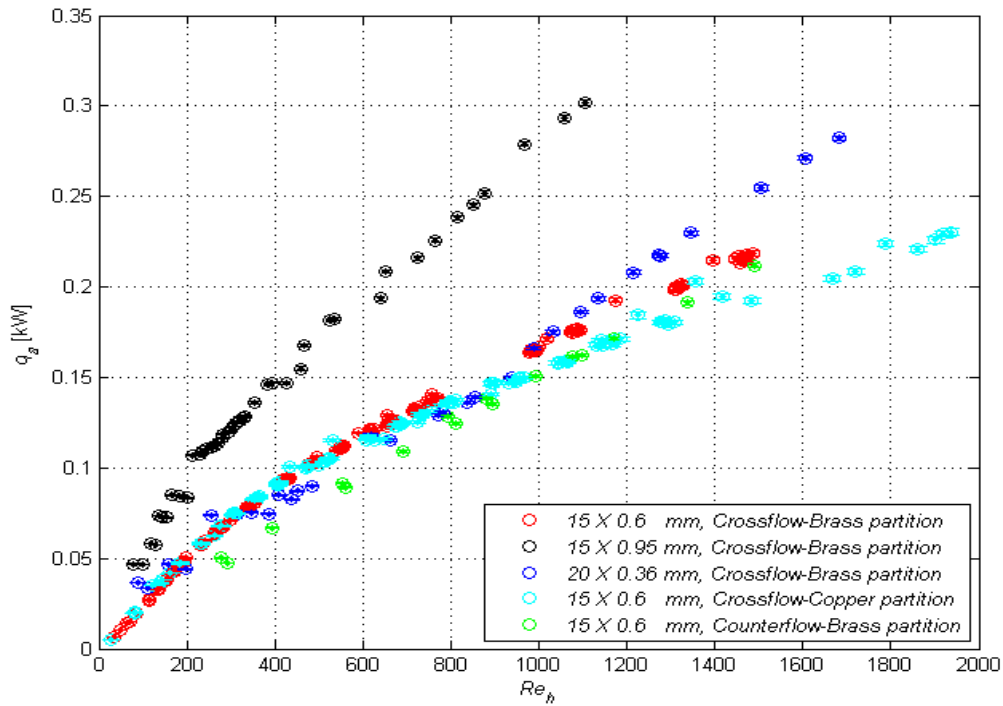
Fig. 5.11 Average heat rate as a function of hot fluid Reynolds number for all heat exchangers.
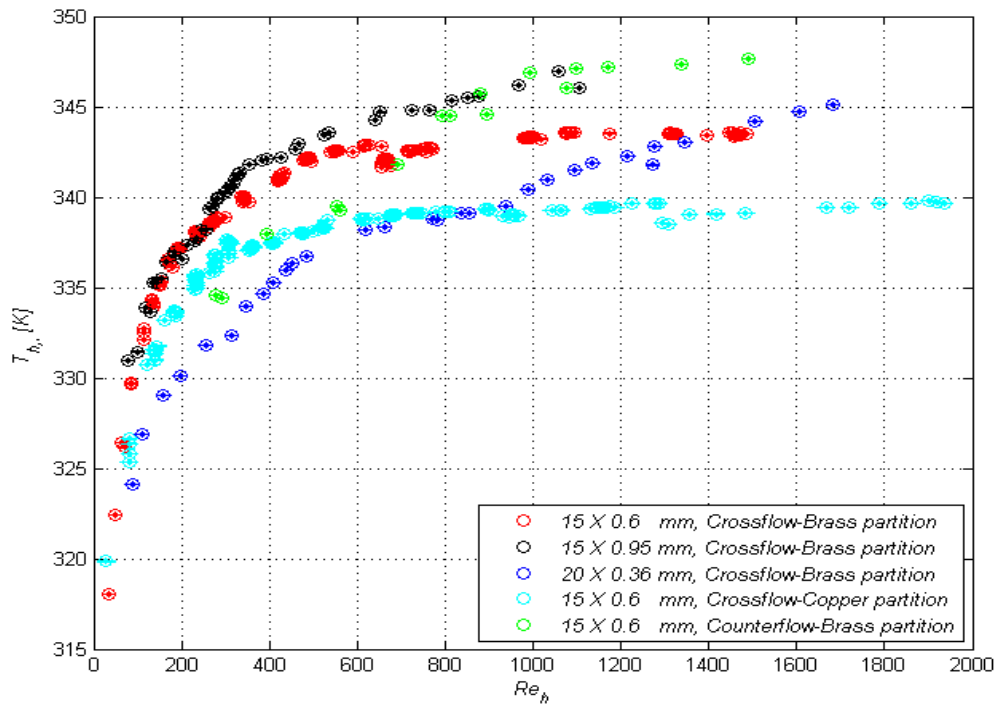
Fig. 5.12 Re_h effect on hot fluid inlet temperature
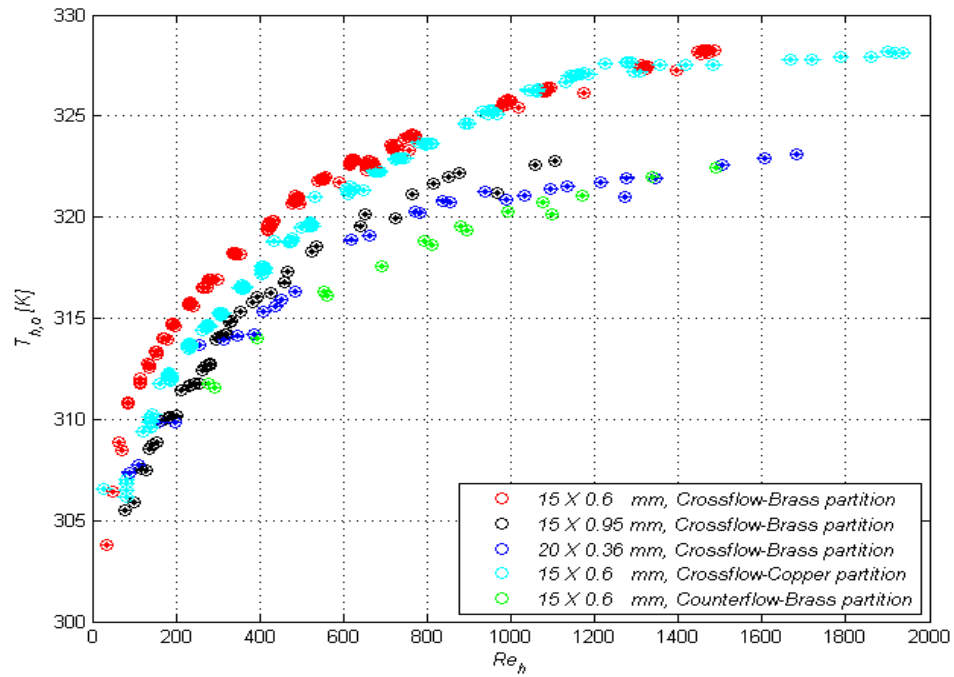
Fig. 5.13 Effect of hot fluid Reynolds number on its outlet temperature
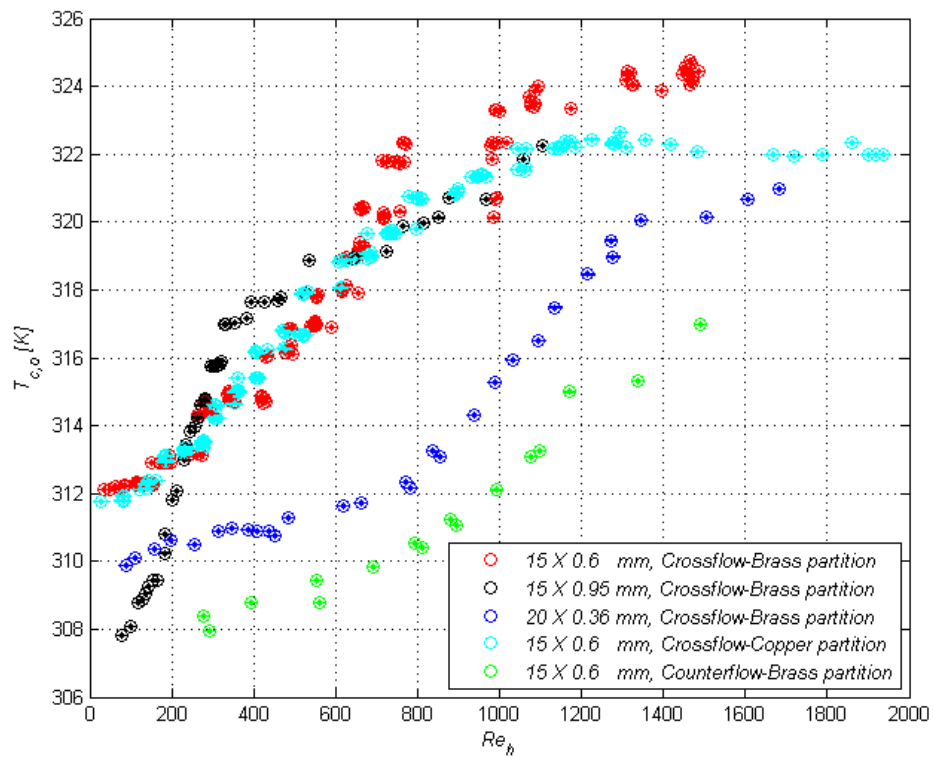
Fig. 5.14 Cold fluid outlet temperature as a function of hot fluid Reynolds number
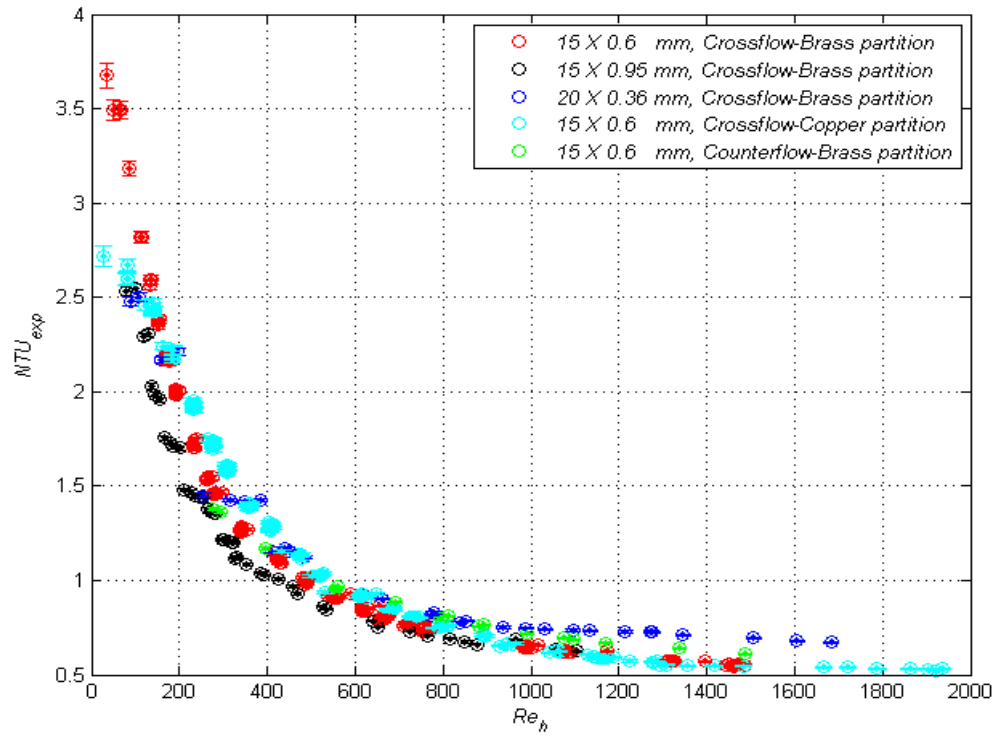
Fig. 5.15 Experimental *NTU* as a function of hot fluid Reynolds number
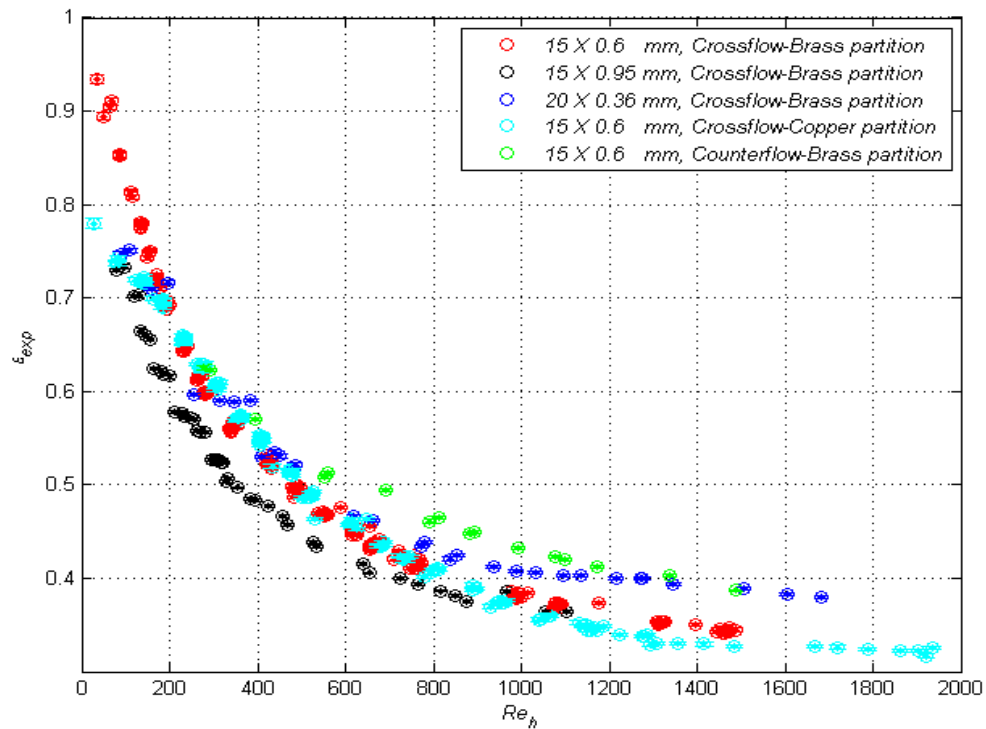
Fig. 5.16 Experimental heat exchanger effectiveness as a function of hot fluid Reynolds number
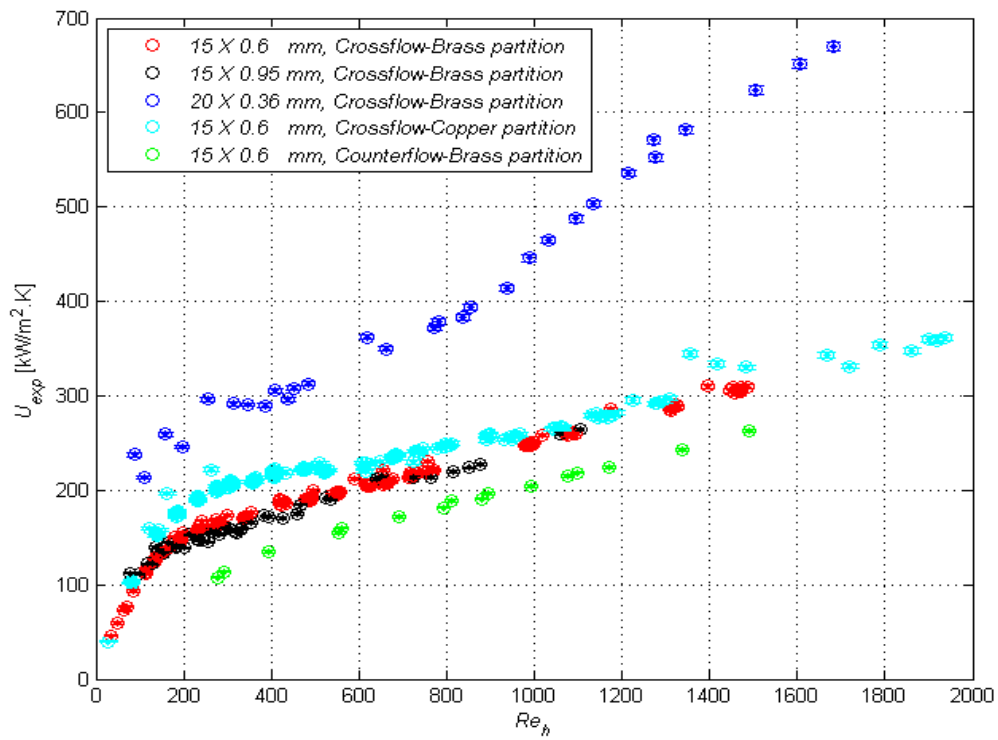
Fig. 5.17 Effect of hot fluid Reynolds number on the experimental overall heat transfer coefficient for all five heat exchangers.
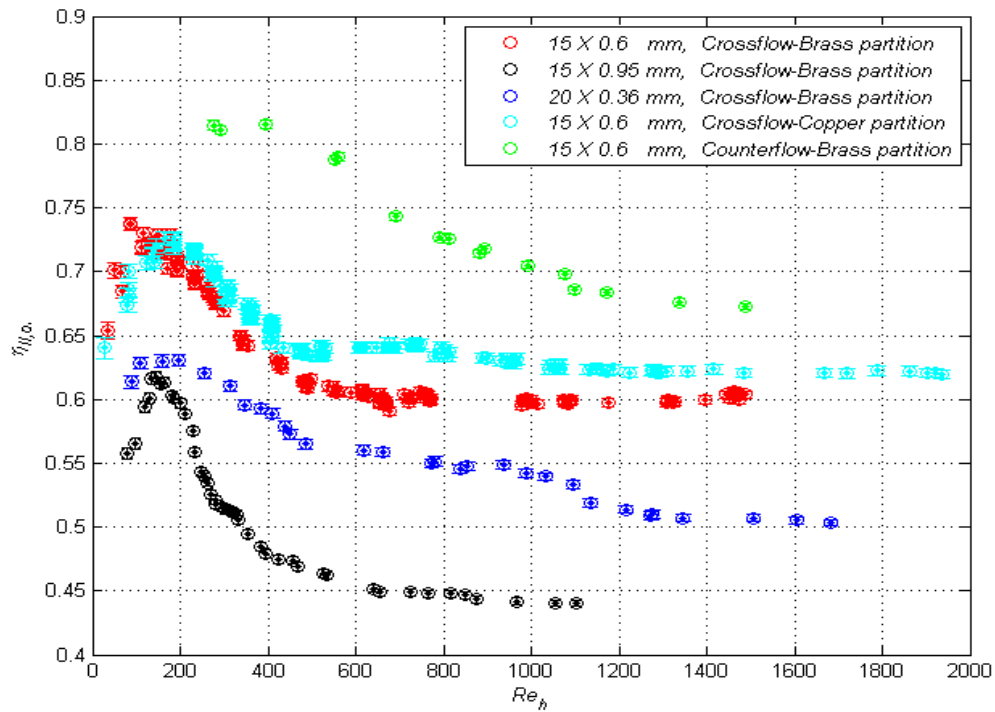
Fig. 5.18 Effect of Re_h on $\eta_{II,ch}$ for all five heat exchangers.
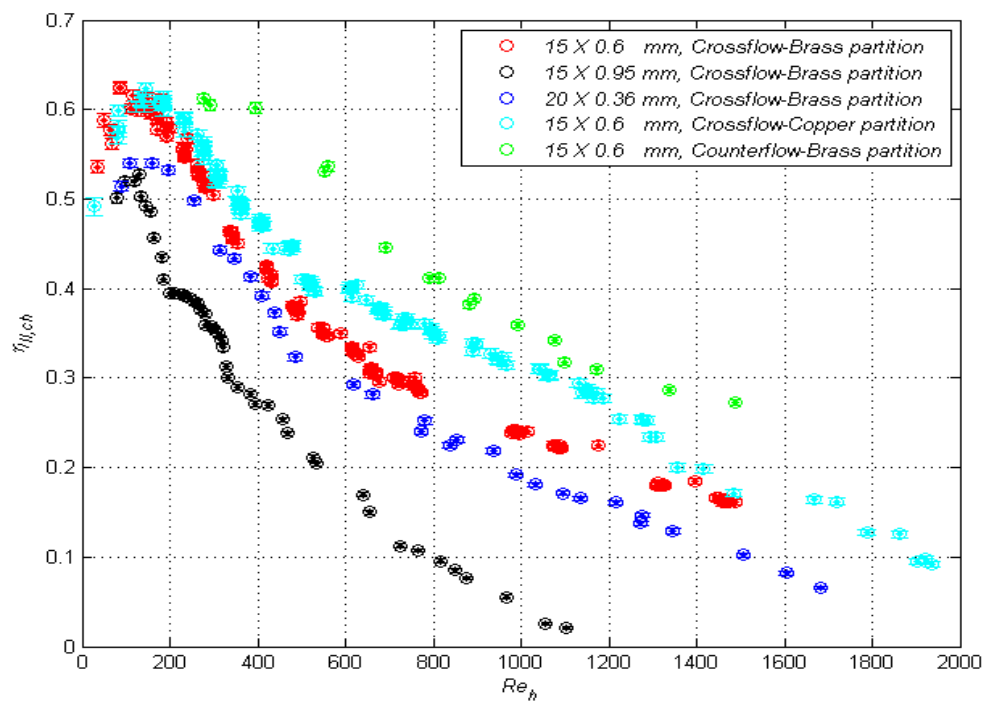
Fig. 5.19 Effect of Re_h on $\eta_{II,oi}$ for all five heat exchangers.

CHAPTER 6

CONCLUSIONS AND RECOMMENDATIONS

6.1 Project Summary

Xurography has been demonstrated to be a useful research tool that enables the rapid prototyping of microfluidic devices at low cost. This study was motivated by the desire to expand the type of microfluidic devices that can be created to include those that incorporate heat transfer. Given that sealing is accomplished using adhesives it was unknown how a xerographic device would perform under elevated temperatures and pressures. To answer these fundamental questions, five microchannel heat exchangers were fabricated by xurography. For the first time, a laser cutting process was employed to create the desired patterns in the double-side adhesive tape that is a core component of one of these structures. The laser cutting process enables the creation of narrower microchannels and allows curved features to be generated. The microchannels were characterized; however, this process was hampered by the black edges formed by the laser cutting.

An existing flow loop was modified to allow a second fluid to be used. Unfortunately, due to equipment failure, the flow loop did not have the ability to individually control the two fluid mass flow rates. This led to less than desirable control over the study parameters. Experiments were designed that focused on rarely reported heat exchanger data, namely NTU, ε, C_r, and η_{II}. Most microchannel heat exchanger

studies in the literature concentrate on ascertaining the heat transfer coefficients, the overall heat transfer coefficient, and friction factors.

The experiments demonstrate the feasibility of creating practical crossflow and counterflow heat exchangers using xurography. This finding may lead to others adapting this technology to create simple and inexpensive microchannel heat exchangers, especially when time is critical. In general, the heat exchangers were found to perform in a manner that agrees with theory.

6.2 Conclusions

6.2.1 Major Conclusions - Performance

The principle conclusions related to heat exchanger performance are reported here.

1) Practical two-layer xerographic devices that operate at elevated temperatures can be fabricated using xurography.

2) Laser cutting of the polyimide tape produces well-defined microchannels with the possibility of curved features. The laser cut channels have fewer defects, more precise dimensions, and better repeatability, than razor cut channels. Laser cutting can leave a residue in the microchannels and may produce melted or burned cut edges.

3) The maximum heat exchanger effectiveness correlates with the lowest mass flow rate and Reynolds number.

4) The most efficient heat exchanger operation occurs at $50 < Re < 150$, based on the exergy analysis.

5)   All devices were able to at least *NTU* = 2.5, and some obtained higher values.

6)   Inter-fluid heat transfer was nearly the same for all devices, with the exception of the 950 μm channel width crossflow heat exchanger.

7)   Effectiveness and *NTU* are approximately inversely proportional to *Re*.

8)   The overall heat transfer coefficient is proportional to *Re*.

9)   As expected, the Kapton® tape was not a good conductor. Thus, the partition material must have high thermal conductivity.

10)   The maximum fluid temperature at which the xurographic devices operated without leaking was 75°C.

11)   The maximum pressure that the heat exchangers withstood without leaking was 2,516.6 *kPa*.

12)   Copper, due to its higher thermal conductivity, is a better partition material than brass

6.2.2 Minor Conclusions – Construction, Data Acquisition, Etc.

In the process of manufacturing and testing the devices, lessons were learned. The summary of this experience is reported as advantages in this section and as disadvantages with recommendations in the following section. Conclusions are as follows.

1)   Curing is required to insure good adhesion between the glass and Kapton® tape. Glass produces a strong bond due to its high surface smoothness.

2)   Brass and copper enhance the interfluid heat transfer and do not add any difficulties in the manufacturing process.

3)   The closer the location of the thermocouple to the microchannel inlet/outlet ports, the greater the accuracy of the measured temperature.

4) To minimize the effect of mass flow rate uncertainty, the time interval between mass measurements must be selected to minimize, within reason, the mass flow rate uncertainty. For example, for *Re* = 50, the time interval was 3 *min*, while for *Re* ≥ 1000 the time interval was 30 *s*.

5) The laser settings must be selected for the specific tape to be cut. Only with the proper combination of laser cutting parameters can the tape be cut without damaging the tape edges and substrate.

6.3 Recommendations

6.3.1 Improving the Design, Fabrication, and Experiment

While the experiment was not without flaw, it did produce results with good agreement to theory. Some recommendations are suggested to improve the accuracy of the data and the overall performance of the experiment.

1) Nano-ports were used as inlet and outlet connections. Replacement of the Nano-ports by a male-female threaded connection would save time and increase confidence that a leak-free device can be produced.

2) Replacement of the glass slides with a PMMA slide is recommended. The PMMA slide could include the female thread to host the male thread and together these connections could serve as the device inlets and outlets for the working fluids.

3) Consider using slides with an increased length and width to create an air-gap around the device to enhance the insulation of the device. The air-gap should be sandwiched between the two slides of PMMA or glass if either is used.

4)   Pressure sensors with a smaller operating range should be used for the lower mass

flow rates, because the uncertainty of the pressure sensor is based upon the full

scale of the sensor. Replacement of the small-scale pressure sensors with higher

scale pressure sensors would then be required for higher flow rates. For example,

for the inlet the recommended pressure sensors are 138 *kPa* (20 *psi*), 551 *kPa* (80

psi), and 1030 *kPa* (150 *psi*) and for the outlet a pair of 34 *kPa* (5 *psi*) and 69 *kPa*

(10 *psi*) sensors will suffice.

6.3.2 Extending the Work

Important ideas emerged as a result of the educational process of this experiment.
The ideas for extending this work are as follows,

1)   The accumulator capacity was acceptable for low flow rates, but was insufficient

for higher flow rates (*Re* > 700). Micro-pumps may be more effective than the

accumulator.

2)   Separate pressure sources and valves should be incorporated into the flow loop so

that both flows can be controlled.

3)   The mass balances (600 *g* maximum load capacity) were insufficient for the high

flow rates (*Re* > 700) due to the time required for the system to achieve steady

state.

4)   Flow visualization may provide insight into how the flow could be modified to

enhance the heat transfer.

5)   To extend the applications of xurographic microfluidic systems, a multi-stack heat

exchanger, either crossflow or counterflow, should be considered for future study.

6)   A similar study should be designed to determine the two fluid heat transfer coefficients and the overall heat transfer coefficient. This study would require more precise measurement of all channel dimensions.

APPENDIX

Output from the Pretest uncertainty analysis is presented in this section. "Measured" data, such as temperatures and pressures, were approximated Pretest using the models created to design the test sections. Measurement uncertainties were taken from manufacturer's published data with the exception of thermocouples, which were assumed to be calibrated ($\Delta T = \pm 0.1 \degree C$). For each output parameter, data are provided for the calculated value, the absolute uncertainty (FLUCTUATION), and the relative uncertainty (UNCERTAINTY) given as a percentage. Contributor is the product of the sensitivity coefficient and the measurement uncertainty.

```
INPUT DATA                           ε = 0.00001


----------------------------------------------------------------
#       PARAMETER        ACTUAL VALUE        UNCERTAINTY
----------------------------------------------------------------
```

#	PARAMETER		ACTUAL VALUE	UNCERTAINTY
1	T_{hi}	(°K)	3.4300e+002	1.0000e-001
2	T_{ho}	(°K)	3.1340e+002	1.0000e-001
3	T_{ci}	(°K)	2.9300e+002	1.0000e-001
4	T_{co}	(°K)	3.2300e+002	1.0000e-001
5	t_1	(s)	1.0000e+000	1.0000e-005
6	t_2	(s)	6.0000e+000	1.0000e-005
7	M_{h1}	(kg)	1.1000e+000	1.0000e-005
8	M_{h2}	(kg)	1.1005e+000	1.0000e-005
9	M_{c1}	(kg)	1.1000e+000	1.0000e-005
10	M_{c2}	(kg)	1.1012e+000	1.0000e-005
11	P_{hi}	(MPa)	2.6237e-001	5.1710e-003
12	P_{ho}	(MPa)	9.3232e-002	3.1026e-003
13	P_{ci}	(MPa)	2.6237e-001	5.1710e-003
14	P_{co}	(MPa)	9.2045e-002	3.1026e-003
15	L_h	(m)	2.0000e-002	1.0000e-006
16	W_h	(m)	6.0000e-004	1.0000e-006
17	Z_h	(m)	1.0000e-004	1.0000e-006
18	L_c	(m)	2.0000e-002	1.0000e-006
19	W_c	(m)	6.0000e-004	1.0000e-006
20	Z_c	(m)	1.0000e-004	1.0000e-006
21	T_r	(°K)	2.9815e+002	1.0000e-002
22	P_r	(MPa)	1.0133e-001	1.0000e-003

```
----------------------------------------------------------------
          HEAT EXCHANGER GENERAL PARAMETERS
----------------------------------------------------------------
----------------------------------------------------------------
```

Uncertainty Pretest for $\dot{m}_h$ (Kg/s)

```
-------------------------------------------------------------
INPUT PAR.    SENS. COEFF.     MEAS. UNCER.   Contributor
-------------------------------------------------------------
```

INPUT PAR.		SENS. COEFF.	MEAS. UNCER.	Contributor
T_{hi}	(°K)	0.0000e+000	1.0000e-001	0.0000e+000
T_{ho}	(°K)	0.0000e+000	1.0000e-001	0.0000e+000
T_{ci}	(°K)	0.0000e+000	1.0000e-001	0.0000e+000
T_{co}	(°K)	0.0000e+000	1.0000e-001	0.0000e+000
t_1	(s)	2.0000e-005	1.0000e-005	4.0000e-020
t_2	(s)	-2.0000e-005	1.0000e-005	4.0000e-020
M_{h1}	(kg)	-2.0000e-001	1.0000e-005	4.0000e-012
M_{h2}	(kg)	2.0000e-001	1.0000e-005	4.0000e-012
M_{c1}	(kg)	0.0000e+000	1.0000e-005	0.0000e+000
M_{c2}	(kg)	0.0000e+000	1.0000e-005	0.0000e+000
P_{hi}	(MPa)	0.0000e+000	5.1710e-003	0.0000e+000
P_{ho}	(MPa)	0.0000e+000	3.1026e-003	0.0000e+000
P_{ci}	(MPa)	0.0000e+000	5.1710e-003	0.0000e+000
P_{co}	(MPa)	0.0000e+000	3.1026e-003	0.0000e+000
L_h	(m)	0.0000e+000	1.0000e-006	0.0000e+000
W_h	(m)	0.0000e+000	1.0000e-006	0.0000e+000
Z_h	(m)	0.0000e+000	1.0000e-006	0.0000e+000
L_c	(m)	0.0000e+000	1.0000e-006	0.0000e+000
W_c	(m)	0.0000e+000	1.0000e-006	0.0000e+000
Z_c	(m)	0.0000e+000	1.0000e-006	0.0000e+000
T_r	(°K)	0.0000e+000	1.0000e-002	0.0000e+000
P_r	(MPa)	0.0000e+000	1.0000e-003	0.0000e+000

```
^^^^^^^^^^^^^^^^^^^^^^^^^^^^^^^^^^^^^^^^^^^^^^^^^^^^^^^^^^^^^^^^
```

$\dot{m}_h$ (Kg/s)   = 0.000100
FLUCTUATION   = 0.000003
UNCERTAINTY   = 2.828427

```
^^^^^^^^^^^^^^^^^^^^^^^^^^^^^^^^^^^^^^^^^^^^^^^^^^^^^^^^^^^^^^^^
-------------------------------------------------------------
```

Uncertainty Pretest for $\dot{m}_c$ (Kg/s)

```
-------------------------------------------------------------
INPUT PAR.    SENS. COEFF.     MEAS. UNCER.   Contributor
-------------------------------------------------------------
```

INPUT PAR.		SENS. COEFF.	MEAS. UNCER.	Contributor
T_{hi}	(°K)	0.0000e+000	1.0000e-001	0.0000e+000
T_{ho}	(°K)	0.0000e+000	1.0000e-001	0.0000e+000
T_{ci}	(°K)	0.0000e+000	1.0000e-001	0.0000e+000
T_{co}	(°K)	0.0000e+000	1.0000e-001	0.0000e+000
t_1	(s)	4.8000e-005	1.0000e-005	2.3040e-019
t_2	(s)	-4.8000e-005	1.0000e-005	2.3040e-019
M_{h1}	(kg)	0.0000e+000	1.0000e-005	0.0000e+000
M_{h2}	(kg)	0.0000e+000	1.0000e-005	0.0000e+000
M_{c1}	(kg)	-2.0000e-001	1.0000e-005	4.0000e-012
M_{c2}	(kg)	2.0000e-001	1.0000e-005	4.0000e-012
P_{hi}	(MPa)	0.0000e+000	5.1710e-003	0.0000e+000
P_{ho}	(MPa)	0.0000e+000	3.1026e-003	0.0000e+000
P_{ci}	(MPa)	0.0000e+000	5.1710e-003	0.0000e+000
P_{co}	(MPa)	0.0000e+000	3.1026e-003	0.0000e+000
L_h	(m)	0.0000e+000	1.0000e-006	0.0000e+000

```
Wₕ      (m)    0.0000e+000          1.0000e-006          0.0000e+000
Zₕ      (m)    0.0000e+000          1.0000e-006          0.0000e+000
L_c     (m)    0.0000e+000          1.0000e-006          0.0000e+000
W_c     (m)    0.0000e+000          1.0000e-006          0.0000e+000
Z_c     (m)    0.0000e+000          1.0000e-006          0.0000e+000
Tᵣ      (°K)   0.0000e+000          1.0000e-002          0.0000e+000
Pᵣ     (MPa)   0.0000e+000          1.0000e-003          0.0000e+000
```

W_h (m) $0.0000e+000$ $1.0000e-006$ $0.0000e+000$
Z_h (m) $0.0000e+000$ $1.0000e-006$ $0.0000e+000$
L_c (m) $0.0000e+000$ $1.0000e-006$ $0.0000e+000$
W_c (m) $0.0000e+000$ $1.0000e-006$ $0.0000e+000$
Z_c (m) $0.0000e+000$ $1.0000e-006$ $0.0000e+000$
T_r (°K) $0.0000e+000$ $1.0000e-002$ $0.0000e+000$
P_r (MPa) $0.0000e+000$ $1.0000e-003$ $0.0000e+000$

```
^^^^^^^^^^^^^^^^^^^^^^^^^^^^^^^^^^^^^^^^^^^^^^^^^^^^^^^^^^^^^^^^
```

$\dot{m}_h$ (Kg/s) = 0.000240
FLUCTUATION   = 0.000003
UNCERTAINTY   = 1.178511

```
^^^^^^^^^^^^^^^^^^^^^^^^^^^^^^^^^^^^^^^^^^^^^^^^^^^^^^^^^^^^^^^^
```

                Uncertainty Pretest for DP_h (MPa)

INPUT PAR.   SENS. COEFF.   MEAS. UNCER.   Contributor

T_{hi} (°K) $0.0000e+000$ $1.0000e-001$ $0.0000e+000$
T_{ho} (°K) $0.0000e+000$ $1.0000e-001$ $0.0000e+000$
T_{ci} (°K) $0.0000e+000$ $1.0000e-001$ $0.0000e+000$
T_{co} (°K) $0.0000e+000$ $1.0000e-001$ $0.0000e+000$
t_1 (s) $0.0000e+000$ $1.0000e-005$ $0.0000e+000$
t_2 (s) $0.0000e+000$ $1.0000e-005$ $0.0000e+000$
M_{h1} (kg) $0.0000e+000$ $1.0000e-005$ $0.0000e+000$
M_{h2} (kg) $0.0000e+000$ $1.0000e-005$ $0.0000e+000$
M_{c1} (kg) $0.0000e+000$ $1.0000e-005$ $0.0000e+000$
M_{c2} (kg) $0.0000e+000$ $1.0000e-005$ $0.0000e+000$
P_{hi} (MPa) $1.0000e+000$ $5.1710e-003$ $2.6739e-005$
P_{ho} (MPa) $-1.0000e+000$ $3.1026e-003$ $9.6264e-006$
P_{ci} (MPa) $0.0000e+000$ $5.1710e-003$ $0.0000e+000$
P_{co} (MPa) $0.0000e+000$ $3.1026e-003$ $0.0000e+000$
L_h (m) $0.0000e+000$ $1.0000e-006$ $0.0000e+000$
W_h (m) $0.0000e+000$ $1.0000e-006$ $0.0000e+000$
Z_h (m) $0.0000e+000$ $1.0000e-006$ $0.0000e+000$
L_c (m) $0.0000e+000$ $1.0000e-006$ $0.0000e+000$
W_c (m) $0.0000e+000$ $1.0000e-006$ $0.0000e+000$
Z_c (m) $0.0000e+000$ $1.0000e-006$ $0.0000e+000$
T_r (°K) $0.0000e+000$ $1.0000e-002$ $0.0000e+000$
P_r (MPa) $0.0000e+000$ $1.0000e-003$ $0.0000e+000$

```
^^^^^^^^^^^^^^^^^^^^^^^^^^^^^^^^^^^^^^^^^^^^^^^^^^^^^^^^^^^^^^^^
```

DP_h (MPa)= 0.169137
FLUCTUATION   = 0.006030
UNCERTAINTY   = 3.565390

```
^^^^^^^^^^^^^^^^^^^^^^^^^^^^^^^^^^^^^^^^^^^^^^^^^^^^^^^^^^^^^^^^
```

                Uncertainty Pretest for DP_c (MPa)

INPUT PAR.   SENS. COEFF.   MEAS. UNCER.   Contributor

T_{hi} (°K) $0.0000e+000$ $1.0000e-001$ $0.0000e+000$

T_{ho}	(°K)	0.0000e+000	1.0000e-001	0.0000e+000
T_{ci}	(°K)	0.0000e+000	1.0000e-001	0.0000e+000
T_{co}	(°K)	0.0000e+000	1.0000e-001	0.0000e+000
t_1	(s)	0.0000e+000	1.0000e-005	0.0000e+000
t_2	(s)	0.0000e+000	1.0000e-005	0.0000e+000
M_{h1}	(kg)	0.0000e+000	1.0000e-005	0.0000e+000
M_{h2}	(kg)	0.0000e+000	1.0000e-005	0.0000e+000
M_{c1}	(kg)	0.0000e+000	1.0000e-005	0.0000e+000
M_{c2}	(kg)	0.0000e+000	1.0000e-005	0.0000e+000
P_{hi}	(MPa)	0.0000e+000	5.1710e-003	0.0000e+000
P_{ho}	(MPa)	0.0000e+000	3.1026e-003	0.0000e+000
P_{ci}	(MPa)	1.0000e+000	5.1710e-003	2.6739e-005
P_{co}	(MPa)	−1.0000e+000	3.1026e-003	9.6264e-006
L_h	(m)	0.0000e+000	1.0000e-006	0.0000e+000
W_h	(m)	0.0000e+000	1.0000e-006	0.0000e+000
Z_h	(m)	0.0000e+000	1.0000e-006	0.0000e+000
L_c	(m)	0.0000e+000	1.0000e-006	0.0000e+000
W_c	(m)	0.0000e+000	1.0000e-006	0.0000e+000
Z_c	(m)	0.0000e+000	1.0000e-006	0.0000e+000
T_r	(°K)	0.0000e+000	1.0000e-002	0.0000e+000
P_r	(MPa)	0.0000e+000	1.0000e-003	0.0000e+000

^^^

```
DP_c    (MPa)= 0.170324
FLUCTUATION  = 0.006030
UNCERTAINTY  = 3.540542
```

^^^

Uncertainty Pretest for DP_{avg} (MPa)

INPUT PAR.		SENS. COEFF.	MEAS. UNCER.	Contributor
T_{hi}	(°K)	0.0000e+000	1.0000e-001	0.0000e+000
T_{ho}	(°K)	0.0000e+000	1.0000e-001	0.0000e+000
T_{ci}	(°K)	0.0000e+000	1.0000e-001	0.0000e+000
T_{co}	(°K)	0.0000e+000	1.0000e-001	0.0000e+000
t_1	(s)	0.0000e+000	1.0000e-005	0.0000e+000
t_2	(s)	0.0000e+000	1.0000e-005	0.0000e+000
M_{h1}	(kg)	0.0000e+000	1.0000e-005	0.0000e+000
M_{h2}	(kg)	0.0000e+000	1.0000e-005	0.0000e+000
M_{c1}	(kg)	0.0000e+000	1.0000e-005	0.0000e+000
M_{c2}	(kg)	0.0000e+000	1.0000e-005	0.0000e+000
P_{hi}	(MPa)	5.0000e-001	5.1710e-003	6.6848e-006
P_{ho}	(MPa)	−5.0000e-001	3.1026e-003	2.4066e-006
P_{ci}	(MPa)	5.0000e-001	5.1710e-003	6.6848e-006
P_{co}	(MPa)	−5.0000e-001	3.1026e-003	2.4066e-006
L_h	(m)	0.0000e+000	1.0000e-006	0.0000e+000
W_h	(m)	0.0000e+000	1.0000e-006	0.0000e+000
Z_h	(m)	0.0000e+000	1.0000e-006	0.0000e+000
L_c	(m)	0.0000e+000	1.0000e-006	0.0000e+000
W_c	(m)	0.0000e+000	1.0000e-006	0.0000e+000

```
Z_c      (m)     0.0000e+000       1.0000e-006       0.0000e+000
T_r      (°K)    0.0000e+000       1.0000e-002       0.0000e+000
P_r      (MPa)   0.0000e+000       1.0000e-003       0.0000e+000
```

Z_c (m)   0.0000e+000   1.0000e-006   0.0000e+000
T_r (°K)   0.0000e+000   1.0000e-002   0.0000e+000
P_r (MPa)   0.0000e+000   1.0000e-003   0.0000e+000

^^

DP_{avg} (MPa)= 0.169730
FLUCTUATION   = 0.004264
UNCERTAINTY   = 2.512296

^^

      Uncertainty Pretest for C_{min} (kW/°K)

INPUT PAR.   SENS. COEFF.   MEAS. UNCER.   Contributor

INPUT PAR.		SENS. COEFF.	MEAS. UNCER.	Contributor
T_{hi}	(°K)	1.6150e-008	1.0000e-001	2.6081e-018
T_{ho}	(°K)	1.6150e-008	1.0000e-001	2.6081e-018
T_{ci}	(°K)	0.0000e+000	1.0000e-001	0.0000e+000
T_{co}	(°K)	0.0000e+000	1.0000e-001	0.0000e+000
t_1	(s)	8.3615e-005	1.0000e-005	6.9914e-019
t_2	(s)	-8.3615e-005	1.0000e-005	6.9914e-019
M_{h1}	(kg)	-8.3615e-001	1.0000e-005	6.9914e-011
M_{h2}	(kg)	8.3615e-001	1.0000e-005	6.9914e-011
M_{c1}	(kg)	0.0000e+000	1.0000e-005	0.0000e+000
M_{c2}	(kg)	0.0000e+000	1.0000e-005	0.0000e+000
P_{hi}	(MPa)	-1.1321e-007	5.1710e-003	3.4271e-019
P_{ho}	(MPa)	-1.1321e-007	3.1026e-003	1.2338e-019
P_{ci}	(MPa)	0.0000e+000	5.1710e-003	0.0000e+000
P_{co}	(MPa)	0.0000e+000	3.1026e-003	0.0000e+000
L_h	(m)	0.0000e+000	1.0000e-006	0.0000e+000
W_h	(m)	0.0000e+000	1.0000e-006	0.0000e+000
Z_h	(m)	0.0000e+000	1.0000e-006	0.0000e+000
L_c	(m)	0.0000e+000	1.0000e-006	0.0000e+000
W_c	(m)	0.0000e+000	1.0000e-006	0.0000e+000
Z_c	(m)	0.0000e+000	1.0000e-006	0.0000e+000
T_r	(°K)	0.0000e+000	1.0000e-002	0.0000e+000
P_r	(MPa)	0.0000e+000	1.0000e-003	0.0000e+000

^^

C_{min} (kW/°K)= 0.000418
FLUCTUATION   = 0.000012
UNCERTAINTY   = 2.828427

^^

      Uncertainty Pretest for C_{max} (kW/°K)

INPUT PAR.		SENS. COEFF.	MEAS. UNCER.	Contributor
T_{hi}	(°K)	0.0000e+000	1.0000e-001	0.0000e+000
T_{ho}	(°K)	0.0000e+000	1.0000e-001	0.0000e+000
T_{ci}	(°K)	-1.7511e-008	1.0000e-001	3.0665e-018
T_{co}	(°K)	-1.7511e-008	1.0000e-001	3.0665e-018
t_1	(s)	2.0058e-004	1.0000e-005	4.0233e-018

t_2	(s)	-2.0058e-004	1.0000e-005	4.0233e-018
M_{h1}	(kg)	0.0000e+000	1.0000e-005	0.0000e+000
M_{h2}	(kg)	0.0000e+000	1.0000e-005	0.0000e+000
M_{c1}	(kg)	-8.3575e-001	1.0000e-005	6.9849e-011
M_{c2}	(kg)	8.3575e-001	1.0000e-005	6.9849e-011
P_{hi}	(MPa)	0.0000e+000	5.1710e-003	0.0000e+000
P_{ho}	(MPa)	0.0000e+000	3.1026e-003	0.0000e+000
P_{ci}	(MPa)	-3.0932e-007	5.1710e-003	2.5584e-018
P_{co}	(MPa)	-3.0932e-007	3.1026e-003	9.2105e-019
L_h	(m)	0.0000e+000	1.0000e-006	0.0000e+000
W_h	(m)	0.0000e+000	1.0000e-006	0.0000e+000
Z_h	(m)	0.0000e+000	1.0000e-006	0.0000e+000
L_c	(m)	0.0000e+000	1.0000e-006	0.0000e+000
W_c	(m)	0.0000e+000	1.0000e-006	0.0000e+000
Z_c	(m)	0.0000e+000	1.0000e-006	0.0000e+000
T_r	(°K)	0.0000e+000	1.0000e-002	0.0000e+000
P_r	(MPa)	0.0000e+000	1.0000e-003	0.0000e+000

^^

```
Cmax      (kW/°K)= 0.001003
FLUCTUATION   = 0.000012
UNCERTAINTY   = 1.178511
```
^^

Uncertainty Pretest for C_h (kW/°K)

INPUT PAR.		SENS. COEFF.	MEAS. UNCER.	Contributor
T_{hi}	(°K)	1.6150e-008	1.0000e-001	2.6081e-018
T_{ho}	(°K)	1.6150e-008	1.0000e-001	2.6081e-018
T_{ci}	(°K)	0.0000e+000	1.0000e-001	0.0000e+000
T_{co}	(°K)	0.0000e+000	1.0000e-001	0.0000e+000
t_1	(s)	8.3615e-005	1.0000e-005	6.9914e-019
t_2	(s)	-8.3615e-005	1.0000e-005	6.9914e-019
M_{h1}	(kg)	-8.3615e-001	1.0000e-005	6.9914e-011
M_{h2}	(kg)	8.3615e-001	1.0000e-005	6.9914e-011
M_{c1}	(kg)	0.0000e+000	1.0000e-005	0.0000e+000
M_{c2}	(kg)	0.0000e+000	1.0000e-005	0.0000e+000
P_{hi}	(MPa)	-1.1321e-007	5.1710e-003	3.4271e-019
P_{ho}	(MPa)	-1.1321e-007	3.1026e-003	1.2338e-019
P_{ci}	(MPa)	0.0000e+000	5.1710e-003	0.0000e+000
P_{co}	(MPa)	0.0000e+000	3.1026e-003	0.0000e+000
L_h	(m)	0.0000e+000	1.0000e-006	0.0000e+000
W_h	(m)	0.0000e+000	1.0000e-006	0.0000e+000
Z_h	(m)	0.0000e+000	1.0000e-006	0.0000e+000
L_c	(m)	0.0000e+000	1.0000e-006	0.0000e+000
W_c	(m)	0.0000e+000	1.0000e-006	0.0000e+000
Z_c	(m)	0.0000e+000	1.0000e-006	0.0000e+000
T_r	(°K)	0.0000e+000	1.0000e-002	0.0000e+000
P_r	(MPa)	0.0000e+000	1.0000e-003	0.0000e+000

```
^^^^^^^^^^^^^^^^^^^^^^^^^^^^^^^^^^^^^^^^^^^^^^^^^^^^^^^^^^^^^^^
```
C_h (kW/°K)= 0.000418
 FLUCTUATION   = 0.000012
 UNCERTAINTY   = 2.828427
```
^^^^^^^^^^^^^^^^^^^^^^^^^^^^^^^^^^^^^^^^^^^^^^^^^^^^^^^^^^^^^^^
-------------------------------------------------------------
```
             Uncertainty Pretest for C_c (kW/°K)
```
-------------------------------------------------------------
```
INPUT PAR.   SENS. COEFF.   MEAS. UNCER.   Contributor
```
-------------------------------------------------------------
```

INPUT PAR.		SENS. COEFF.	MEAS. UNCER.	Contributor
T_{hi}	(°K)	0.0000e+000	1.0000e-001	0.0000e+000
T_{ho}	(°K)	0.0000e+000	1.0000e-001	0.0000e+000
T_{ci}	(°K)	-1.7511e-008	1.0000e-001	3.0665e-018
T_{co}	(°K)	-1.7511e-008	1.0000e-001	3.0665e-018
t_1	(s)	2.0058e-004	1.0000e-005	4.0233e-018
t_2	(s)	-2.0058e-004	1.0000e-005	4.0233e-018
M_{h1}	(kg)	0.0000e+000	1.0000e-005	0.0000e+000
M_{h2}	(kg)	0.0000e+000	1.0000e-005	0.0000e+000
M_{c1}	(kg)	-8.3575e-001	1.0000e-005	6.9849e-011
M_{c2}	(kg)	8.3575e-001	1.0000e-005	6.9849e-011
P_{hi}	(MPa)	0.0000e+000	5.1710e-003	0.0000e+000
P_{ho}	(MPa)	0.0000e+000	3.1026e-003	0.0000e+000
P_{ci}	(MPa)	-3.0932e-007	5.1710e-003	2.5584e-018
P_{co}	(MPa)	-3.0932e-007	3.1026e-003	9.2105e-019
L_h	(m)	0.0000e+000	1.0000e-006	0.0000e+000
W_h	(m)	0.0000e+000	1.0000e-006	0.0000e+000
Z_h	(m)	0.0000e+000	1.0000e-006	0.0000e+000
L_c	(m)	0.0000e+000	1.0000e-006	0.0000e+000
W_c	(m)	0.0000e+000	1.0000e-006	0.0000e+000
Z_c	(m)	0.0000e+000	1.0000e-006	0.0000e+000
T_r	(°K)	0.0000e+000	1.0000e-002	0.0000e+000
P_r	(MPa)	0.0000e+000	1.0000e-003	0.0000e+000

```
^^^^^^^^^^^^^^^^^^^^^^^^^^^^^^^^^^^^^^^^^^^^^^^^^^^^^^^^^^^^^^^
```
C_c (kW/°K)= 0.001003
 FLUCTUATION   = 0.000012
 UNCERTAINTY   = 1.178511
```
^^^^^^^^^^^^^^^^^^^^^^^^^^^^^^^^^^^^^^^^^^^^^^^^^^^^^^^^^^^^^^^
-------------------------------------------------------------
```
             Uncertainty Pretest for C_r
```
-------------------------------------------------------------
```
INPUT PAR.   SENS. COEFF.   MEAS. UNCER.   Contributor
```
-------------------------------------------------------------
```

INPUT PAR.		SENS. COEFF.	MEAS. UNCER.	Contributor
T_{hi}	(°K)	1.6103e-005	1.0000e-001	2.5930e-012
T_{ho}	(°K)	1.6103e-005	1.0000e-001	2.5930e-012
T_{ci}	(°K)	7.2787e-006	1.0000e-001	5.2980e-013
T_{co}	(°K)	7.2787e-006	1.0000e-001	5.2980e-013
t_1	(s)	-2.7756e-012	1.0000e-005	7.7037e-034
t_2	(s)	-9.2519e-013	1.0000e-005	8.5597e-035
M_{h1}	(kg)	-8.3372e+002	1.0000e-005	6.9510e-005
M_{h2}	(kg)	8.3372e+002	1.0000e-005	6.9510e-005

```
M_c1    (kg)   3.4741e+002        1.0000e-005      1.2070e-005
M_c2    (kg)  -3.4741e+002        1.0000e-005      1.2070e-005
P_hi    (MPa) -1.1288e-004        5.1710e-003      3.4073e-013
P_ho    (MPa) -1.1288e-004        3.1026e-003      1.2266e-013
P_ci    (MPa)  1.2857e-004        5.1710e-003      4.4201e-013
P_co    (MPa)  1.2857e-004        3.1026e-003      1.5913e-013
L_h     (m)    0.0000e+000        1.0000e-006      0.0000e+000
W_h     (m)    0.0000e+000        1.0000e-006      0.0000e+000
Z_h     (m)    0.0000e+000        1.0000e-006      0.0000e+000
L_c     (m)    0.0000e+000        1.0000e-006      0.0000e+000
W_c     (m)    0.0000e+000        1.0000e-006      0.0000e+000
Z_c     (m)    0.0000e+000        1.0000e-006      0.0000e+000
T_r     (°K)   0.0000e+000        1.0000e-002      0.0000e+000
P_r     (MPa)  0.0000e+000        1.0000e-003      0.0000e+000
^^^^^^^^^^^^^^^^^^^^^^^^^^^^^^^^^^^^^^^^^^^^^^^^^^^^^^^^^^^^^^^^^

C_r          = 0.416862
FLUCTUATION  = 0.012773
UNCERTAINTY  = 3.064168
^^^^^^^^^^^^^^^^^^^^^^^^^^^^^^^^^^^^^^^^^^^^^^^^^^^^^^^^^^^^^^^^^

-----------------------------------------------------------------
            Uncertainty Pretest for q_h        (kW)
-----------------------------------------------------------------
INPUT PAR.   SENS. COEFF.      MEAS. UNCER.   Contributor
-----------------------------------------------------------------

T_hi    (°K)   4.1855e-004        1.0000e-001      1.7519e-009
T_ho    (°K)  -4.1760e-004        1.0000e-001      1.7439e-009
T_ci    (°K)   0.0000e+000        1.0000e-001      0.0000e+000
T_co    (°K)   0.0000e+000        1.0000e-001      0.0000e+000
t_1     (s)    2.4750e-003        1.0000e-005      6.1256e-016
t_2     (s)   -2.4750e-003        1.0000e-005      6.1256e-016
M_h1    (kg)  -2.4750e+001        1.0000e-005      6.1256e-008
M_h2    (kg)   2.4750e+001        1.0000e-005      6.1256e-008
M_c1    (kg)   0.0000e+000        1.0000e-005      0.0000e+000
M_c2    (kg)   0.0000e+000        1.0000e-005      0.0000e+000
P_hi    (MPa) -3.3510e-006        5.1710e-003      3.0027e-016
P_ho    (MPa) -3.3510e-006        3.1026e-003      1.0810e-016
P_ci    (MPa)  0.0000e+000        5.1710e-003      0.0000e+000
P_co    (MPa)  0.0000e+000        3.1026e-003      0.0000e+000
L_h     (m)    0.0000e+000        1.0000e-006      0.0000e+000
W_h     (m)    0.0000e+000        1.0000e-006      0.0000e+000
Z_h     (m)    0.0000e+000        1.0000e-006      0.0000e+000
L_c     (m)    0.0000e+000        1.0000e-006      0.0000e+000
W_c     (m)    0.0000e+000        1.0000e-006      0.0000e+000
Z_c     (m)    0.0000e+000        1.0000e-006      0.0000e+000
T_r     (°K)   0.0000e+000        1.0000e-002      0.0000e+000
P_r     (MPa)  0.0000e+000        1.0000e-003      0.0000e+000
^^^^^^^^^^^^^^^^^^^^^^^^^^^^^^^^^^^^^^^^^^^^^^^^^^^^^^^^^^^^^^^^^

q_h         (kW)= 0.012375
FLUCTUATION  = 0.000355
UNCERTAINTY  = 2.868496
```

```
^^^^^^^^^^^^^^^^^^^^^^^^^^^^^^^^^^^^^^^^^^^^^^^^^^^^^^^^^^^^^^^^^^^^^
-----------------------------------------------------------------
              Uncertainty Pretest for qc        (kW)
-----------------------------------------------------------------
INPUT PAR.    SENS. COEFF.      MEAS. UNCER.   Contributor
-----------------------------------------------------------------
```

INPUT PAR.		SENS. COEFF.	MEAS. UNCER.	Contributor
T_{hi}	(°K)	0.0000e+000	1.0000e-001	0.0000e+000
T_{ho}	(°K)	0.0000e+000	1.0000e-001	0.0000e+000
T_{ci}	(°K)	−1.0034e-003	1.0000e-001	1.0069e-008
T_{co}	(°K)	1.0024e-003	1.0000e-001	1.0048e-008
t_1	(s)	6.0174e-003	1.0000e-005	3.6210e-015
t_2	(s)	−6.0174e-003	1.0000e-005	3.6210e-015
M_{h1}	(kg)	0.0000e+000	1.0000e-005	0.0000e+000
M_{h2}	(kg)	0.0000e+000	1.0000e-005	0.0000e+000
M_{c1}	(kg)	−2.5073e+001	1.0000e-005	6.2864e-008
M_{c2}	(kg)	2.5073e+001	1.0000e-005	6.2864e-008
P_{hi}	(MPa)	0.0000e+000	5.1710e-003	0.0000e+000
P_{ho}	(MPa)	0.0000e+000	3.1026e-003	0.0000e+000
P_{ci}	(MPa)	−9.2797e-006	5.1710e-003	2.3026e-015
P_{co}	(MPa)	−9.2797e-006	3.1026e-003	8.2895e-016
L_h	(m)	0.0000e+000	1.0000e-006	0.0000e+000
W_h	(m)	0.0000e+000	1.0000e-006	0.0000e+000
Z_h	(m)	0.0000e+000	1.0000e-006	0.0000e+000
L_c	(m)	0.0000e+000	1.0000e-006	0.0000e+000
W_c	(m)	0.0000e+000	1.0000e-006	0.0000e+000
Z_c	(m)	0.0000e+000	1.0000e-006	0.0000e+000
T_r	(°K)	0.0000e+000	1.0000e-002	0.0000e+000
P_r	(MPa)	0.0000e+000	1.0000e-003	0.0000e+000

```
^^^^^^^^^^^^^^^^^^^^^^^^^^^^^^^^^^^^^^^^^^^^^^^^^^^^^^^^^^^^^^^^^^^^^

qc          (kW)= 0.030087
 FLUCTUATION    = 0.000382
 UNCERTAINTY    = 1.269296
^^^^^^^^^^^^^^^^^^^^^^^^^^^^^^^^^^^^^^^^^^^^^^^^^^^^^^^^^^^^^^^^^^^^^
-----------------------------------------------------------------
              Uncertainty Pretest for qavg       (kW)
-----------------------------------------------------------------
INPUT PAR.    SENS. COEFF.      MEAS. UNCER.   Contributor
-----------------------------------------------------------------
```

INPUT PAR.		SENS. COEFF.	MEAS. UNCER.	Contributor
T_{hi}	(°K)	2.0928e-004	1.0000e-001	4.3796e-010
T_{ho}	(°K)	−2.0880e-004	1.0000e-001	4.3596e-010
T_{ci}	(°K)	−5.0172e-004	1.0000e-001	2.5172e-009
T_{co}	(°K)	5.0119e-004	1.0000e-001	2.5119e-009
t_1	(s)	4.2462e-003	1.0000e-005	1.8030e-015
t_2	(s)	−4.2462e-003	1.0000e-005	1.8030e-015
M_{h1}	(kg)	−1.2375e+001	1.0000e-005	1.5314e-008
M_{h2}	(kg)	1.2375e+001	1.0000e-005	1.5314e-008
M_{c1}	(kg)	−1.2536e+001	1.0000e-005	1.5716e-008
M_{c2}	(kg)	1.2536e+001	1.0000e-005	1.5716e-008
P_{hi}	(MPa)	−1.6755e-006	5.1710e-003	7.5067e-017
P_{ho}	(MPa)	−1.6755e-006	3.1026e-003	2.7025e-017

```
Pci   (MPa)   -4.6398e-006      5.1710e-003      5.7564e-016
Pco   (MPa)   -4.6398e-006      3.1026e-003      2.0724e-016
Lh    (m)     0.0000e+000       1.0000e-006      0.0000e+000
Wh    (m)     0.0000e+000       1.0000e-006      0.0000e+000
Zh    (m)     0.0000e+000       1.0000e-006      0.0000e+000
Lc    (m)     0.0000e+000       1.0000e-006      0.0000e+000
Wc    (m)     0.0000e+000       1.0000e-006      0.0000e+000
Zc    (m)     0.0000e+000       1.0000e-006      0.0000e+000
Tr    (°K)    0.0000e+000       1.0000e-002      0.0000e+000
Pr    (MPa)   0.0000e+000       1.0000e-003      0.0000e+000
```

q_{avg} and its subscripts:

P_{ci}, P_{co}, L_h, W_h, Z_h, L_c, W_c, Z_c, T_r, P_r

```
^^^^^^^^^^^^^^^^^^^^^^^^^^^^^^^^^^^^^^^^^^^^^^^^^^^^^^^^^^^^^^^^

 q_avg       (kW)= 0.021231
 FLUCTUATION   = 0.000261
 UNCERTAINTY   = 1.227903
^^^^^^^^^^^^^^^^^^^^^^^^^^^^^^^^^^^^^^^^^^^^^^^^^^^^^^^^^^^^^^^^

----------------------------------------------------------------
          Uncertainty Pretest for q_max        (kW)
----------------------------------------------------------------

INPUT PAR.   SENS. COEFF.     MEAS. UNCER.   Contributor
----------------------------------------------------------------

 Thi   (°K)   4.1888e-004      1.0000e-001      1.7546e-009
 Tho   (°K)   8.0748e-007      1.0000e-001      6.5203e-015
 Tci   (°K)  -4.1807e-004      1.0000e-001      1.7479e-009
 Tco   (°K)   0.0000e+000      1.0000e-001      0.0000e+000
 t1    (s)    4.1807e-003      1.0000e-005      1.7479e-015
 t2    (s)   -4.1807e-003      1.0000e-005      1.7479e-015
 Mh1   (kg)  -4.1807e+001      1.0000e-005      1.7479e-007
 Mh2   (kg)   4.1807e+001      1.0000e-005      1.7479e-007
 Mc1   (kg)   0.0000e+000      1.0000e-005      0.0000e+000
 Mc2   (kg)   0.0000e+000      1.0000e-005      0.0000e+000
 Phi   (MPa) -5.6605e-006      5.1710e-003      8.5677e-016
 Pho   (MPa) -5.6605e-006      3.1026e-003      3.0845e-016
 Pci   (MPa)  0.0000e+000      5.1710e-003      0.0000e+000
 Pco   (MPa)  0.0000e+000      3.1026e-003      0.0000e+000
 Lh    (m)    0.0000e+000      1.0000e-006      0.0000e+000
 Wh    (m)    0.0000e+000      1.0000e-006      0.0000e+000
 Zh    (m)    0.0000e+000      1.0000e-006      0.0000e+000
 Lc    (m)    0.0000e+000      1.0000e-006      0.0000e+000
 Wc    (m)    0.0000e+000      1.0000e-006      0.0000e+000
 Zc    (m)    0.0000e+000      1.0000e-006      0.0000e+000
 Tr    (°K)   0.0000e+000      1.0000e-002      0.0000e+000
 Pr    (MPa)  0.0000e+000      1.0000e-003      0.0000e+000
^^^^^^^^^^^^^^^^^^^^^^^^^^^^^^^^^^^^^^^^^^^^^^^^^^^^^^^^^^^^^^^^

 q_max       (kW)= 0.020904
 FLUCTUATION   = 0.000594
 UNCERTAINTY   = 2.842561
^^^^^^^^^^^^^^^^^^^^^^^^^^^^^^^^^^^^^^^^^^^^^^^^^^^^^^^^^^^^^^^^

----------------------------------------------------------------
          Uncertainty Pretest for EFFECTIVENESS
----------------------------------------------------------------
```

```
INPUT PAR.    SENS. COEFF.      MEAS. UNCER.    Contributor
------------------------------------------------------------
```

INPUT PAR.		SENS. COEFF.	MEAS. UNCER.	Contributor
T_{hi}	(°K)	8.4933e-005	1.0000e-001	7.2136e-011
T_{ho}	(°K)	8.4933e-005	1.0000e-001	7.2136e-011
T_{ci}	(°K)	1.2870e-004	1.0000e-001	1.6563e-010
T_{co}	(°K)	1.2870e-004	1.0000e-001	1.6563e-010
t_1	(s)	-4.8615e-002	1.0000e-005	2.3634e-013
t_2	(s)	4.8615e-002	1.0000e-005	2.3634e-013
M_{h1}	(kg)	7.0913e+002	1.0000e-005	5.0287e-005
M_{h2}	(kg)	-7.0913e+002	1.0000e-005	5.0287e-005
M_{c1}	(kg)	-9.2946e+001	1.0000e-005	8.6390e-007
M_{c2}	(kg)	9.2946e+001	1.0000e-005	8.6390e-007
P_{hi}	(MPa)	1.4570e-004	5.1710e-003	5.6767e-013
P_{ho}	(MPa)	1.4570e-004	3.1026e-003	2.0437e-013
P_{ci}	(MPa)	1.5769e-005	5.1710e-003	6.6491e-015
P_{co}	(MPa)	1.5769e-005	3.1026e-003	2.3937e-015
L_h	(m)	6.1922e+000	1.0000e-006	3.8344e-011
W_h	(m)	2.4591e+002	1.0000e-006	6.0472e-008
Z_h	(m)	-1.4755e+003	1.0000e-006	2.1770e-006
L_c	(m)	5.9614e+000	1.0000e-006	3.5539e-011
W_c	(m)	2.3674e+002	1.0000e-006	5.6048e-008
Z_c	(m)	-1.4205e+003	1.0000e-006	2.0177e-006
T_r	(°K)	0.0000e+000	1.0000e-002	0.0000e+000
P_r	(MPa)	0.0000e+000	1.0000e-003	0.0000e+000

```
^^^^^^^^^^^^^^^^^^^^^^^^^^^^^^^^^^^^^^^^^^^^^^^^^^^^^^^^^^^^^^

EFFECTIVENESS = 0.785773
FLUCTUATION   = 0.010325
UNCERTAINTY   = 1.314037
^^^^^^^^^^^^^^^^^^^^^^^^^^^^^^^^^^^^^^^^^^^^^^^^^^^^^^^^^^^^^^

------------------------------------------------------------
              Uncertainty Pretest for NTU
------------------------------------------------------------
INPUT PAR.    SENS. COEFF.      MEAS. UNCER.    Contributor
------------------------------------------------------------
```

INPUT PAR.		SENS. COEFF.	MEAS. UNCER.	Contributor
T_{hi}	(°K)	8.1283e-004	1.0000e-001	6.6069e-009
T_{ho}	(°K)	8.1283e-004	1.0000e-001	6.6069e-009
T_{ci}	(°K)	1.1900e-003	1.0000e-001	1.4160e-008
T_{co}	(°K)	1.1900e-003	1.0000e-001	1.4160e-008
t_1	(s)	-4.4279e-001	1.0000e-005	1.9607e-011
t_2	(s)	4.4279e-001	1.0000e-005	1.9607e-011
M_{h1}	(kg)	4.4301e+003	1.0000e-005	1.9626e-003
M_{h2}	(kg)	-4.4301e+003	1.0000e-005	1.9626e-003
M_{c1}	(kg)	0.0000e+000	1.0000e-005	0.0000e+000
M_{c2}	(kg)	0.0000e+000	1.0000e-005	0.0000e+000
P_{hi}	(MPa)	1.0520e-003	5.1710e-003	2.9595e-011
P_{ho}	(MPa)	1.0520e-003	3.1026e-003	1.0654e-011
P_{ci}	(MPa)	4.5693e-004	5.1710e-003	5.5827e-012
P_{co}	(MPa)	4.5693e-004	3.1026e-003	2.0098e-012
L_h	(m)	5.6400e+001	1.0000e-006	3.1810e-009
W_h	(m)	2.2398e+003	1.0000e-006	5.0167e-006

```
Zₕ     (m)    -1.3439e+004    1.0000e-006    1.8060e-004
L_c    (m)     5.4298e+001    1.0000e-006    2.9483e-009
W_c    (m)     2.1563e+003    1.0000e-006    4.6497e-006
Z_c    (m)    -1.2938e+004    1.0000e-006    1.6739e-004
T_r    (°K)    0.0000e+000    1.0000e-002    0.0000e+000
P_r    (MPa)   0.0000e+000    1.0000e-003    0.0000e+000
```

Z_h (m) $-1.3439e+004$ $1.0000e-006$ $1.8060e-004$
L_c (m) $5.4298e+001$ $1.0000e-006$ $2.9483e-009$
W_c (m) $2.1563e+003$ $1.0000e-006$ $4.6497e-006$
Z_c (m) $-1.2938e+004$ $1.0000e-006$ $1.6739e-004$
T_r (°K) $0.0000e+000$ $1.0000e-002$ $0.0000e+000$
P_r (MPa) $0.0000e+000$ $1.0000e-003$ $0.0000e+000$

^^^

NTU   = 2.213971
FLUCTUATION   = 0.065443
UNCERTAINTY   = 2.955930

^^^

              Uncertainty Pretest for U (W/m^2.°K)

INPUT PAR.   SENS. COEFF.   MEAS. UNCER.   Contributor

INPUT PAR.		SENS. COEFF.	MEAS. UNCER.	Contributor
T_{hi}	(°K)	1.5649e+001	1.0000e-001	2.4489e+000
T_{ho}	(°K)	1.5649e+001	1.0000e-001	2.4489e+000
T_{ci}	(°K)	2.0729e+001	1.0000e-001	4.2968e+000
T_{co}	(°K)	2.0729e+001	1.0000e-001	4.2968e+000
t_1	(s)	0.0000e+000	1.0000e-005	0.0000e+000
t_2	(s)	0.0000e+000	1.0000e-005	0.0000e+000
M_{h1}	(kg)	0.0000e+000	1.0000e-005	0.0000e+000
M_{h2}	(kg)	0.0000e+000	1.0000e-005	0.0000e+000
M_{c1}	(kg)	0.0000e+000	1.0000e-005	0.0000e+000
M_{c2}	(kg)	0.0000e+000	1.0000e-005	0.0000e+000
P_{hi}	(MPa)	7.8827e+000	5.1710e-003	1.6615e-003
P_{ho}	(MPa)	7.8826e+000	3.1026e-003	5.9815e-004
P_{ci}	(MPa)	7.9596e+000	5.1710e-003	1.6941e-003
P_{co}	(MPa)	7.9596e+000	3.1026e-003	6.0988e-004
L_h	(m)	9.8248e+005	1.0000e-006	9.6526e-001
W_h	(m)	3.9017e+007	1.0000e-006	1.5223e+003
Z_h	(m)	-2.3410e+008	1.0000e-006	5.4803e+004
L_c	(m)	-9.8248e+005	1.0000e-006	9.6526e-001
W_c	(m)	-2.6715e+007	1.0000e-006	7.1371e+002
Z_c	(m)	-2.2538e+008	1.0000e-006	5.0794e+004
T_r	(°K)	0.0000e+000	1.0000e-002	0.0000e+000
P_r	(MPa)	0.0000e+000	1.0000e-003	0.0000e+000

^^^

U (W/m^2.°K)= 38566.764413
FLUCTUATION   = 328.403449
UNCERTAINTY   = 0.851519

^^^

              Uncertainty Pretest for Re_h

INPUT PAR.   SENS. COEFF.   MEAS. UNCER.   Contributor

INPUT PAR.		SENS. COEFF.	MEAS. UNCER.	Contributor
T_{hi}	(°K)	3.0105e-001	1.0000e-001	9.0634e-004
T_{ho}	(°K)	3.0105e-001	1.0000e-001	9.0634e-004
T_{ci}	(°K)	0.0000e+000	1.0000e-001	0.0000e+000

T_{co}	(°K)	0.0000e+000	1.0000e-001	0.0000e+000
t_1	(s)	7.5699e+000	1.0000e-005	5.7303e-009
t_2	(s)	-7.5699e+000	1.0000e-005	5.7303e-009
M_{h1}	(kg)	-7.5699e+004	1.0000e-005	5.7303e-001
M_{h2}	(kg)	7.5699e+004	1.0000e-005	5.7303e-001
M_{c1}	(kg)	0.0000e+000	1.0000e-005	0.0000e+000
M_{c2}	(kg)	0.0000e+000	1.0000e-005	0.0000e+000
P_{hi}	(MPa)	-8.4083e-003	5.1710e-003	1.8904e-009
P_{ho}	(MPa)	-8.4083e-003	3.1026e-003	6.8058e-010
P_{ci}	(MPa)	0.0000e+000	5.1710e-003	0.0000e+000
P_{co}	(MPa)	0.0000e+000	3.1026e-003	0.0000e+000
L_h	(m)	0.0000e+000	1.0000e-006	0.0000e+000
W_h	(m)	-5.4070e+004	1.0000e-006	2.9236e-003
Z_h	(m)	-5.4070e+004	1.0000e-006	2.9236e-003
L_c	(m)	0.0000e+000	1.0000e-006	0.0000e+000
W_c	(m)	0.0000e+000	1.0000e-006	0.0000e+000
Z_c	(m)	0.0000e+000	1.0000e-006	0.0000e+000
T_r	(°K)	0.0000e+000	1.0000e-002	0.0000e+000
P_r	(MPa)	0.0000e+000	1.0000e-003	0.0000e+000

^^

```
Re_h          = 37.849347
FLUCTUATION   = 1.074113
UNCERTAINTY   = 2.837864
```
^^

Uncertainty Pretest for Re_c

INPUT PAR.		SENS. COEFF.	MEAS. UNCER.	Contributor
T_{hi}	(°K)	0.0000e+000	1.0000e-001	0.0000e+000
T_{ho}	(°K)	0.0000e+000	1.0000e-001	0.0000e+000
T_{ci}	(°K)	6.3405e-001	1.0000e-001	4.0202e-003
T_{co}	(°K)	6.3405e-001	1.0000e-001	4.0202e-003
t_1	(s)	1.2676e+001	1.0000e-005	1.6067e-008
t_2	(s)	-1.2676e+001	1.0000e-005	1.6067e-008
M_{h1}	(kg)	0.0000e+000	1.0000e-005	0.0000e+000
M_{h2}	(kg)	0.0000e+000	1.0000e-005	0.0000e+000
M_{c1}	(kg)	-5.2815e+004	1.0000e-005	2.7895e-001
M_{c2}	(kg)	5.2815e+004	1.0000e-005	2.7895e-001
P_{hi}	(MPa)	0.0000e+000	5.1710e-003	0.0000e+000
P_{ho}	(MPa)	0.0000e+000	3.1026e-003	0.0000e+000
P_{ci}	(MPa)	-2.7366e-003	5.1710e-003	2.0025e-010
P_{co}	(MPa)	-2.7365e-003	3.1026e-003	7.2088e-011
L_h	(m)	0.0000e+000	1.0000e-006	0.0000e+000
W_h	(m)	0.0000e+000	1.0000e-006	0.0000e+000
Z_h	(m)	0.0000e+000	1.0000e-006	0.0000e+000
L_c	(m)	0.0000e+000	1.0000e-006	0.0000e+000
W_c	(m)	-9.0541e+004	1.0000e-006	8.1976e-003
Z_c	(m)	-9.0541e+004	1.0000e-006	8.1976e-003
T_r	(°K)	0.0000e+000	1.0000e-002	0.0000e+000

```
 Pr    (MPa)    0.0000e+000         1.0000e-003       0.0000e+000
^^^^^^^^^^^^^^^^^^^^^^^^^^^^^^^^^^^^^^^^^^^^^^^^^^^^^^^^^^^^^^^^^^^
```

Re_c = 63.378440
FLUCTUATION   = 0.763104
UNCERTAINTY   = 1.204044
```
^^^^^^^^^^^^^^^^^^^^^^^^^^^^^^^^^^^^^^^^^^^^^^^^^^^^^^^^^^^^^^^^^^^
```

Uncertainty Pretest for Re_{avg}

INPUT PAR.		SENS. COEFF.	MEAS. UNCER.	Contributor
T_{hi}	(°K)	1.5053e-001	1.0000e-001	2.2658e-004
T_{ho}	(°K)	1.5053e-001	1.0000e-001	2.2658e-004
T_{ci}	(°K)	3.1703e-001	1.0000e-001	1.0051e-003
T_{co}	(°K)	3.1703e-001	1.0000e-001	1.0051e-003
t_1	(s)	1.0123e+001	1.0000e-005	1.0247e-008
t_2	(s)	-1.0123e+001	1.0000e-005	1.0247e-008
M_{h1}	(kg)	-3.7849e+004	1.0000e-005	1.4326e-001
M_{h2}	(kg)	3.7849e+004	1.0000e-005	1.4326e-001
M_{c1}	(kg)	-2.6408e+004	1.0000e-005	6.9737e-002
M_{c2}	(kg)	2.6408e+004	1.0000e-005	6.9737e-002
P_{hi}	(MPa)	-4.2041e-003	5.1710e-003	4.7261e-010
P_{ho}	(MPa)	-4.2041e-003	3.1026e-003	1.7014e-010
P_{ci}	(MPa)	-1.3682e-003	5.1710e-003	5.0058e-011
P_{co}	(MPa)	-1.3681e-003	3.1026e-003	1.8018e-011
L_h	(m)	0.0000e+000	1.0000e-006	0.0000e+000
W_h	(m)	-2.7035e+004	1.0000e-006	7.3090e-004
Z_h	(m)	-2.7035e+004	1.0000e-006	7.3090e-004
L_c	(m)	0.0000e+000	1.0000e-006	0.0000e+000
W_c	(m)	-4.5270e+004	1.0000e-006	2.0494e-003
Z_c	(m)	-4.5270e+004	1.0000e-006	2.0494e-003
T_r	(°K)	0.0000e+000	1.0000e-002	0.0000e+000
P_r	(MPa)	0.0000e+000	1.0000e-003	0.0000e+000

```
^^^^^^^^^^^^^^^^^^^^^^^^^^^^^^^^^^^^^^^^^^^^^^^^^^^^^^^^^^^^^^^^^^^
```

Re_{avg} = 50.613893
```
FLUCTUATION   = 0.658796
UNCERTAINTY   = 1.301610
```
```
^^^^^^^^^^^^^^^^^^^^^^^^^^^^^^^^^^^^^^^^^^^^^^^^^^^^^^^^^^^^^^^^^^^
```

Uncertainty Pretest for H_c h_{h_i} (kJ/kg)

INPUT PAR.		SENS. COEFF.	MEAS. UNCER.	Contributor
T_{hi}	(°K)	4.1876e+000	1.0000e-001	1.7536e-001
T_{ho}	(°K)	0.0000e+000	1.0000e-001	0.0000e+000
T_{ci}	(°K)	0.0000e+000	1.0000e-001	0.0000e+000
T_{co}	(°K)	0.0000e+000	1.0000e-001	0.0000e+000
t_1	(s)	0.0000e+000	1.0000e-005	0.0000e+000
t_2	(s)	0.0000e+000	1.0000e-005	0.0000e+000
M_{h1}	(kg)	0.0000e+000	1.0000e-005	0.0000e+000

```
M_{h2}   (kg)   0.0000e+000        1.0000e-005        0.0000e+000
M_{c1}   (kg)   0.0000e+000        1.0000e-005        0.0000e+000
M_{c2}   (kg)   0.0000e+000        1.0000e-005        0.0000e+000
P_{hi}   (MPa)  8.1806e-001        5.1710e-003        1.7895e-005
P_{ho}   (MPa)  0.0000e+000        3.1026e-003        0.0000e+000
P_{ci}   (MPa)  0.0000e+000        5.1710e-003        0.0000e+000
P_{co}   (MPa)  0.0000e+000        3.1026e-003        0.0000e+000
L_h      (m)    0.0000e+000        1.0000e-006        0.0000e+000
W_h      (m)    0.0000e+000        1.0000e-006        0.0000e+000
Z_h      (m)    0.0000e+000        1.0000e-006        0.0000e+000
L_c      (m)    0.0000e+000        1.0000e-006        0.0000e+000
W_c      (m)    0.0000e+000        1.0000e-006        0.0000e+000
Z_c      (m)    0.0000e+000        1.0000e-006        0.0000e+000
T_r      (°K)   0.0000e+000        1.0000e-002        0.0000e+000
P_r      (MPa)  0.0000e+000        1.0000e-003        0.0000e+000
^^^^^^^^^^^^^^^^^^^^^^^^^^^^^^^^^^^^^^^^^^^^^^^^^^^^^^^^^^^^^^^^^^
```

h_{h_i} (kJ/kg)= 292.578819
FLUCTUATION   = 0.418786
UNCERTAINTY   = 0.143136

```
^^^^^^^^^^^^^^^^^^^^^^^^^^^^^^^^^^^^^^^^^^^^^^^^^^^^^^^^^^^^^^^^^^

----------------------------------------------------------------
```

Uncertainty Pretest for h_{h_o} (kJ/kg)

```
----------------------------------------------------------------
INPUT PAR.   SENS. COEFF.    MEAS. UNCER.   Contributor
----------------------------------------------------------------
```

```
T_{hi}   (°K)   0.0000e+000        1.0000e-001        0.0000e+000
T_{ho}   (°K)   4.1786e+000        1.0000e-001        1.7460e-001
T_{ci}   (°K)   0.0000e+000        1.0000e-001        0.0000e+000
T_{co}   (°K)   0.0000e+000        1.0000e-001        0.0000e+000
t_1      (s)    0.0000e+000        1.0000e-005        0.0000e+000
t_2      (s)    0.0000e+000        1.0000e-005        0.0000e+000
M_{h1}   (kg)   0.0000e+000        1.0000e-005        0.0000e+000
M_{h2}   (kg)   0.0000e+000        1.0000e-005        0.0000e+000
M_{c1}   (kg)   0.0000e+000        1.0000e-005        0.0000e+000
Mc2      (kg)   0.0000e+000        1.0000e-005        0.0000e+000
P_{hi}   (MPa)  0.0000e+000        5.1710e-003        0.0000e+000
P_{ho}   (MPa)  8.8573e-001        3.1026e-003        7.5521e-006
P_{ci}   (MPa)  0.0000e+000        5.1710e-003        0.0000e+000
P_{co}   (MPa)  0.0000e+000        3.1026e-003        0.0000e+000
L_h      (m)    0.0000e+000        1.0000e-006        0.0000e+000
W_h      (m)    0.0000e+000        1.0000e-006        0.0000e+000
Z_h      (m)    0.0000e+000        1.0000e-006        0.0000e+000
L_c      (m)    0.0000e+000        1.0000e-006        0.0000e+000
W_c      (m)    0.0000e+000        1.0000e-006        0.0000e+000
Z_c      (m)    0.0000e+000        1.0000e-006        0.0000e+000
T_r      (°K)   0.0000e+000        1.0000e-002        0.0000e+000
P_r      (MPa)  0.0000e+000        1.0000e-003        0.0000e+000
^^^^^^^^^^^^^^^^^^^^^^^^^^^^^^^^^^^^^^^^^^^^^^^^^^^^^^^^^^^^^^^^^^
```

h_{h_o} (kJ/kg)= 168.661783
FLUCTUATION   = 0.417866

```
   UNCERTAINTY   = 0.247754
^^^^^^^^^^^^^^^^^^^^^^^^^^^^^^^^^^^^^^^^^^^^^^^^^^^^^^^^^^^^^^^^
---------------------------------------------------------------
          Uncertainty Pretest for Hci      (kJ/kg)
---------------------------------------------------------------
INPUT PAR.    SENS. COEFF.      MEAS. UNCER.    Contributor
---------------------------------------------------------------
 Thi   (°K)   0.0000e+000      1.0000e-001      0.0000e+000
 Tho   (°K)   0.0000e+000      1.0000e-001      0.0000e+000
 Tci   (°K)   4.1844e+000      1.0000e-001      1.7509e-001
 Tco   (°K)   0.0000e+000      1.0000e-001      0.0000e+000
 t1    (s)    0.0000e+000      1.0000e-005      0.0000e+000
 t2    (s)    0.0000e+000      1.0000e-005      0.0000e+000
 Mh1   (kg)   0.0000e+000      1.0000e-005      0.0000e+000
 Mh2   (kg)   0.0000e+000      1.0000e-005      0.0000e+000
 Mc1   (kg)   0.0000e+000      1.0000e-005      0.0000e+000
 Mc2   (kg)   0.0000e+000      1.0000e-005      0.0000e+000
 Phi   (MPa)  0.0000e+000      5.1710e-003      0.0000e+000
 Pho   (MPa)  0.0000e+000      3.1026e-003      0.0000e+000
 Pci   (MPa)  9.4145e-001      5.1710e-003      2.3700e-005
 Pco   (MPa)  0.0000e+000      3.1026e-003      0.0000e+000
 Lh    (m)    0.0000e+000      1.0000e-006      0.0000e+000
 Wh    (m)    0.0000e+000      1.0000e-006      0.0000e+000
 Zh    (m)    0.0000e+000      1.0000e-006      0.0000e+000
 Lc    (m)    0.0000e+000      1.0000e-006      0.0000e+000
 Wc    (m)    0.0000e+000      1.0000e-006      0.0000e+000
 Zc    (m)    0.0000e+000      1.0000e-006      0.0000e+000
 Tr    (°K)   0.0000e+000      1.0000e-002      0.0000e+000
 Pr    (MPa)  0.0000e+000      1.0000e-003      0.0000e+000
^^^^^^^^^^^^^^^^^^^^^^^^^^^^^^^^^^^^^^^^^^^^^^^^^^^^^^^^^^^^^^^^

 hci      (kJ/kg)= 83.536957
 FLUCTUATION    = 0.418468
 UNCERTAINTY    = 0.500938
^^^^^^^^^^^^^^^^^^^^^^^^^^^^^^^^^^^^^^^^^^^^^^^^^^^^^^^^^^^^^^^^
---------------------------------------------------------------
          Uncertainty Pretest for hco      (kJ/kg)
---------------------------------------------------------------
INPUT PAR.    SENS. COEFF.      MEAS. UNCER.    Contributor
---------------------------------------------------------------
 Thi   (°K)   0.0000e+000      1.0000e-001      0.0000e+000
 Tho   (°K)   0.0000e+000      1.0000e-001      0.0000e+000
 Tci   (°K)   0.0000e+000      1.0000e-001      0.0000e+000
 Tco   (°K)   4.1795e+000      1.0000e-001      1.7469e-001
 t1    (s)    0.0000e+000      1.0000e-005      0.0000e+000
 t2    (s)    0.0000e+000      1.0000e-005      0.0000e+000
 Mh1   (kg)   0.0000e+000      1.0000e-005      0.0000e+000
 Mh2   (kg)   0.0000e+000      1.0000e-005      0.0000e+000
 Mc1   (kg)   0.0000e+000      1.0000e-005      0.0000e+000
 Mc2   (kg)   0.0000e+000      1.0000e-005      0.0000e+000
 Phi   (MPa)  0.0000e+000      5.1710e-003      0.0000e+000
```

P_{ho}	(MPa)	0.0000e+000	3.1026e-003	0.0000e+000
P_{ci}	(MPa)	0.0000e+000	5.1710e-003	0.0000e+000
P_{co}	(MPa)	8.6285e-001	3.1026e-003	7.1669e-006
L_h	(m)	0.0000e+000	1.0000e-006	0.0000e+000
W_h	(m)	0.0000e+000	1.0000e-006	0.0000e+000
Z_h	(m)	0.0000e+000	1.0000e-006	0.0000e+000
L_c	(m)	0.0000e+000	1.0000e-006	0.0000e+000
W_c	(m)	0.0000e+000	1.0000e-006	0.0000e+000
Z_c	(m)	0.0000e+000	1.0000e-006	0.0000e+000
T_r	(°K)	0.0000e+000	1.0000e-002	0.0000e+000
P_r	(MPa)	0.0000e+000	1.0000e-003	0.0000e+000

^^

h_{c_o} (kJ/kg)= 208.778003
FLUCTUATION   = 0.417963
UNCERTAINTY   = 0.200195

^^

          Uncertainty Pretest for S_{h_i} (kJ/kg.°K)

INPUT PAR.		SENS. COEFF.	MEAS. UNCER.	Contributor
T_{hi}	(°K)	1.2209e-002	1.0000e-001	1.4906e-006
T_{ho}	(°K)	0.0000e+000	1.0000e-001	0.0000e+000
T_{ci}	(°K)	0.0000e+000	1.0000e-001	0.0000e+000
T_{co}	(°K)	0.0000e+000	1.0000e-001	0.0000e+000
t_1	(s)	0.0000e+000	1.0000e-005	0.0000e+000
t_2	(s)	0.0000e+000	1.0000e-005	0.0000e+000
M_{h1}	(kg)	0.0000e+000	1.0000e-005	0.0000e+000
M_{h2}	(kg)	0.0000e+000	1.0000e-005	0.0000e+000
M_{c1}	(kg)	0.0000e+000	1.0000e-005	0.0000e+000
M_{c2}	(kg)	0.0000e+000	1.0000e-005	0.0000e+000
P_{hi}	(MPa)	-5.9621e-004	5.1710e-003	9.5049e-012
P_{ho}	(MPa)	0.0000e+000	3.1026e-003	0.0000e+000
P_{ci}	(MPa)	0.0000e+000	5.1710e-003	0.0000e+000
P_{co}	(MPa)	0.0000e+000	3.1026e-003	0.0000e+000
L_h	(m)	0.0000e+000	1.0000e-006	0.0000e+000
W_h	(m)	0.0000e+000	1.0000e-006	0.0000e+000
Z_h	(m)	0.0000e+000	1.0000e-006	0.0000e+000
L_c	(m)	0.0000e+000	1.0000e-006	0.0000e+000
W_c	(m)	0.0000e+000	1.0000e-006	0.0000e+000
Z_c	(m)	0.0000e+000	1.0000e-006	0.0000e+000
T_r	(°K)	0.0000e+000	1.0000e-002	0.0000e+000
P_r	(MPa)	0.0000e+000	1.0000e-003	0.0000e+000

^^

S_{h_i} (kJ/kg.°K)= 0.953024
FLUCTUATION   = 0.001221
UNCERTAINTY   = 0.128107

^^

          Uncertainty Pretest for S_{h_o} (kJ/kg.°K)

```
--------------------------------------------------------------
INPUT PAR.    SENS. COEFF.      MEAS. UNCER.   Contributor
--------------------------------------------------------------
```

INPUT PAR.		SENS. COEFF.	MEAS. UNCER.	Contributor
T_{hi}	(°K)	0.0000e+000	1.0000e-001	0.0000e+000
T_{ho}	(°K)	1.3333e-002	1.0000e-001	1.7777e-006
T_{ci}	(°K)	0.0000e+000	1.0000e-001	0.0000e+000
T_{co}	(°K)	0.0000e+000	1.0000e-001	0.0000e+000
t_1	(s)	0.0000e+000	1.0000e-005	0.0000e+000
t_2	(s)	0.0000e+000	1.0000e-005	0.0000e+000
M_{h1}	(kg)	0.0000e+000	1.0000e-005	0.0000e+000
M_{h2}	(kg)	0.0000e+000	1.0000e-005	0.0000e+000
M_{c1}	(kg)	0.0000e+000	1.0000e-005	0.0000e+000
M_{c2}	(kg)	0.0000e+000	1.0000e-005	0.0000e+000
P_{hi}	(MPa)	0.0000e+000	5.1710e-003	0.0000e+000
P_{ho}	(MPa)	−3.8993e-004	3.1026e-003	1.4636e-012
P_{ci}	(MPa)	0.0000e+000	5.1710e-003	0.0000e+000
P_{co}	(MPa)	0.0000e+000	3.1026e-003	0.0000e+000
L_h	(m)	0.0000e+000	1.0000e-006	0.0000e+000
W_h	(m)	0.0000e+000	1.0000e-006	0.0000e+000
Z_h	(m)	0.0000e+000	1.0000e-006	0.0000e+000
L_c	(m)	0.0000e+000	1.0000e-006	0.0000e+000
W_c	(m)	0.0000e+000	1.0000e-006	0.0000e+000
Z_c	(m)	0.0000e+000	1.0000e-006	0.0000e+000
T_r	(°K)	0.0000e+000	1.0000e-002	0.0000e+000
P_r	(MPa)	0.0000e+000	1.0000e-003	0.0000e+000

```
^^^^^^^^^^^^^^^^^^^^^^^^^^^^^^^^^^^^^^^^^^^^^^^^^^^^^^^^^^^^^^
```

S_{h_o} (kJ/kg.°K)= 0.575731
FLUCTUATION   = 0.001333
UNCERTAINTY   = 0.231584

```
^^^^^^^^^^^^^^^^^^^^^^^^^^^^^^^^^^^^^^^^^^^^^^^^^^^^^^^^^^^^^^

--------------------------------------------------------------
```

Uncertainty Pretest for S_{c_i} (kJ/kg.°K)

```
--------------------------------------------------------------
```

INPUT PAR.		SENS. COEFF.	MEAS. UNCER.	Contributor
T_{hi}	(°K)	0.0000e+000	1.0000e-001	0.0000e+000
T_{ho}	(°K)	0.0000e+000	1.0000e-001	0.0000e+000
T_{ci}	(°K)	1.4281e-002	1.0000e-001	2.0395e-006
T_{co}	(°K)	0.0000e+000	1.0000e-001	0.0000e+000
t_1	(s)	0.0000e+000	1.0000e-005	0.0000e+000
t_2	(s)	0.0000e+000	1.0000e-005	0.0000e+000
M_{h1}	(kg)	0.0000e+000	1.0000e-005	0.0000e+000
M_{h2}	(kg)	0.0000e+000	1.0000e-005	0.0000e+000
M_{c1}	(kg)	0.0000e+000	1.0000e-005	0.0000e+000
M_{c2}	(kg)	0.0000e+000	1.0000e-005	0.0000e+000
P_{hi}	(MPa)	0.0000e+000	5.1710e-003	0.0000e+000
P_{ho}	(MPa)	0.0000e+000	3.1026e-003	0.0000e+000
P_{ci}	(MPa)	−2.0562e-004	5.1710e-003	1.1305e-012
P_{co}	(MPa)	0.0000e+000	3.1026e-003	0.0000e+000
L_h	(m)	0.0000e+000	1.0000e-006	0.0000e+000

W_h	(m)	0.0000e+000	1.0000e-006	0.0000e+000
Z_h	(m)	0.0000e+000	1.0000e-006	0.0000e+000
L_c	(m)	0.0000e+000	1.0000e-006	0.0000e+000
W_c	(m)	0.0000e+000	1.0000e-006	0.0000e+000
Z_c	(m)	0.0000e+000	1.0000e-006	0.0000e+000
T_r	(°K)	0.0000e+000	1.0000e-002	0.0000e+000
P_r	(MPa)	0.0000e+000	1.0000e-003	0.0000e+000

```
^^^^^^^^^^^^^^^^^^^^^^^^^^^^^^^^^^^^^^^^^^^^^^^^^^^^^^^^^^^^^
```

S_{c_i} (kJ/kg.°K)= 0.294308
FLUCTUATION   = 0.001428
UNCERTAINTY   = 0.485248

```
^^^^^^^^^^^^^^^^^^^^^^^^^^^^^^^^^^^^^^^^^^^^^^^^^^^^^^^^^^^^^
-------------------------------------------------------------
```

Uncertainty Pretest for S_{c_o} (kJ/kg.°K)

```
-------------------------------------------------------------
```

INPUT PAR.		SENS. COEFF.	MEAS. UNCER.	Contributor
T_{hi}	(°K)	0.0000e+000	1.0000e-001	0.0000e+000
T_{ho}	(°K)	0.0000e+000	1.0000e-001	0.0000e+000
T_{ci}	(°K)	0.0000e+000	1.0000e-001	0.0000e+000
T_{co}	(°K)	1.2940e-002	1.0000e-001	1.6744e-006
t_1	(s)	0.0000e+000	1.0000e-005	0.0000e+000
t_2	(s)	0.0000e+000	1.0000e-005	0.0000e+000
M_{h1}	(kg)	0.0000e+000	1.0000e-005	0.0000e+000
M_{h2}	(kg)	0.0000e+000	1.0000e-005	0.0000e+000
M_{c1}	(kg)	0.0000e+000	1.0000e-005	0.0000e+000
M_{c2}	(kg)	0.0000e+000	1.0000e-005	0.0000e+000
P_{hi}	(MPa)	0.0000e+000	5.1710e-003	0.0000e+000
P_{ho}	(MPa)	0.0000e+000	3.1026e-003	0.0000e+000
P_{ci}	(MPa)	0.0000e+000	5.1710e-003	0.0000e+000
P_{co}	(MPa)	-4.6187e-004	3.1026e-003	2.0535e-012
L_h	(m)	0.0000e+000	1.0000e-006	0.0000e+000
W_h	(m)	0.0000e+000	1.0000e-006	0.0000e+000
Z_h	(m)	0.0000e+000	1.0000e-006	0.0000e+000
L_c	(m)	0.0000e+000	1.0000e-006	0.0000e+000
W_c	(m)	0.0000e+000	1.0000e-006	0.0000e+000
Z_c	(m)	0.0000e+000	1.0000e-006	0.0000e+000
T_r	(°K)	0.0000e+000	1.0000e-002	0.0000e+000
P_r	(MPa)	0.0000e+000	1.0000e-003	0.0000e+000

```
^^^^^^^^^^^^^^^^^^^^^^^^^^^^^^^^^^^^^^^^^^^^^^^^^^^^^^^^^^^^^
```

S_{c_o} (kJ/kg.°K)= 0.701816
FLUCTUATION   = 0.001294
UNCERTAINTY   = 0.184375

```
^^^^^^^^^^^^^^^^^^^^^^^^^^^^^^^^^^^^^^^^^^^^^^^^^^^^^^^^^^^^^
-------------------------------------------------------------
```

Uncertainty Pretest for E_{h_i} (kJ)

```
-------------------------------------------------------------
```

INPUT PAR.		SENS. COEFF.	MEAS. UNCER.	Contributor
T_{hi}	(°K)	5.4757e-005	1.0000e-001	2.9983e-011

T_{ho}	(°K)	0.0000e+000	1.0000e-001	0.0000e+000
T_{ci}	(°K)	0.0000e+000	1.0000e-001	0.0000e+000
T_{co}	(°K)	0.0000e+000	1.0000e-001	0.0000e+000
t_1	(s)	2.5991e-004	1.0000e-005	6.7553e-018
t_2	(s)	-2.5991e-004	1.0000e-005	6.7553e-018
M_{h1}	(kg)	-2.5991e+000	1.0000e-005	6.7553e-010
M_{h2}	(kg)	2.5991e+000	1.0000e-005	6.7553e-010
M_{c1}	(kg)	0.0000e+000	1.0000e-005	0.0000e+000
M_{c2}	(kg)	0.0000e+000	1.0000e-005	0.0000e+000
P_{hi}	(MPa)	9.9582e-005	5.1710e-003	2.6516e-013
P_{ho}	(MPa)	0.0000e+000	3.1026e-003	0.0000e+000
P_{ci}	(MPa)	0.0000e+000	5.1710e-003	0.0000e+000
P_{co}	(MPa)	0.0000e+000	3.1026e-003	0.0000e+000
L_h	(m)	0.0000e+000	1.0000e-006	0.0000e+000
W_h	(m)	0.0000e+000	1.0000e-006	0.0000e+000
Z_h	(m)	0.0000e+000	1.0000e-006	0.0000e+000
L_c	(m)	0.0000e+000	1.0000e-006	0.0000e+000
W_c	(m)	0.0000e+000	1.0000e-006	0.0000e+000
Z_c	(m)	0.0000e+000	1.0000e-006	0.0000e+000
T_r	(°K)	-5.8579e-005	1.0000e-002	3.4315e-013
P_r	(MPa)	-1.0030e-004	1.0000e-003	1.0059e-014

^^

```
E_hi      (kJ)= 0.001300
FLUCTUATION   = 0.000037
UNCERTAINTY   = 2.860280
```

^^

Uncertainty Pretest for E_{h_o} (kJ)

INPUT PAR.		SENS. COEFF.	MEAS. UNCER.	Contributor

T_{hi}	(°K)	0.0000e+000	1.0000e-001	0.0000e+000
T_{ho}	(°K)	2.0333e-005	1.0000e-001	4.1343e-012
T_{ci}	(°K)	0.0000e+000	1.0000e-001	0.0000e+000
T_{co}	(°K)	0.0000e+000	1.0000e-001	0.0000e+000
t_1	(s)	3.1365e-005	1.0000e-005	9.8377e-020
t_2	(s)	-3.1365e-005	1.0000e-005	9.8377e-020
M_{h1}	(kg)	-3.1365e-001	1.0000e-005	9.8377e-012
M_{h2}	(kg)	3.1365e-001	1.0000e-005	9.8377e-012
M_{c1}	(kg)	0.0000e+000	1.0000e-005	0.0000e+000
M_{c2}	(kg)	0.0000e+000	1.0000e-005	0.0000e+000
P_{hi}	(MPa)	0.0000e+000	5.1710e-003	0.0000e+000
P_{ho}	(MPa)	1.0020e-004	3.1026e-003	9.6647e-014
P_{ci}	(MPa)	0.0000e+000	5.1710e-003	0.0000e+000
P_{co}	(MPa)	0.0000e+000	3.1026e-003	0.0000e+000
L_h	(m)	0.0000e+000	1.0000e-006	0.0000e+000
W_h	(m)	0.0000e+000	1.0000e-006	0.0000e+000
Z_h	(m)	0.0000e+000	1.0000e-006	0.0000e+000
L_c	(m)	0.0000e+000	1.0000e-006	0.0000e+000
W_c	(m)	0.0000e+000	1.0000e-006	0.0000e+000

Z_c	(m)	0.0000e+000	1.0000e-006	0.0000e+000
T_r	(°K)	-2.0850e-005	1.0000e-002	4.3472e-014
P_r	(MPa)	-1.0030e-004	1.0000e-003	1.0059e-014

^^

E_{h_o} (kJ)= 0.000157
FLUCTUATION   = 0.000005
UNCERTAINTY   = 3.121226

^^

           Uncertainty Pretest for E_{c_i} (kJ)

INPUT PAR.		SENS. COEFF.	MEAS. UNCER.	Contributor
T_{hi}	(°K)	0.0000e+000	1.0000e-001	0.0000e+000
T_{ho}	(°K)	0.0000e+000	1.0000e-001	0.0000e+000
T_{ci}	(°K)	-1.7652e-005	1.0000e-001	3.1158e-012
T_{co}	(°K)	0.0000e+000	1.0000e-001	0.0000e+000
t_1	(s)	1.6788e-005	1.0000e-005	2.8184e-020
t_2	(s)	-1.6788e-005	1.0000e-005	2.8184e-020
M_{h1}	(kg)	0.0000e+000	1.0000e-005	0.0000e+000
M_{h2}	(kg)	0.0000e+000	1.0000e-005	0.0000e+000
M_{c1}	(kg)	-6.9951e-002	1.0000e-005	4.8931e-013
M_{c2}	(kg)	6.9951e-002	1.0000e-005	4.8931e-013
P_{hi}	(MPa)	0.0000e+000	5.1710e-003	0.0000e+000
P_{ho}	(MPa)	0.0000e+000	3.1026e-003	0.0000e+000
P_{ci}	(MPa)	2.4066e-004	5.1710e-003	1.5487e-012
P_{co}	(MPa)	0.0000e+000	3.1026e-003	0.0000e+000
L_h	(m)	0.0000e+000	1.0000e-006	0.0000e+000
W_h	(m)	0.0000e+000	1.0000e-006	0.0000e+000
Z_h	(m)	0.0000e+000	1.0000e-006	0.0000e+000
L_c	(m)	0.0000e+000	1.0000e-006	0.0000e+000
W_c	(m)	0.0000e+000	1.0000e-006	0.0000e+000
Z_c	(m)	0.0000e+000	1.0000e-006	0.0000e+000
T_r	(°K)	1.7502e-005	1.0000e-002	3.0631e-014
P_r	(MPa)	-2.4071e-004	1.0000e-003	5.7942e-014

^^

E_{c_i} (kJ)= 0.000084
FLUCTUATION   = 0.000002
UNCERTAINTY   = 2.852116

^^

           Uncertainty Pretest for E_{c_o} (kJ)

INPUT PAR.		SENS. COEFF.	MEAS. UNCER.	Contributor
T_{hi}	(°K)	0.0000e+000	1.0000e-001	0.0000e+000
T_{ho}	(°K)	0.0000e+000	1.0000e-001	0.0000e+000
T_{ci}	(°K)	0.0000e+000	1.0000e-001	0.0000e+000
T_{co}	(°K)	7.7173e-005	1.0000e-001	5.9556e-011
t_1	(s)	1.9642e-004	1.0000e-005	3.8580e-018

```
t₂       (s)     -1.9642e-004      1.0000e-005      3.8580e-018
```
M_{h1} (kg)   0.0000e+000   1.0000e-005   0.0000e+000
M_{h2} (kg)   0.0000e+000   1.0000e-005   0.0000e+000
M_{c1} (kg)   -8.1841e-001   1.0000e-005   6.6979e-011
M_{c2} (kg)   8.1841e-001   1.0000e-005   6.6979e-011
P_{hi} (MPa)   0.0000e+000   5.1710e-003   0.0000e+000
P_{ho} (MPa)   0.0000e+000   3.1026e-003   0.0000e+000
P_{ci} (MPa)   0.0000e+000   5.1710e-003   0.0000e+000
P_{co} (MPa)   2.4013e-004   3.1026e-003   5.5509e-013
L_h (m)   0.0000e+000   1.0000e-006   0.0000e+000
W_h (m)   0.0000e+000   1.0000e-006   0.0000e+000
Z_h (m)   0.0000e+000   1.0000e-006   0.0000e+000
L_c (m)   0.0000e+000   1.0000e-006   0.0000e+000
W_c (m)   0.0000e+000   1.0000e-006   0.0000e+000
Z_c (m)   0.0000e+000   1.0000e-006   0.0000e+000
T_r (°K)   -8.0301e-005   1.0000e-002   6.4482e-013
P_r (MPa) -2.4071e-004   1.0000e-003   5.7942e-014

^^

E_{c_o} (kJ)= 0.000982
FLUCTUATION   = 0.000014
UNCERTAINTY   = 1.421060
^^

              Uncertainty Pretest for $\eta_{I_{c,h}}$

INPUT PAR.   SENS. COEFF.   MEAS. UNCER.   Contributor

T_{hi} (°K)   -3.7662e-002   1.0000e-001   1.4185e-005
T_{ho} (°K)   1.3985e-002   1.0000e-001   1.9558e-006
T_{ci} (°K)   1.5447e-002   1.0000e-001   2.3861e-006
T_{co} (°K)   6.7534e-002   1.0000e-001   4.5609e-005
t_1 (s)   5.5511e-012   1.0000e-005   3.0815e-033
t_2 (s)   -9.2519e-013   1.0000e-005   8.5597e-035
M_{h1} (kg)   1.5727e+003   1.0000e-005   2.4734e-004
M_{h2} (kg)   -1.5727e+003   1.0000e-005   2.4734e-004
M_{c1} (kg)   -6.5498e+002   1.0000e-005   4.2900e-005
M_{c2} (kg)   6.5498e+002   1.0000e-005   4.2900e-005
P_{hi} (MPa) -6.8494e-002   5.1710e-003   1.2544e-007
P_{ho} (MPa)   6.8918e-002   3.1026e-003   4.5722e-008
P_{ci} (MPa) -2.1060e-001   5.1710e-003   1.1860e-006
P_{co} (MPa)   2.1014e-001   3.1026e-003   4.2510e-007
L_h (m)   0.0000e+000   1.0000e-006   0.0000e+000
W_h (m)   0.0000e+000   1.0000e-006   0.0000e+000
Z_h (m)   0.0000e+000   1.0000e-006   0.0000e+000
L_c (m)   0.0000e+000   1.0000e-006   0.0000e+000
W_c (m)   0.0000e+000   1.0000e-006   0.0000e+000
Z_c (m)   0.0000e+000   1.0000e-006   0.0000e+000
T_r (°K)   -5.9636e-002   1.0000e-002   3.5565e-007
P_r (MPa)   0.0000e+000   1.0000e-003   0.0000e+000

```
^^^^^^^^^^^^^^^^^^^^^^^^^^^^^^^^^^^^^^^^^^^^^^^^^^^^^^^^^^^^^^^^^
```
$\eta_{I_{c,h}}$ = 0.785976
 FLUCTUATION   = 0.025431
 UNCERTAINTY   = 3.235652
```
^^^^^^^^^^^^^^^^^^^^^^^^^^^^^^^^^^^^^^^^^^^^^^^^^^^^^^^^^^^^^^^^^
-----------------------------------------------------------------
```
            Uncertainty Pretest for $\eta_{II_{o,i}}$
```
-----------------------------------------------------------------
```

INPUT PAR.		SENS. COEFF.	MEAS. UNCER.	Contributor
T_{hi}	(°K)	-3.2582e-002	1.0000e-001	1.0616e-005
T_{ho}	(°K)	1.4697e-002	1.0000e-001	2.1600e-006
T_{ci}	(°K)	1.0503e-002	1.0000e-001	1.1032e-006
T_{co}	(°K)	5.5781e-002	1.0000e-001	3.1116e-005
t_1	(s)	5.5511e-012	1.0000e-005	3.0815e-033
t_2	(s)	-9.2519e-013	1.0000e-005	8.5597e-035
M_{h1}	(kg)	1.3204e+003	1.0000e-005	1.7435e-004
M_{h2}	(kg)	-1.3204e+003	1.0000e-005	1.7435e-004
M_{c1}	(kg)	-5.4993e+002	1.0000e-005	3.0243e-005
M_{c2}	(kg)	5.4993e+002	1.0000e-005	3.0243e-005
P_{hi}	(MPa)	-5.9255e-002	5.1710e-003	9.3885e-008
P_{ho}	(MPa)	7.2425e-002	3.1026e-003	5.0494e-008
P_{ci}	(MPa)	-1.4320e-001	5.1710e-003	5.4833e-007
P_{co}	(MPa)	1.7357e-001	3.1026e-003	2.9001e-007
L_h	(m)	0.0000e+000	1.0000e-006	0.0000e+000
W_h	(m)	0.0000e+000	1.0000e-006	0.0000e+000
Z_h	(m)	0.0000e+000	1.0000e-006	0.0000e+000
L_c	(m)	0.0000e+000	1.0000e-006	0.0000e+000
W_c	(m)	0.0000e+000	1.0000e-006	0.0000e+000
Z_c	(m)	0.0000e+000	1.0000e-006	0.0000e+000
T_r	(°K)	-4.8670e-002	1.0000e-002	2.3688e-007
P_r	(MPa)	-4.3573e-002	1.0000e-003	1.8986e-009

```
^^^^^^^^^^^^^^^^^^^^^^^^^^^^^^^^^^^^^^^^^^^^^^^^^^^^^^^^^^^^^^^^^
```
$\eta_{II_{o,i}}$ = 0.823222
 FLUCTUATION   = 0.021340
 UNCERTAINTY   = 2.592250
```
^^^^^^^^^^^^^^^^^^^^^^^^^^^^^^^^^^^^^^^^^^^^^^^^^^^^^^^^^^^^^^^^^
```

REFERENCES

[1] R. Shah, D. Sekulić, Fundamentals of Heat Exchanger Design, illustrated ed., Wiley, New York, 2003, pp 790.

[2] Z. Y. Guo, Z. X. Li, Size effect on microscale single-phase flow and heat transfer, International Journal of Heat and Mass Transfer (46) (2005) 149-159.

[3] S. B. Choi, R.F. Barron, R.O. Warrington, Fluid flow and heat transfer in microtubes, Micromechanical Sensors, Actuators, and Systems, ASME (32) (1991) 123-134.

[4] S. Kakaç, L.L. Vasiliev, Y. Bayazitoğlu, Y. Yener (Eds.), Microscale Heat Transfer Fundamentals and applications, Springer, Norwell, MA, 2005, pp 9-20.

[5] G. Hestroni, A. Mosyak, E. Pogrebnyak, L.P. Yarin, Heat transfer in micro-channel: comparison of experiments with theory and numerical results, International journal of Heat and Mass Transfer (48) (2005) 5580-5601.

[6] B. H. Jo, L. M. Van Lerberghe, K. M. Motsegood, D. J. Beebe, Three-dimensional micro-channel fabrication in polydimethylsiloxane (PDMS) elastomer, Journal of Microelectromechanical Systems, 1(1) (2000) 76-83.

[7] C. Liu, Foundations of MEMS, second ed., Pearson Prentice Hall, New Jersey, 2006, pp 453-460.

[8] D. Bartholomeusz, R. Boutte, J. Andrade, Xurography: Rapid prototyping of microstructures using a cutting plotter, Journal of Microelectromechanical Systems 14 (6) (2005)1364-1374.

[9] R. Kolekar, Fluid Flow Characteristics in Xurographic Microchannels, Master's Thesis, University of Utah, Salt Lake City, UT, 2009.

[10] N. T. Obot, Toward a better understanding of friction and heat/mass transfer in microchannels – a literature review, Microscale Thermophysical Engineering 6 (2002) 155-173.

[11] B. X. Wang, X. F. Peng, Experimental investigation of liquid forced-convection heat transfer through microchannels, International journal of Heat and Mass Transfer 37 (suppl.1) (1994) 73-82.

[12] X. F. Peng, G. P. Peterson, B. X. Wang, Frictional flow characteristics of water flowing through microchannels, Experimental Heat Transfer 7 (1994) 249-264.

[13] Wu and W. A. Little, Measurement of friction factor for the flow of gases in very fine channels used for microminiature Joule-Thomson refrigerators, Cryogenics 23 (5) (1984) 273-277.

[14] R. E. Acosta, R. H. Muller, W. C. Tobias, Transport process in narrow (capillary) channels, AIChE J. Fluids Eng. 110 (1985) 473-482.

[15] J. Pfahler, J. Harley, H. Bau, J. Zemel, Liquid transport in micron and sub-micron channels, Sensors and Actuators 21 (23) (1990) 431-434.

[16] X. F. Peng, G. P. Peterson, B. X. Wang, Heat transfer characterization of water flowing through micro-channels, Experimental Heat Transfer 7 (1994) 265-283.

[17] D. Yu, R. Warrington, R. Baron, An experimental investigation of fluid flow and heat transfer in microtubes, in: T. Ameel (Ed.), Proceedings of the 5th ASME/JSME Joint Thermal Engineering Conference, ASME, New York, NY,1995, pp. 523-530.

 [18] I.Papautsky, J. Brazzle, T. Ameel, A. B. Frazier, Laminar fluid behavior in microchannels using micropolar fluid theory, Sensors and Actuators 73 (1999) 101-108.

[19] J. Pfahler, J. Harley, H. Bau, J. Zemel, Gas and liquid flow in small channels, Micromechanical Sensors, Actuators, and Systems ASME DSC-32 (1991) 49-60.

[20] M. Makihara, K. Sasakura, A. Nagayama, The flow of liquids in micro-capillary tubes – consideration to application of the Navier-Stokes equations, Journal of the Japan Society of Precision Engineering 59 (3) (1993) 399-404.

[21] F. Gui, R. P. Scaringe, Enhanced heat transfer in the entrance region of microchannels, IECEC Paper No. ES-40 ASME (1995) 289-294.

[22] M. M. Rahman, F. Gui, Experimental measurements of fluid flow and heat transfer in microchannel cooling passages in a chip substrate, Advances in Electronic Packaging ASME EEP 4 (2) (1993) 685-692.

[23] T. L. Bergman, A. S. Levine, F. P. Incropera, and D. P. DeWitt, Fundamentals of Heat and Mass Transfer, seventh ed., Wiley, New York, 2011, pp. 544.

[24] G.L. Morini, Single-phase convective heat transfer in microchannels: a review of experimental results, International Journal of Thermal Sciences 43 (2004) 631-651.

[25] Kandlikar, S. G., Steinke, M. E., Single-phase liquid heat transfer in microchannels, ASME ICMM 75071 (2005) 667-677.

[26] R. A. Bowman, A.C. Mueller, W. M. Nagle, Mean Temperature Difference in Design, Transactions of the ASME 62 (1940) 283-294.

[27] W. Bier, W. Keller, G. Linder, D. Seidel, K. Schubert, Manufacturing and testing of compact micro heat exchanger with high volumetric heat transfer coefficients, ASME Dynamic Systems and Control Division (Publication) DSC 19 (1990) 189-197.

[28] C. R. Friedrich, S. D. Kang, Micro heat exchangers fabricated by diamond machining, Precision Engineering 16 (1) (1994) 56-59.

[29] T. S. Ravigururajan, J. Cuta, C. E. McDonald, M. K. Drost, Single-phase flow thermal performance characteristics of a parallel micro-channel heat exchanger, ASME Heat Transfer Division (publication) HTD 329 (1996) 157-161.

[30] P. X. Jiang, M. H. Fan, G. S. Si, Z. P. Ren, Thermal-hydraulic performance of small scale micro-channel and porous-media heat-exchanger, International Journal of Heat and Mass Transfer 44 (2001) 1039-1051.

[31] C. Harris, K. Kelly, T. Wang, A. McCandless, S. Motakef, Fabrication, modeling, and testing of micro-crossflow heat exchangers, Journal of Microelectromechanical Systems 11 (6) (2002) 726-735.

[32] B. Alm, U. Imke, R. Knitter, U. Schygulla, S. Zimmermann, Testing and simulation of ceramic micro heat exchangers, Chemical Engineering Journal 135S (2002) 726-735.

[33] N. Garcia-Hernando, A. Acosta-Iborra, U. Ruiz-Rivas, M. Izquierdo, Experimental investigation of fluid flow and heat transfer in a single-phase liquid flow micro-heat exchanger, International Journal of Heat and Mass Transfer 52 (2009) 5433-5446.

[34] J. J. Brandner, K. Schubert, Fabrication and testing of microstructure heat exchanger for thermal applications ASME ICMM 75071 (2005) 657-665.

[35] K. W. Kelly, C. Harris, L. S. Stephens, C. Marques, D. Foley, Industrial applications for LIGA-fabricated micro heat exchangers, SPIE - The International Society for Optical Engineering 4559 (2001) 73-84.

[36] Mohamed Gad-el-Hak (Ed.), The MEMES Handbook , CRC Press LLC, Danvers, MA 2002, pp. 1-1.

[37] J. H. Spurk, N. Aksel, Fluid Mechanics, second ed., Springer, New York, 2008, pp. 516.

[38] F. M. White, E. Benjamin Wylie, Fluid Mechanics, third ed., McGraw Hill, New York, 1994, pp 701.

[39] V. L. Streeter, Fundamentals of Fluid Mechanics, eight ed., McGraw Hill, New York, 1985, pp 557.

[40] S. Alshareef, Experimental study of xurographic microchannel single-pass single-phase counterflow heat exchanger, Master's Thesis, University of Utah, Salt Lake City, UT, 2012.

[41] S. J. Kline, The purpose of uncertainty analysis, Journal of Fluids Engineering 107 (153) (1984).

[42] R. J. Moffat, Contributes to the theory of uncertainty analysis for single-sample experiments, Thermosciences Division, Dept. of Mech. Engr., Stanford University, Stanford, California (1981) 40-57.

[43] R. J. Moffat, Describing the uncertainties in experimental results, Experimental Thermal and Fluid Science 1 (1998) 3–17.

[44] R. J. Moffat, Contributions to the theory of uncertainty analysis for single-sample experiments, ASME Journal of Fluids Engineering 104 (250) (1982).

[45] S. Ashman, S. Kandlikar, A review of manufacturing processes for microchannel heat exchanger fabrication, Fourth International Conference on Nanochannels, Microchannels and Minichannels, Limerick, Ireland, 2006.

[46] L.T. Nguyen, Contraction/expansion effects in 90º miter bends in rectangular xurographic microchannel, Master's Thesis, University of Utah, Salt Lake City, UT, 2011.

[47] D. Bartholomeusz, R. Boutté, J. Andrade, Xurography: rapid prototyping of microstructures using a cutting plotter, Journal of Microelectromechanical Systems 14 (6) (2005) 1364-1374.

[48] D. Torgerson, R. Kolekar, B. Gale, Minor losses in rectangular xurographic microchannels, in: T. Ameel (Ed.), Proceedings of the ASME International Mechanical Engineering Conference and Exposition, Vancouver, Canada, 2010 IMECE2010 39401.

[49] J. Greer, S. O. Sundberg, C. T. Wittwer, Comparison of glass etching to xurography prototyping of microfluidic channels for DNA melting analysis, Journal of Micromechanics and Microengineering 17 (12) (2007) 2407-2413.

[50] F. White, Fluid Mechanics, third ed., McGraw Hill, New York, 1994, pp. 701.

[51] Department of Technical Thermodynamics - Mechanical Engineering - University of Applied Sciences Zittau/Görlitz, Prof. Hans-Joachim Kretzschmar, Dr. Ines Stöcker. (*http://thermodynamik.hszigr.de/cmsfg/lehre/index.php?rubic=downloads+f%FCr+Studierende*) Last date visited: Nov.2011.

[52] K. Wark, Advanced Thermodynamics for Engineers, illustrated ed., McGraw Hill, New York, 1995, pp. 122.